

Technische Universität München
Lehrstuhl für Technische Chemie II

Autothermal Reforming of n-Hexane over Supported Metal Catalysts

Maria Brandmair

Vollständiger Abdruck der von der Fakultät für Chemie der Technischen Universität
München zur Erlangung des akademischen Grades eines

Doktors der Naturwissenschaften

genehmigten Dissertation.

Vorsitzender:

Univ. Prof. K.-O. Hinrichsen

Prüfer der Dissertation:

1. Univ. Prof. J. A. Lercher

2. Priv.-Doz. Dr. P. Härter

Die Dissertation wurde am 30.08.2005 bei der Technischen Universität München eingereicht
und durch die Fakultät für Chemie am 18.10.2005 angenommen.

***“Mehr als die Vergangenheit interessiert mich
die Zukunft, denn in ihr gedenke ich zu leben.“***

Albert Einstein

Für meine Familie.

Acknowledgements

Now, that I have finished writing, I want to thank all the people who have contributed to my work in one way or the other.

Prof. J.A. Lercher for getting me into his truly international group (not less than ten nations from all over the world). He gave me the opportunity to work on a very interesting project with a good prospect. Thank you, I have really learnt a lot.

Special thanks to Josef, for supervising me during the first period until he got the job in industry he was looking for and Roberta for corrections and plenty of discussions when I was approaching the end of my work.

I would like to thank all the members of TC-II for many discussions and wonderful moments inside and outside of the lab. The people who were already there when I started my work in the group: first Qing, Jan-Olaf and Stevie (starting at the same time) thank you for your friendship and keeping my spirits up when research process was slow, Renate, Adam, Bertha and Laurent sharing the office with me, thanks also to Jochen, Hilton, Fred, Alex H., Shourong, Christian S., Martin S., Ngyuen, Anil, Dr. Bratz, Hiroaki, Andreas F., Jan, Gabriela, Dr. Bratz, Thomas and Andy J.. Many others entering the group during my PhD: Hendrik, Elvira, Virginia and Carsten moving in the office, when the others left to the “french getto” for writing, Christian W., Philipp, Ben, Wolfgang, Andi S., Florencia, Helen and Peter S. (my “chauffeurs”), Wolfram, Alex G., Oriol, Iker, Olga, Chintan, Krishna, Rino, Lay Hwa, Aonsourong, Xuebing, Mahdi, Jürgen and Manuel thanks for your support and the nice atmosphere. Thanks to all the other colleagues at the institute making the last years more comfortable: Heike making bureaucracy easier and Heidi always taking care of the finances, Xaver, Andreas M., Martin N. for measurements and for a lot of technical support and all the members of the TC-workshop.

Some were only staying for a short time for some reason or the other: Toshi working on a similar topic giving me some ideas and helpful discussions, Linda, Peter H., Chirag, Hitri, Stefan V. Hope I have forgotten nobody, if so it was only because of the numerous former and actual members of the chair.

I am thankful for the financial support by the Bayerisches Staatsministerium für Wirtschaft, Verkehr und Technologie (Project 13 03/892 66/1396/02) and the project partners from Industry, Prof. Stimming and Holger from the physical department.

Besonderer Dank gilt natürlich auch meiner Familie: meinen Eltern, meiner Tante Sefi und meinem Bruder Martin (mit seiner kleinen Familie), mit deren Unterstützung und Rückhalt dieser Werdegang erst möglich wurde.

Table of Contents

<i>Chapter 1</i>	General Introduction	1
1.1	Fuel cells	2
1.2	PEMFC and SOFC	5
1.3	Reformer – hydrogen from gasoline	7
1.4	Scope and structure of the thesis	9
1.5	References	11
<i>Chapter 2</i>	Hexane to Synthesis Gas – Thermodynamic Calculations	12
2.1	Introduction	12
2.2	Thermodynamics of hexane to synthesis gas	13
2.3	Autothermal Reforming	16
2.3.1	Thermodynamic equilibrium for ATR of n-hexane	17
2.3.2	Thermo-neutrality of the autothermal reforming	20
2.4	Mechanistic Aspects	21
2.4.1	Partial Oxidation	22
2.4.2	Steam Reforming	26
2.4.3	Inverse spillover in steam reforming	27
2.4.4	Mechanism of WGS reaction	28
2.5	References	29
<i>Chapter 3</i>	Autothermal Reforming of Hexane over Ni, Pt and Rh Supported Metal Catalysts	31
3.1	Introduction	32
3.2	Experimental	34
3.2.1	Catalyst Preparation	34

3.2.2	Chemical and Physico-chemical Characterization	35
3.2.3	Catalytic Activity	36
3.3	Results	39
3.3.1	Characterization	39
3.3.2	Catalytic Activity	41
3.3.2.1	Comparison of different metals supported on alumina	41
3.3.2.2	Comparison of different metals supported on yttria-stabilized zirconia	43
3.3.2.3	Comparison of different metals supported on zirconia	46
3.3.2.4	Comparison of different metals supported on ceria	49
3.4	Discussion	51
3.4.1	Effect of Noble Metal	51
3.4.2	Effect of Support	52
3.5	Conclusion	54
3.6	References	55

Chapter 4 **Autothermal Reforming of n-Hexane over Structured Catalysts**

		56
4.1	Introduction	57
4.2	Experimental	57
4.2.1	Impregnation of monolithic catalysts	57
4.2.2	Characterization techniques	58
4.2.3	Catalytic experiments	59
4.3	Results	62
4.3.1	Characterization	62
4.3.2	Catalytic activity at 775°C - Effect of feed composition	65
4.3.3	Effect of reaction temperature on catalytic activity (ratio hexane/oxygen/water=1/3/7)	71

4.4	Discussion	75
4.5	Conclusion	78
4.6	References	79
<i>Chapter 5</i>	Kinetic parameters for the autothermal reforming of n-hexane on Al₂O₃-supported Rh catalysts	80
5.1	Introduction	81
5.2	Catalytic Experiments	82
5.3	Results and Interpretation	85
5.3.1	Variation of WHSV	86
5.3.1.1	Rh/ γ -Al ₂ O ₃ (M)	87
5.3.1.2	Umicore A-Type	89
5.3.1.2.1	Partial poisoning with sulfur (hexane containing 10 ppm S)	92
5.3.1.1	Rh/ γ -Al ₂ O ₃ (P)	93
5.3.2	Variation of O ₂ /C ₆ H ₁₄ and H ₂ O/C ₆ H ₁₄	95
5.3.3	Oscillations during autothermal reforming	97
5.3.4	Discussion	98
5.5	Hydrogenolysis	103
5.6	Conclusions	106
5.7	References	107
<i>Chapter 6</i>	Summary	108
	<i>Curriculum Vitae</i>	113

General Introduction

Abstract

This chapter gives a general background for the work presented in this thesis. First fuel cell systems are described and their advantages and types discussed. Two fuel cell types – proton exchange membrane fuel cell and solid oxide fuel cell - are described in more detail. In the following the reforming process for converting hydrocarbons to hydrogen (syngas) for fuel cells is shortly depicted. Finally, the scope of the thesis and its structure are presented.

1. Fuel cells

Due to the decrease of worldwide capacity of crude oil and due to political reasons, the price for fuels - gasoline and diesel – are increasing dramatically. In Germany one litre of gasoline (super) cost 35.3 cents in 1972 at a fuel station while in August 2004 a top price of 121.9 cents was reached. Therefore the call for alternatives to fossil fuels is becoming stronger. Besides Bio-Diesel (in Germany price maintenance to fossil fuels) and solar energy, hydrogen - used in fuel cells - seems to be the most promising energy source.

Fuel cells at the moment hold an almost irrational attraction. Although the principle of fuel cells was already discovered in 1839 by William Grove (“gas voltaic battery”: hydrogen reacts with oxygen producing electricity and water), their role as a practical power generator did not emerge until the 1960s when the U.S. space program developed fuel cells to power the Gemini and Apollo spacecraft ¹. The term “fuel cell” was coined later in 1889 by Ludwig Mond and Charles Langer, who attempted to build the first practical device using air and industrial coal gas ².

Fuel cells are electrochemical devices similar to a battery, but differing from the later in that they are designed for continuous replenishment of the reactants consumed, i.e. they produce electricity from an external fuel supply as opposed to the limited internal energy storage capacity of a battery. Typical reactants used in a fuel cell are hydrogen or carbon monoxide on the anode side and oxygen on the cathode side. Fuel cells, being electrochemical devices, are not constrained by the maximum thermal (Carnot) efficiency as combustion engines are. Consequently, they can have very high efficiencies in converting chemical energy to electrical energy without detour of heat. Moreover, because electrical energy is generated without combusting fuel, fuel cells are extremely attractive from an environmental stand point. Attractive fuel cell characteristics include:

- High electrical efficiencies in wide range of load (see Fig. 1.1)
- No emission running on hydrogen
- Only low emission running on hydrocarbons with a previous reformer
- High overall efficiency coupled with heat exploitation
- Easy power adjustment through modular construction
- Mechanically simple systems without moving parts
- No vibrations
- Quiet operation

Many industrial branches are interested in fuel cells that can be used as batteries, e.g. for mobile phones or notebooks (miniaturisation problem), for vehicles (mobile application) and to generate heat and power for households (stationary application).

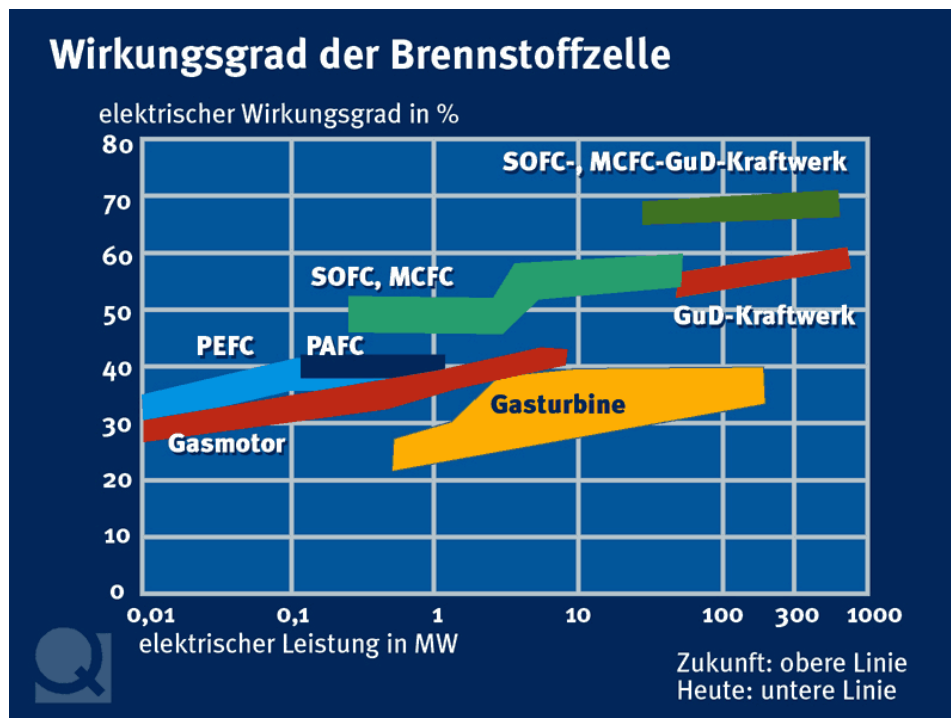


Figure 1.1: Efficiencies and power range of different fuel cells compared to conventional systems³.

Different types of fuel cells are concurring against each other (see Table 1.1). The type of fuel cell is named after the electrolyte used that determines the working temperature required for the ionic transport. The proton exchange membrane fuel cell (PEMFC) gains at the moment the highest interest in research. Both high temperature cells – molten carbonate fuel cell (MCFC) and solid oxide fuel cell (SOFC) - are developed especially for stationary applications allowing CO as fuel besides H₂.

Which kind of fuel cell will win the race is still outstanding. Each fuel cell has its specific advantages and disadvantages depending on the application wanted (see Table 1.2). In the following paragraph two types of fuel cells (PEMFC and SOFC) are presented in more detail.

Table 2.1 Overview of the different fuel cell types ⁴.

FC-Type	Fuel (primary) (Anode)	Electrolyte T-Range (Cell)	Oxidant (Cathode)	System Components	System-efficiency (%)	Comment	Stand of Art (max. power)
Alkaline (AFC)	pure H ₂	30% KOH 60...90°C	Air	Cell, Water removal	60	CO ₂ -sensitive	20 kW
Proton-exchange-Membrane (PEMFC)	H ₂ , Methane, Methanol	PEM NAFION 80...200°C	Air, Oxygen	Reformer, Gas Cleaning, Cell	60 (H ₂) 40 (CH ₄)	CO-sensitive	250 kW
Direct-Methanol (DMFC)	Methanol	PEM NAFION 80...200°C	Air, Oxygen	Cell	40	Promising: H ₂ -production has not to take place	Under development
Phosphoric Acid (PAFC)	Methane, H ₂	conc. H ₃ PO ₄ 130...220°C	Air, Oxygen	Reformer, Converter, Cell, Heat Exchanger	40	weak CO-sensitive	11 MW
Molten Carbonate (MCFC)	Methane, Coal gas, Biogas, Biomass-Gas	Li ₂ CO ₃ /K ₂ CO ₃ 600...650°C	Air, Oxygen	Gasification or Reformer, Cell, Heat Exchanger	48-60	CO ₂ has to run in cycles back to cell	2,2 MW
Solid Oxide (SOFC)	Methane, Coal gas, H ₂ , Biogas, Biomass-Gas	Zr(Y)O ₂ 800...1000°C	Air, Oxygen	Cell, Heat Exchanger	50-65	Reforming of fuel (CH ₄) not necessarily required	10 kW (planar) 25 kW (tubular)

Table 1.2: Applications of fuel cells.

Application for Fuel Cell Types	AFC	PEMFC	PAFC	SOFC	MCFC	DMFC
Mobile (e.g. vehicles)	✓	✓	✗	✓	✗	✓
Portable (e.g. Mobile Phones and Notebooks)	✓	✓	✗	✗	✗	✓
Home electricity and heat production	✗	✓	✗	✓	✗	✗
Stationary power units Middle power range	✗	✓	✓	✓	✓	✗
Stationary power units High power range	✗	✗	✗	✓	✓	✗

1.2 PEMFC and SOFC

Out of the four candidates considered for mobile applications there are currently two types of favoured fuel cell systems: i) the proton-exchange membrane fuel cell (PEMFC) and the solid oxide fuel cell (SOFC). The basic differences between these two fuel cells are the type of electrolyte and therefore the working temperature necessary to achieve an adequate ionic conductivity (Fig. 1.2). In a SOFC the transport of oxygen ions (O^{2-}) through the electrolyte requires high temperatures (800-1000°C), while in a PEMFC low temperatures (80-200°C) are sufficient for the transport of hydrogen ions (H^+).

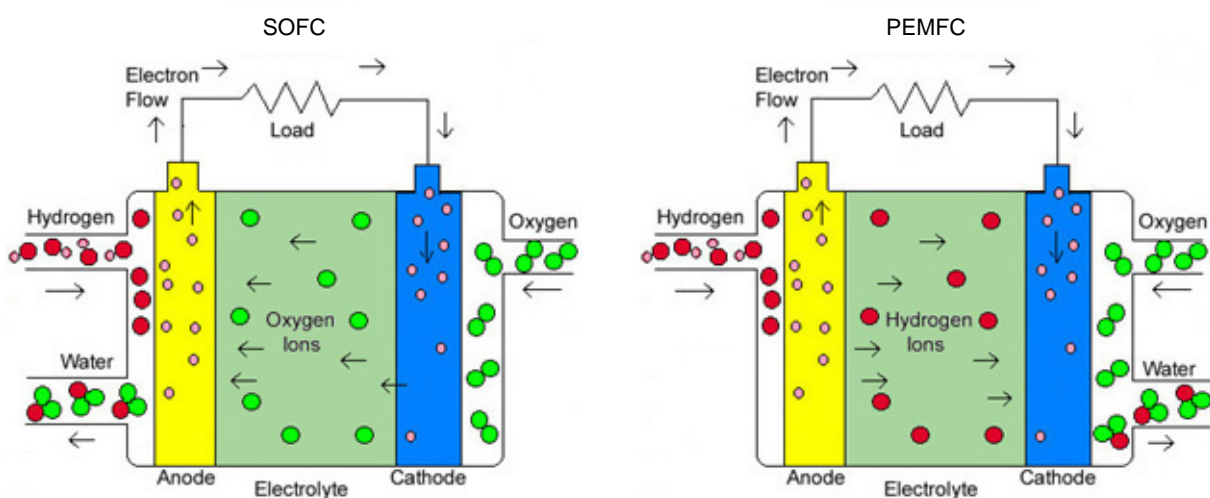


Figure 1.2: Ionic transport through the electrolyte of a SOFC compared to a PEMFC.

In addition to pure hydrogen, the PEMFC and SOFC can also operate on reformed hydrocarbon fuels. For the PEMFC the traces of CO produced during the reforming process must be removed up to less than 40 ppm^{5,6} because CO poisons the anode (platinum). Therefore synthesis gas must be “cleaned” converting CO stepwise into CO₂. This is performed by a high-temperature water gas shift (HTS, 450 °C) followed by a low-temperature water gas shift (LTS, 180 °C, CO between 0.5 and 1%) and finally by selective CO-oxidation at 180 °C (CO < 10 ppm). Despite the need of high purity hydrogen, the benefits of the PEMFC-system are the low process temperature, the narrow construction of single cells and the expected low manufacture cost of the polymer electrolyte (the most part known from synthetics). Unlike PEMFC, in SOFC CO does not act as a poison and can be used directly as a fuel allowing the use of a simple single-stage reformer. Additionally the high operating temperature of the SOFC offers the possibility of internal reforming.

Furthermore, of all fuel cell types, the SOFC is the least sensitive to impurities and it can tolerate several orders of magnitude more sulfur than other fuel cells. In SOFC no expensive precious metals are required for the electrodes (anodes are based on Ni). All these characteristics render the SOFC more appropriate for use of gasoline and diesel.

Common for both PEMFC and SOFC are a desulfurization step and an after-burner. The heat released from the after-burner is used for heating up the air and the reformer increasing the overall efficiency (Fig. 1.3).

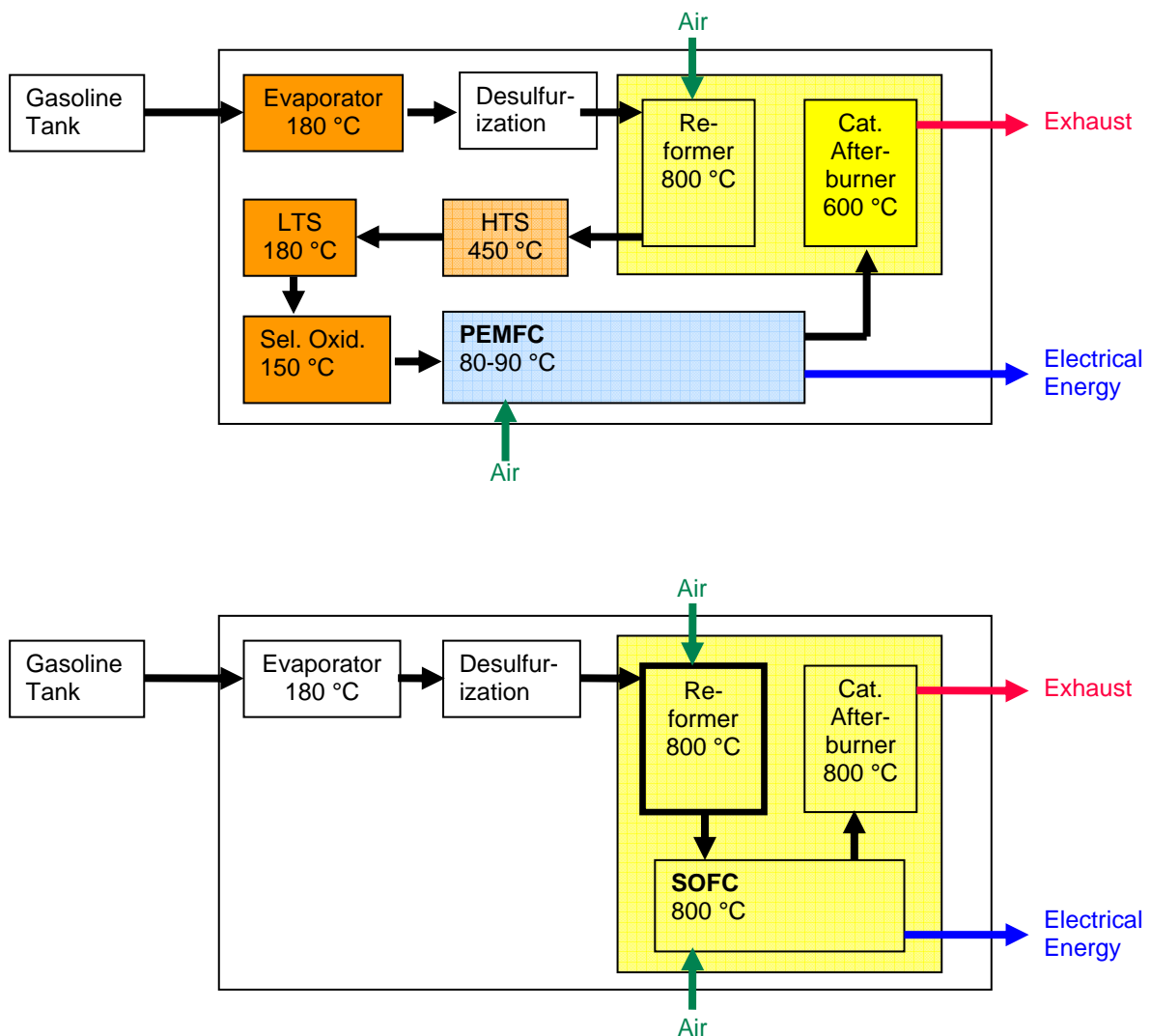


Figure 1.3: Integrated scheme for PEMFC (above) and SOFC (below). (LTS: low temperature shift; HTS high temperature shift; Sel. Oxid.: selective oxidation).

Considering the complete energy conversion (reformer and fuel cell) significantly less CO₂ is produced compared to conventional systems burning fossil fuels. At present, Mercedes Benz is developing a PEMFC system. In the Nekar 5 the

tank, the reformer and the fuel cell (PEMFC from Ballard Power) fits into a standard A-Klasse. Other companies studying fuel cell-driven cars are Opel, Honda and Toyota. The SOFC so far is used only as an auxiliary power unit in cars under development by Delphi ⁷ together with BMW and Renault. They integrated a fuel reformer that generates hydrogen rich gas by partial oxidation of gasoline or diesel fuel at 800°C. One of the most important aspects is a long life-time of the cell. Westinghouse tested a tubular SOFC with more than 60000 h, while Dornier reported 18000 h for a planar SOFC. Both fuel cell types offer advantages. However, which is to be favored is a matter of opinion.

1.3 Reformer – hydrogen from gasoline

Hydrogen, the simplest element and most plentiful gas in the universe, does not exist alone in nature. It always combines with other elements such as oxygen and carbon. Natural gas contains hydrogen (about 95% of natural gas is methane), as do biomass and hydrocarbons, like coal. Once it has been separated from hydrogen-containing feedstocks, hydrogen is the ultimate clean energy carrier. Almost all of the hydrogen produced today (95% of the hydrogen produced in the U.S.) is obtained by steam reforming of natural gas or other hydrocarbons. For the near term, this method of production will continue to dominate, although several other methods have been developed. Many of them involve splitting water. For example hydrogen can be produced by electrolysis. A variation of the conventional electrolysis is the steam electrolysis that uses heat, instead of electricity, to provide some of the energy needed to split water, making the process more energy efficient. Photochemical, photobiological, biological and thermal methods for water decomposition have also been developed.

While electricity, that is the energy carrier in the today's system, is easily transported and delivered to end-users, storage, transportation and delivery of hydrogen are still critical steps toward a future hydrogen economy. The need of an infrastructure that allows easy and cost-effective hydrogen transportation could be overcome by combining the production of hydrogen and its use in fuel cells. Thus, methane, methanol or other fuels could be converted into hydrogen within a reformer that straightway supplies it to the fuel cell. As an intermediate step for introduction of fuel cells on the market, the automobile industry works on the on-board production of

hydrogen from gasoline or diesel. The resulting reformer/fuel cell system should have an efficiency 10% higher than that of the conventional engines.

The reformer is a light, multifunctional reactor with integrated heat and material management. Inside the reformer hydrogen can be obtained by partial oxidation (POX), steam reforming (SR) or autothermal reforming (ATR - a combination of POX and SR) of gasoline or diesel. Gasoline, as exemplary fuel, is mixed with air and water (ATR) at 800°C (latest works 650°C⁸). The gas mixture generated contains mainly hydrogen, carbon monoxide, carbon dioxide, nitrogen and water.

Autothermal reforming and partial oxidation systems have a much better dynamic than steam reforming systems since they do not require external heating and can be heated up relatively quick by internal combustion of fuel⁹. Autothermal reforming and partial oxidation can take place in both non-catalytic (at temperatures higher than 1000 °C) and catalytic reactions. Two examples⁹ are shown in Figure 1.4. The non-catalytic thermal POX (Fig. 1.4a) uses water to prevent coking. Very high temperatures (approximately 1400°C) are required thus resulting in a good gas phase kinetics and therefore generating a reformate of good quality. The non-catalytic thermal POX combined with catalytic steam reforming (=ATR) (Fig. 1.4b) operates at lower temperature, resulting in unwanted by-products. However by means of the steam reforming these by-products can be converted to H₂ and CO. The composition of the product gas is determined by the thermodynamic equilibrium corresponding to the outlet temperature of the catalytic bed, which is dictated by the inlet temperature and the adiabatic temperature rise.

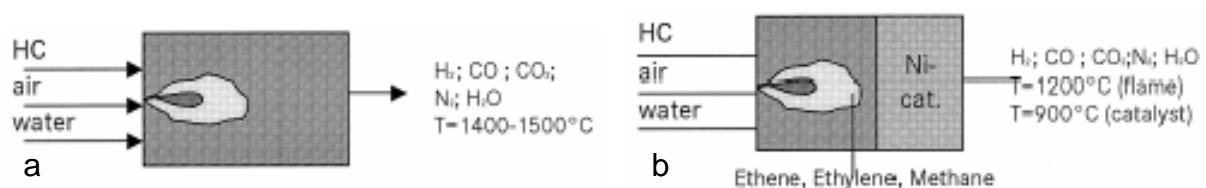


Figure 1.4: Examples for reforming reactor types: a) thermal partial oxidation with water injection and b) thermal partial oxidation combined with steam reforming.

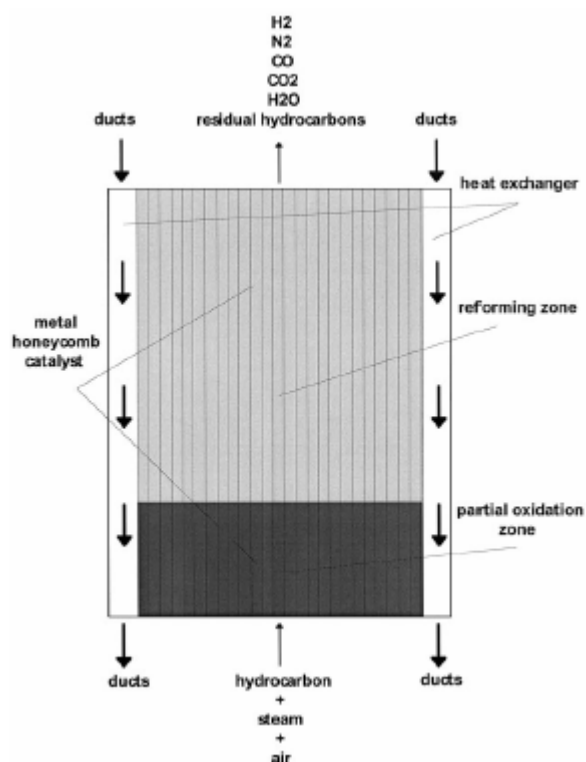


Figure 1.5: Schematic design of an autothermal propane reformer.

Figure 2.7 shows an example for an ATR running on propane¹⁰ including a heat exchanger for the internal preheating of ducts. Due to the different reaction rates of combustion and reforming, the catalyst structure may be divided into two zones: in the first zone the oxidation of the hydrocarbon prevails while the second zone is mainly required for complete reforming. Thus the catalyst at the inlet of the reactor is mainly heated by direct heat transfer of the combustion reaction while the second zone is heated by the heat content of the product gas flowing counter current to the feed stream.

Therefore, ATR allows flexible operation, compact design and low investment costs. However some problems have to be solved such as the large size of the reformer and the high costs. In this context it is important to observe that in combination with an SOFC the size of the reformer can be minimized because a single-stage reformer is sufficient.

1.4 Scope and Structure of the Thesis

Reforming of hydrocarbon based liquid fuels has the advantage of an easily adaptable fuel infrastructure and ease of refueling. Methanol, gasoline, and diesel are considered as liquid fuel sources for on-board hydrogen production. Catalytic partial oxidation and autothermal reforming are considered as alternative to steam reforming. However the mentioned processes have been less broadly explored in the open literature where a strong focus on methane and light hydrocarbons exists. Especially for alkanes in fuels for automotive applications (e.g. diesel and gasoline) more information is needed for efficient hydrogen production on a small scale. In this thesis the production of syngas through autothermal reforming for SOFC application was investigated. As gasoline is a complex mixture of hydrocarbons hexane was chosen as a model component. Additionally, one major concern in autothermal reforming of hydrocarbons is carbon deposition causing catalyst deactivation.

Chapter 2 presents the reactions involved in autothermal reforming process and possible side reactions for the conversion of hexane. Included is the simulation of the thermodynamic equilibrium in a temperature range interesting for reformer application in a SOFC depending on changes in feed composition.

Chapter 3 deals with the suitability of various supported metal catalysts for autothermal reforming of hexane (Ni, Pt and Rh supported on ceria, zirconia, yttria-stabilized zirconia and alumina).

Chapter 4 focuses on Ni, Pt and Rh supported on structured support (alumina monolith). The effect of feed composition on their stability and activity was investigated at constant temperature (775°C). Additionally, the catalytic activity of Pt and Rh containing catalysts were compared to those of an industrial catalyst in the temperature range interesting for a reformer operating with fuel cells (500-800°C).

In **chapter 5** the product distribution over Rh catalysts was studied under reaction conditions (changes in feed compositions and load) typical for a pre-reformer in fuel cells. Mechanistic aspects of autothermal reforming are also discussed in this section. Furthermore, the possibility to increase the methane content in the reformat through hydrogenolysis of hexane is discussed.

In **chapter 6** the major results are summarized.

1.5 References

- (1) www.cmt.anl.gov.
- (2) <http://chem.ch.huji.ac.il/~eugeniik/history/grove.htm>.
- (3) www.quarks.de/energie.
- (4) Wendt, H.; V., P. *Brennstoffzellen-Typen, Entwicklungslinien, Marktchancen*; VDI-Verlag: Düsseldorf, 1990.
- (5) Gray, P. G.; Frost, J. C. "Impact of catalysis on clean energy"; 2nd Asia Pacific Conf. On Sustainable Energy and Environmental Technologies, 1998, Gold Coast, Australia.
- (6) Avci, A. K.; Önsan, Z. I.; Trimm, D. L. *Applied Catalysis A-General* **2001**, 216, 243.
- (7) www.delphi.com.
- (8) Megede, D.; Sommer, M. "On-Board Hydrogen Production for Fuel Cell Application in Vehicles"; Proceedings of the DGMK-Conference "Innovation in the Manufacture and Use of Hydrogen", 2003, Dresden, Germany.
- (9) Docter, A.; Lamm, A. *Journal of Power Sources* **1999**, 84, 194.
- (10) Rampe, T.; Heinzl, A.; Vogel, B. *Journal of Power Sources* **2000**, 86, 536.

Hexane to Synthesis Gas – Thermodynamic Calculations

2.1 Introduction

As an intermediate target for introducing fuel cells on the market – unless the problem for hydrogen infrastructure is solved – reformers running on gasoline (or diesel) are developed for on-board production of hydrogen. As gasoline is a complex mixture of hydrocarbons, hexane was used in this study as a model component. In fact its properties are similar to those of gasoline, e.g. the lower heating values for hexane and gasoline are 3886.6 kJ/mol (= 44.7 kJ/g) and 4050 kJ/mol (= 42 kJ/g), respectively. This chapter summarizes the reactions for converting hexane to synthesis gas including mechanistic aspects. Their thermodynamic equilibria are discussed and the advantages of autothermal reforming over other reactions for synthesis gas production underlined.

2.2 Thermodynamics of hexane to synthesis gas

The production of synthesis gas (carbon monoxide + hydrogen) is currently carried out via **steam reforming (SR)**, reaction 2.1). Steam passes over a carbon source, often methane or coal, and is heated to produce a hydrogen rich gas.



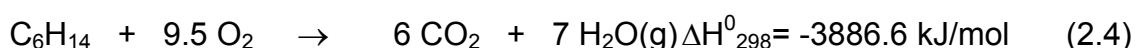
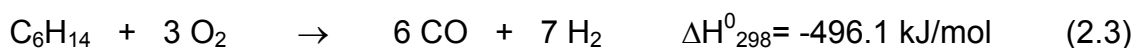
To describe the composition of the feed for steam reforming often the parameter “steam to carbon molar ratio” (S/C) is used (S/C=1 for reaction 2.1).

Steam reforming can be replaced by the even more endothermic **carbon dioxide reforming** (reaction 2.2), also called dry-reforming, yielding a CO rich gas:



If sufficient steam is fed, the global reaction of hexane to synthesis gas corresponds to steam reforming because CO is converted with H₂O to CO₂ and H₂ via water-gas-shift reaction (see reaction 2.8).

Reforming has the major disadvantage of being highly endothermic and hence requires a large amount of wasted energy. An interesting alternative to reforming is the **partial oxidation (POX)**, reaction 2.3) of the hydrocarbon. The major advantage is that the process is exothermic, so energy is not consumed in order to drive the reaction. The partial oxidation of hexane to synthesis gas and its **total oxidation (TOX)**, reaction 2.4) to carbon dioxide and water may proceed concurrently:



If air is used as oxygen source, the so-called “λ-value” is introduced corresponding to the ratio between the amount of air (oxygen) present and the amount of air (oxygen)

needed for total oxidation. In the case of the total oxidation λ is equal to 1 while for the reaction (2.3) λ is 0.32.

From Le Chatelier's principle it is clear that low pressure favours both reforming and oxidation equilibria. Figure 2.1 shows the product distribution for steam reforming, CO₂ reforming and partial oxidation (complete oxygen consumption). The thermodynamic equilibria were calculated with the version 5.1 of the software HSC Chemistry[®] from Outokumpu. The conversion of hexane does not require high temperature. However high temperatures (about 850 °C) are required to reduce the production of methane. In the POX, at low temperature the equilibrium composition corresponds to a mixture of methane and TOX products (CO₂ and H₂O). These results are similar to those obtained for methane by Stobbe¹.

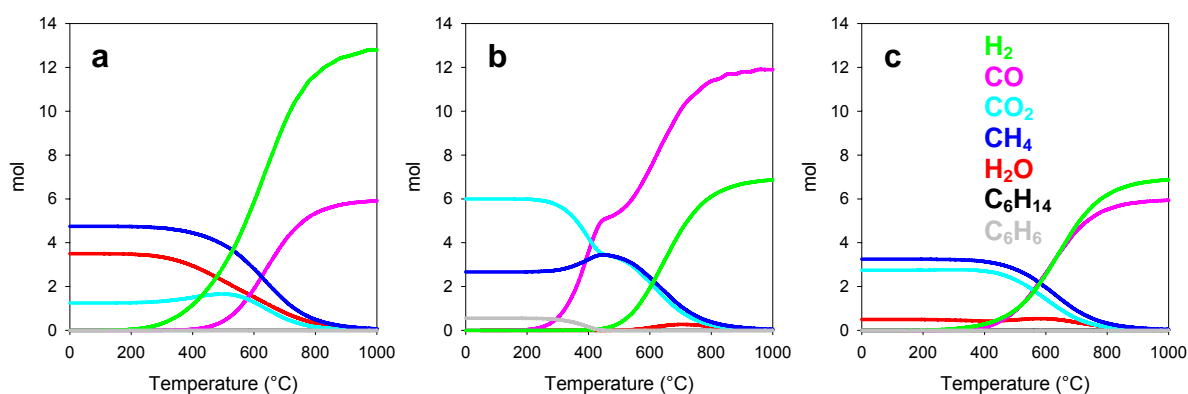


Figure 2.1: Equilibrium composition as a function of temperature at 1 bar for **a)** SR: hexane/steam=1:6, **b)** CO₂ reforming: hexane/carbon dioxide = 1:6 and **c)** POX: hexane/oxygen = 1:3. Carbon formation was excluded from the equilibrium calculations. For POX the O₂ consumption was complete over whole temperature range and therefore it is not shown. In all cases C₆H₁₄ was fully converted.

Replacing hexane by methane in SR (2.5), POX (2.6) or CO₂ reforming (2.7) reactions leads to different CO/H₂ ratios. As these reactions are reversible they can be a source for methane formation.

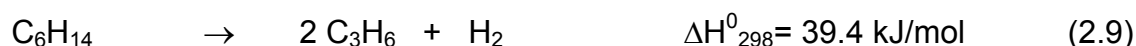




The **water-gas shift** equilibrium (**WGS**, reaction 2.8) changes the ratio between CO and H₂ produced by reforming (reactions 2.1 and 2.2). The position of the WGS reaction depends only upon temperature and not upon pressure.



Unlike methane, hexane can undergo additional reactions. The most important are the slight endothermic cracking reactions. Through **catalytic cracking** (2.9) the share of propene would be higher while through **thermal cracking** (2.10) the share of ethylene is predominant:



Another possible side reaction is the **dehydration** (2.11) of hexane resulting in hydrogen and cyclic products like benzene. This reaction is thermodynamically favoured during carbon dioxide reforming at temperature below about 400 °C, as seen in Fig. 2.1b.



A complicating factor in the conversion of both hexane and methane is the formation of carbonaceous deposits that may proceed through a number of complex reactions. At high temperature coke (carbon) can be formed from hexane through a sequence of irreversible reactions giving first olefins, then polymers and finally coke. This series of reaction is summarized as hexane **pyrolysis** in reaction 2.12. Three of the intermediate steps are mentioned above: thermal and catalytic cracking and dehydration. Also methane can undergo to pyrolysis (reaction 2.13). Other reaction

such as **Boudouard equilibrium** (reaction 2.14), or **CO reduction** to carbon and water (reaction 2.15) are involved.



Low temperatures and high pressures favour the Boudouard reaction and the CO reduction while high temperatures and low pressures favour hexane and methane pyrolysis.

Deposition of carbon can be prevented kinetically by selecting the appropriate catalyst and thermodynamically by operating the process outside the carbon boundaries, *i.e.* with a proper choice of the oxygen/hydrocarbon or steam/hydrocarbon ratios^{2,3}.

2.3 Autothermal reforming

Autothermal reforming (ATR) is the combination of partial oxidation and steam reforming, where steam reforming is carried out in the presence of oxygen. Exothermic, endothermic and thermo-neutral conditions can be selected by changing the hydrocarbon/oxygen/steam ratios^{4, 5, 6, 7}. The gross ATR reaction for a general hydrocarbon C_nH_m can be described by the following equation:



Docter *et al.*³ calculated a theoretical value of a lying between 3.0 and 3.5 for n-heptane to get maximum efficiency for their reformer system (connected to a

PEMFC). A prediction of a out of a stoichiometric calculation is not possible (i.e. heat loss of the system components cannot be included), but calculations of the thermodynamic equilibrium allow to predict the optimal operating condition for the autothermal reforming reactor and possible values for a . To reduce the coke formation high oxygen/hydrocarbon and water/hydrocarbon ratios have to be used⁸. Investigations at Mercedes Benz⁹ for ATR applied to a PEMFC system showed that in the case of POX a $\lambda \geq 0.35$ (corresponding to oxygen/hexane ratio $\geq 3.325/1$) is sufficient to prevent coking. With increasing steam to carbon ratio (S/C) the boundary value for λ decrease to 0.275 (for S/C = 0.7).

2.3.1 Thermodynamic equilibrium for ATR of n-hexane

As the equilibrium composition in autothermal reforming depends on three variable (i) temperature, ii) ratio fuel/oxygen and iii) ratio fuel/water), the equilibrium composition from ATR of n-hexane was calculated for two special cases in a temperature range of 500-900 °C:

- a) at constant hexane/oxygen molar ratio (1:3) with variation of water/hexane molar ratio from 3 to 15,
- b) at constant hexane/water ratio (1:7) with variation of oxygen/hexane molar ratio from 1 to 6.

For a constant hexane/oxygen ratio of 1:3, thermodynamic calculations (Fig. 1a-c) show that with increasing water content in the feed stream (from 3 to 15 mol per mol hexane) the fraction of hydrogen increased, while methane and carbon monoxide fractions decrease. With increasing temperature the carbon monoxide concentration increased from 500 °C to 800 °C, while the methane concentration followed the opposite trend. Interestingly, the hydrogen concentration passed through a maximum at 650 °C.

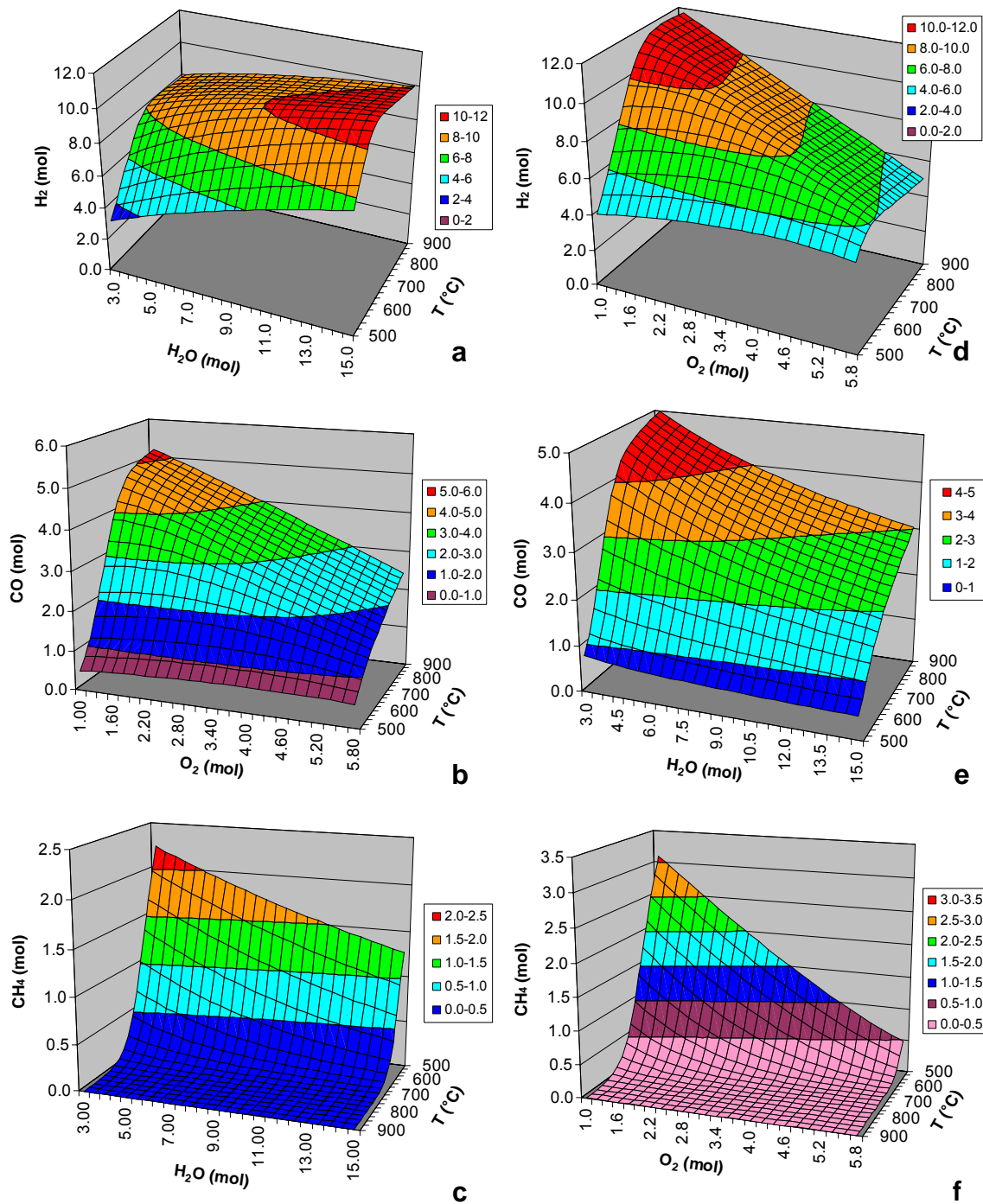


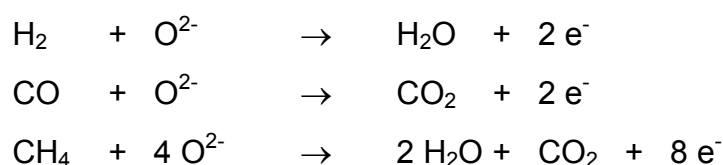
Figure 2.2: Thermodynamic equilibrium. On the left hand side: **a)** hydrogen, **b)** carbon monoxide and **c)** methane as function of temperature and water amount (1bar; 1mol C₆H₁₄; 3mol O₂). On the right hand side: **d)** hydrogen, **e)** carbon monoxide and **f)** methane as function of temperature and oxygen amount (1bar; 1mol C₆H₁₄; 7mol H₂O).

For a constant hexane/water ratio of 1:7, the increase of oxygen from one to six moles per mol hexane (Fig. 1d-f) led to higher concentrations of combustion

products and, therefore, to a lower concentration of the desired products (carbon monoxide, methane and hydrogen). With increasing temperature carbon monoxide fraction increased and methane fraction decreased, while the fraction of hydrogen formed passed through a maximum, which shifted to lower temperatures with higher oxygen concentrations.

Compared to POX (Figure 2.1c) and SR (Figure 2.1a), for ATR methane disappears from the equilibrium composition already at 700 °C (Figure 2.2c and 2.2f) instead that at 900 °C.

When a mixture $C_6H_{14}/O_2/H_2O$ undergoes to ATR, the distribution of the products and, among them, of H_2 , CO and CH_4 , changes depending on the temperature. This is exemplified in figure 2.3a for a feed containing $C_6H_{14}/O_2/H_2O$ with molar ratios 1/3/7. If the effluent from the autothermal reformer is fed to a SOFC, the following anodic reactions involving the three compounds above mentioned (H_2 , CO and CH_4) occur:



It is interesting to observe that the sum of redox-equivalents (from H_2 , CO and CH_4) is invariant with temperature. For example for the mixture $C_6H_{14}/O_2/H_2O$ 1/3/7 it is constant at 26 mol electrons per mol of hexane autothermal reformed (Fig. 2.3b). Additionally, the ratio C_6H_{14}/H_2O (Fig. 2.4a) does not affect the number of equivalents produced, while the number of redox-equivalents linearly decreases with increasing O_2/C_6H_{14} ratios (see Fig. 2.4b). These features are extremely important. First the power of the SOFC is not affected by the temperature of the ATR. Second it is possible to increase the SOFC power by changing the hydrocarbon/oxygen ratio.

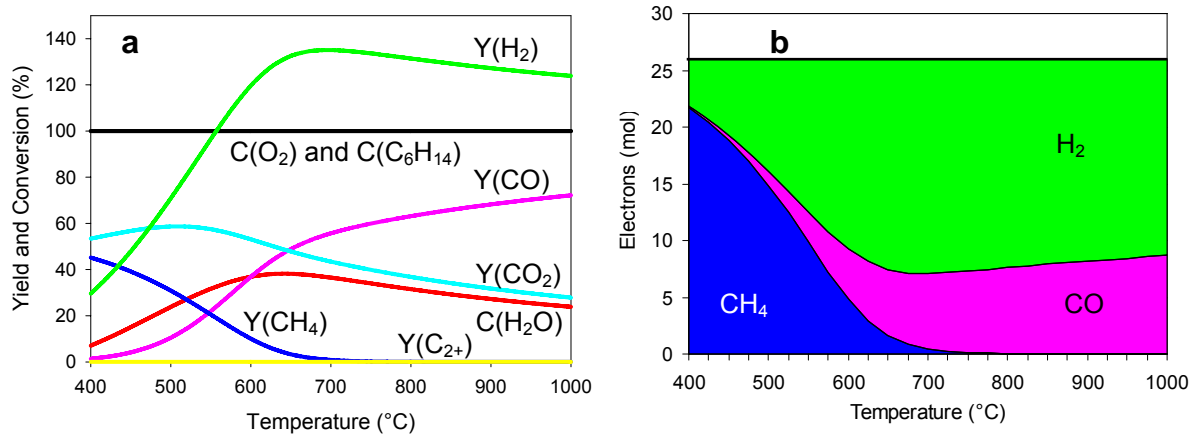


Figure 2.3: a) Conversion and yields for the thermodynamic equilibrium calculated for a feed $C_6H_{14} : O_2 : H_2O = 1 : 3 : 7$ vs. temperature ($P=1\text{bar}$) and b) sum and distribution of redox-equivalents (as mol) produced by the anodic reactions of CH_4 , CO and H_2 in a fuel cell vs. temperature of the ATR that produced these compounds ($P=1\text{bar}$).

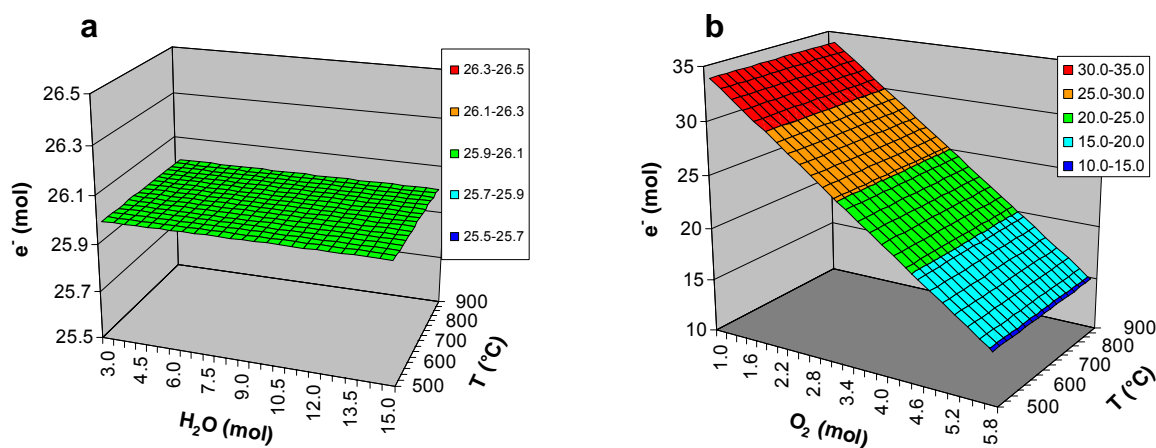
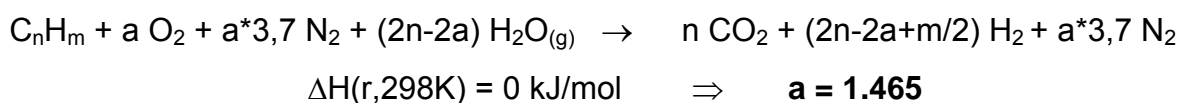


Figure 2.4: Distribution of redox-equivalents (as mol) at thermodynamic equilibrium as function of temperature and a) water amount (1bar; 1mol C_6H_{14} ; 3mol O_2) or b) oxygen amount (1bar; 1mol C_6H_{14} ; 7mol H_2O).

2.3.2 Thermo-neutrality of the autothermal reforming

The amount of oxygen to be fed in order to perform autothermal reforming of hexane thermoneutrally at standard conditions can be calculate from the reaction (2.16) by assuming $n=6$:



If water is present in the liquid phase instead than in the gaseous one, the value of a would change to **2.162**. For the ratio $C_6H_{14} : O_2 : H_2O = 1 : 3 : 7$ the reaction 2.16

becomes exothermic with a $\Delta H(r,298K)$ of -742.9 kJ/mol (considering only CO_2 and H_2 as products, and water in the gas phase).

In Figure 2.5 the thermodynamic composition for $a = 1.465$ and $a = 2.162$ is shown. The corresponding curves are just intersections of the surfaces of Figure 2.2. It has to be noted that the parameter “a” only affects the value of the yields not the relative distribution of the compounds.

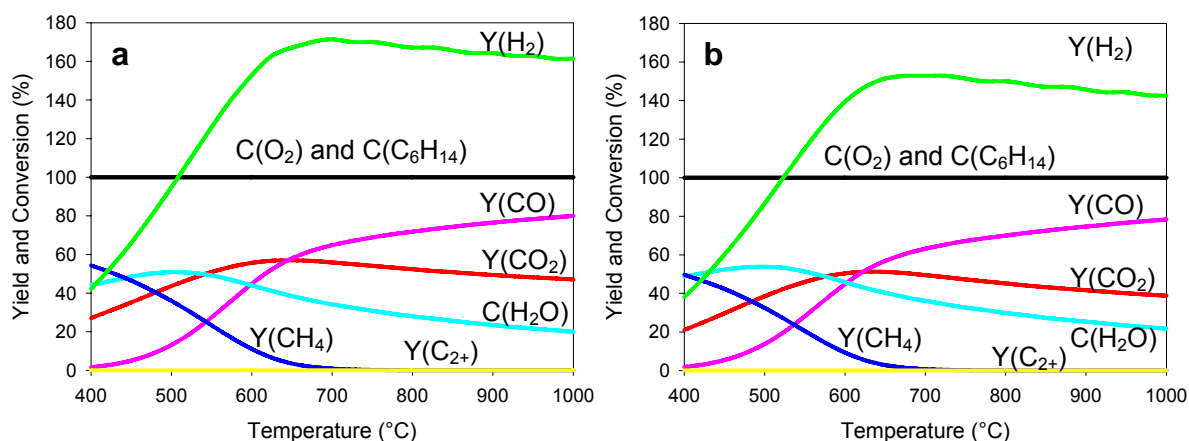


Figure 2.5: Conversion and yields for the thermodynamic equilibrium calculated for a) $\text{C}_6\text{H}_{14} : \text{O}_2 : \text{H}_2\text{O} = 1 : 1.465 : 9.07$ ratio and b) $\text{C}_6\text{H}_{14} : \text{O}_2 : \text{H}_2\text{O} = 1 : 2.162 : 7.676$ ratio vs. temperature ($P=1$ bar).

Other important parameters have to be considered for an autothermal regime of the reformer, i.e. the preheating of the fed air, water and fuel, the chemical composition of the fuel, the heat dispersion from the system and the pressure inside the reactor.

2.4 Mechanistic Aspects

In this section mechanistic aspects of partial oxidation and steam reforming are reviewed. As most research was performed with methane as hydrocarbon fuel it will capture the major part.

2.4.1 Partial Oxidation

Partial oxidation of hydrocarbons is normally catalyzed by metal (Pt, Pd, Rh, Ru) supported on oxides (mainly Al_2O_3). Oxygen adsorbs dissociatively on metal sites (reaction 2.17). The adsorption of the hydrocarbon on the metal is a sequence of C-H cleavages which produces atomic hydrogen and hydrocarbon fragments^{10, 11} (see reactions 2.18-2.22 for methane). Finally molecular hydrogen desorbs (reaction 2.35). The initial dissociative chemisorption step of methane (equation 2.19) is generally considered to be the rate determining step (e.g. Wu¹² *et al.*). Further dissociation steps to CH_2 , CH and C are significantly faster.

The presence of oxygen adsorbed on the metal sites is reported to enhance the chemisorption rate of methane^{13, 14}. The main role of oxygen seems to be the formation of hydroxyl groups by interaction with adsorbed hydrogen atoms (reaction 2.23). Additionally, adsorbed oxygen species allow the formation of adsorbed CO as described in reaction 2.24 (oxidation of carbon^{15, 16}) or in reactions 2.29-2.31 and 2.33-2.34. CO can be also formed *via* reduction of adsorbed CO_2 with hydrogen (equilibration of the water-gas shift).

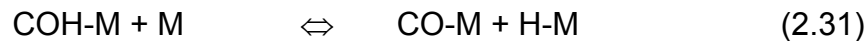
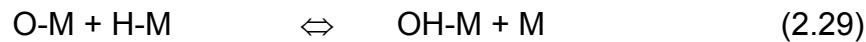
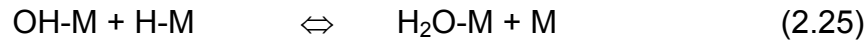
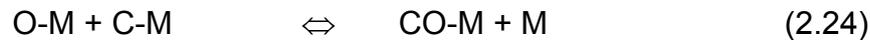
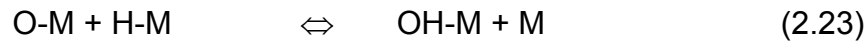
Wang *et al.*¹¹ proposed that the reaction (2.28) of adsorbed CO with adsorbed hydroxyl group to form CO_2 is only important if the concentration of the latter is high or when there is a considerable amount of water on the support (inverse spill over see section 2.4.3).

Reactions on metal site (M):

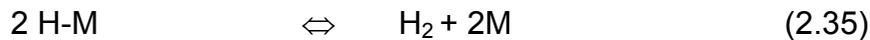
i) adsorption steps and dissociation of methane:



ii) surface reactions:



iii) desorption steps:



Reaction conditions strongly affect the product distribution. Thus, if the ratio C/O is high (low concentration of adsorbed oxygen), the residence time short or the temperature high (fast desorption of oxygen fast), formation of CO and H₂ is favored and only small amounts of CO₂ and H₂O are produced.

It has been suggested that synthesis gas can be a primary or a secondary product of hydrocarbon partial oxidation. In the first case H₂ and CO are formed directly by partial oxidization of the hydrocarbon^{11, 7, 17}. In the latter case, first a fraction of the fed hydrocarbon is combusted to CO₂ and H₂O (primary products), then the hydrocarbon undergoes steam and CO₂-reforming with formation of CO and H₂ (secondary products)^{11, 18}. The prevailing of one of these pathways depends upon the reaction conditions and the catalytic system.

The measurements of Baerns *et al.*¹⁹ and Buyevskaya *et al.*²⁰ showed that CO₂ was formed as primary reaction product over supported noble metal catalysts (Ru, Pd, Pt and Rh supported on γ -alumina and Rh supported on magnesia or zirconia) while CO was suggested to result from the reaction of CO₂ with surface carbon deposits as secondary product. Their results support the idea that high concentrations of reactive adsorbed oxygen at steady state conditions are responsible for fast complete oxidation of surface hydrocarbon adsorbates on transition metal catalysts.

On Pt sponge catalysts the selectivity to H₂ and CO was lower than that observed for Rh supported sponge catalyst - independent of a support. This feature was correlated with the different nature of the oxygen species adsorbed on the two metals²¹.

Tulenin *et al.*²² showed that on Ni-containing catalyst the route of direct formation of syngas prevails at a C/O ratio of 1.875 and at high flow rates, while at low flow rates and temperatures above 700 °C total oxidation predominates.

Wu *et al.*¹² showed on a Rh/SiO₂ catalyst that CO and H₂ were formed through the reaction of surface CH_x with adsorbed oxygen, while CO₂ could be formed either from CO or CH_x (or other C-species) reacting with adsorbed oxygen.

Weng *et al.*²³ compared the performance in POX of methane of Rh and Ru supported on SiO₂ and γ -Al₂O₃. Direct oxidation of methane was identified to be the main pathway over pre-reduced Rh/SiO₂ with CO as primary product. CO₂ was formed through consecutive oxidation of surface CO. However, over Ru/ γ -Al₂O₃ and Ru/SiO₂ the primary product was CO₂ and CO was formed via steam reforming and CO₂-reforming of methane. The authors concluded that the different reaction mechanisms may result from the different concentration of oxygen adsorbed on Rh and Ru under reaction conditions. A higher concentration of metal oxide species (surface oxygen) in Ru/SiO₂ catalyst compared to Rh/SiO₂ was found by Yan *et al.*²⁴ by *in situ* Raman spectroscopy.

H₂O is dissociatively adsorbed on the Al surface sites of the support (γ -Al₂O₃) (see section 2.4.3). At high temperatures (450-750 °C) the hydroxyl surface groups migrate to the metal sites. The resulting hydroxyl on the metal together with dissociatively adsorbed O₂ oxidize adsorbed hydrocarbon species²⁵ forming CO (e.g.

on Rh). On ceria as support²⁶ for Pt catalyst, the authors observed bidentate type carbonate adsorbed on Ce^{n+} and carbon as intermediate, but no formaldehyde or methanol. CO was formed from the reaction of C with lattice oxygen of ceria. The Pt accelerated the recombination and desorption of H_2 , which was identified as rate determining step through a reverse spill over mechanism. In contrast, at temperatures higher than 600 °C, the activation of methane was found to be the rate determining step in the syngas production over yttria-stabilized zirconia (=YSZ)^{10, 27}. Besides syngas, CO_2 and H_2O traces of other hydrocarbons, formaldehyde and formic acid were detected, especially at high temperatures. As reaction intermediate adsorbed formate was identified. CO_2 was mainly formed by the decomposition of the formate, while CO and H_2 were formed by the decomposition of adsorbed formate and formaldehyde. The formation of formate was also observed on other oxides (TiO_2 , ZrO_2 and SiO_2)²⁸ and explained by the amphoteric character of these oxides with their acid and basic sites playing a synergetic role in the reaction pathway.

The reaction mechanisms for partial oxidation of light paraffins (ethane and propane) are in principle the same as for methane. It has been shown that over supported Pt catalysts syngas was produced directly by partial oxidation of ethane and propane²⁹, while over Rh supported catalysts syngas was formed both directly by partial oxidation and indirectly by steam reforming. For Pt the product distribution was strongly affected by the reaction temperature. Below 550 °C CO_2 and H_2O were formed, between 550 °C and 700 °C mainly CO and H_2 , and above 700 °C large amounts of gas phase olefinic products were observed. Secondary reforming reactions were negligible at short contact times. Rh exhibited high selectivity to syngas even for temperatures above 700 °C (no olefin formation). Even if homogeneous reactions took place, conversion of C_2 may still proceed on the catalyst surface through secondary reactions at sufficiently long contact time or sufficient catalyst load. Additional experiments performed by Beretta *et al.*²⁹ on supported Rh confirmed that after partial replacing of a paraffin by the corresponding olefin the catalytic partial oxidation of gas-phase products was faster. Thus Rh would convert both the feed gas and the gas phase products into CO and H_2 .

2.4.2 Steam Reforming

The mechanism of steam reforming is similar on several metals (Ni, Ru, Rh, Pd, Ir and Pt)^{30, 31}. Methane is dissociatively adsorbed on the metal site (see reaction steps 2.18 to 2.22 in POX mechanism), while H₂O can be adsorbed dissociatively on the metal site forming hydrogen and surface oxygen:



H₂O can also be adsorbed on an empty site on the support surface and then transferred to the metal site *via* inverse spill over (see section 2.4.3). Surface carbon, formed in the dissociation of methane, reacts at high temperatures with surface oxygen forming CO. Rostrup-Nielsen *et al.*³¹ showed that Ru and Rh exhibit highest selectivity for carbon-free operation followed by similar high selectivity of sulphur-passivated Ni catalyst. They ascribed this to high reforming rates and low carbon formation rates.

For methane steam reforming (under differential conditions) over Ru/ α -Al₂O₃ promoted with Mn³⁰, a reaction order <1 in methane was found in a temperature range of 450-500 °C, while it was close to 1 at temperatures between 700-900 °C. The reaction order in H₂O was negative for all temperatures. Praharso *et al.*³² found different reaction orders in the steam reforming of isooctane over Ni/ γ -Al₂O₃: 0.2 in *i*-C₈H₁₈ and 0.5 in H₂O (differential conditions, temperature between 310°C and 350°C), indicating a dissociative adsorption of steam. The authors³² considered a Langmuir-Hishelwood mechanism the most plausible pathway, which requires dissociative adsorption of both isooctane and H₂O on two different sites. The rate determining step involves a reaction between dissociatively adsorbed species of isooctane and H₂O. Besides CO, CO₂, H₂ and CH₄ occasionally acetylene was observed as product in the SR of isooctane. Investigations of the optimal steam to carbon ratios (= S/C) showed that reoxidation of Ni occurred at S/C ratios ≥ 7 and carbon was deposited at S/C ratios ≤ 3 .

2.4.3 Inverse spillover in steam reforming

The spillover of water from the support to the metal site, usually referred to as “inverse spillover”, is a step of the steam reforming mechanism. Water spilled over to the metal site (Rh) dissociates into adsorbed oxygen and hydroxyl group, which in turn are able to oxidize the adsorbed CH_x species. Wang *et al.*¹¹ showed with pulse experiments that water adsorbed on alumina acts as a reactant in methane steam reforming. Inverse spillover of H₂O was also suggested by Rostrup-Nielsen² to explain the differences in the steam reforming rates observed on catalysts with different supports. This does not imply that H₂O adsorbed on the metal results exclusively from inverse spillover from the support. Besides inverse spillover, Rostrup-Nielsen reported a desorption–readsorption mechanism of water directly on the metal.

The mechanism of H₂O adsorption on the metal depends upon that of adsorption/desorption of H₂O on the support. H₂O adsorbed on metal mainly comes from inverse spillover when the partial pressure of H₂O in the bulk gas phase is low or at a temperature where the desorption from support is low.

Wang *et al.*¹¹ observed the water partial pressure in the gas phase does not significantly change with the water loading. This indicates that an inverse spillover mechanism from the support to the metal is operative, rather than desorption–readsorption. The temperature range for inverse spillover process from alumina was found to be 450–750 °C^{11, 33}. As at higher temperatures a rapid loss of water from the support (Al₂O₃) occurs. It is likely that inverse spill over becomes more important when the support is highly hydrated. It may be assumed that water dissociatively adsorbs forming acidic and basic hydroxyl groups. By recombination of these groups a mobile H₂O adsorbed species is formed, which can spillover the metal. The following equilibria were suggested for the inverse spillover from support (Al₂O₃ = S) to metal (e.g. Rh = M):

Dissociative adsorption H₂O on support:



Non-dissociative adsorption H₂O on support:

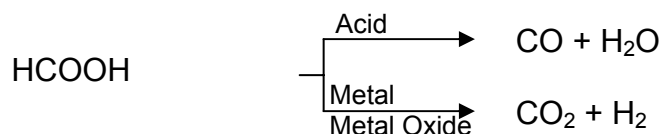


Spillover from support to metal:



2.4.4 Mechanism of WGS reaction

Several reaction schemes were reported in the literature for the water–gas shift reaction. Grenoble *et al.*³⁴ proposed a mechanism consisting of a spillover of CO from the metal to the support (Al₂O₃), forming formic acid (HCOOH) on the support. The formic acid in principle can decompose on acid sites to CO and H₂O or migrating to the metal (or metal oxide) site decomposing to CO₂ and H₂:



These bifunctional features are used to explain the differences in the rate of the WGS-reaction on catalysts with different supports. The existence of formate on Al₂O₃ was reported also by Amenomiya *et al.*³⁵. It was suggested that the mechanism including formate species is depending on temperature. Below 300 °C the above mentioned mechanism occurs. At higher temperatures a different mechanism on the metal site is likely as the CO-desorption from the metal and the dissociation of formate on the support are fast. For the temperature range covered in the POX (of CH₄) the proposed steps^{11, 36, 37, 38} in the overall WGS-reaction are the oxygen transfer from CO₂ or H₂O to the catalyst and from that to H₂ or CO. Over Rh/Al₂O₃¹¹ the reaction pathway was similar, but includes an inverse spillover step attributing an active role to the support (see section 2.4.3).

2.5 References

- (1) Stobbe, E. R. Catalytic routes for the conversion of methane to synthesis gas. PhD-Thesis, University of Utrecht, 1999.
- (2) Rostrup-Nielsen, J. R. Catalytic steam reforming. In *Catalysis Science and Technology*; Anderson, J., Boudart, M., Eds.; Springer, 1984.
- (3) Docter, A.; Lamm, A. *Journal of Power Sources* **1999**, *84*, 194.
- (4) Ayabe, S.; Omoto, H.; Utaka, T.; Kikuchi, R.; Sasaki, K.; Teraoka, Y.; Eguchi, K. *Applied Catalysis A-General* **2003**, *241*, 261.
- (5) Ma, L.; Trimm, D. L. *Applied Catalysis A-General*. **1996**, *138*, 265.
- (6) Bharadwaj, S. S.; Schmidt, L. D. *Fuel Processing Technology* **1995**, *42*, 109.
- (7) Hickman, D. A.; Schmidt, L. D. *AIChE J* **1993**, *39*, 1164.
- (8) Ahmed, S.; Krumpelt, M. *International Journal of Hydrogen Energy* **2001**, *26*, 291.
- (9) Lamm, A. "PEM-BZ-Systeme für den mobilen Einsatz," Forschung und Technologie 1, Forschungszentrum Ulm, 2003.
- (10) Steghuis, A. G. Catalyzed partial oxidation of methane to synthesis gas. PhD-Thesis, University of Twente, 1998.
- (11) Wang, D.; Dewaele, O.; Groote, A. M. D.; Froment, G. F. *Journal of Catalysis* **1996**, *159*, 418.
- (12) Wu, T.; Yan, Q. G.; Mao, F.; Niu, Z.; Zhang, Q.; Li, Z.; Wan, H. L. *Catalysis Today* **2004**, *93-95*, 121.
- (13) Baerns, M.; Buyevskaya, O. V.; Mlezcko, L.; Wolf, D. *Studies in Surface Science Catalysis* **1997**, *107*, 421.
- (14) Buyevskaya, O. V.; Walter, K.; Wolf, D.; Baerns, M. *Catalysis Letters* **1996**, *38*, 81.
- (15) Garcia, L.; French, R.; Czernik, S.; Chornet, E. *Applied Catalysis A-General* **2000**, *201*, 225.
- (16) Ross, J. R. H.; Steel, M. C. F.; Zeini-Isfahani, A. *Journal of Catalysis* **1978**, *52*, 280.
- (17) Huff, M.; Schmidt, L. D. *Journal of Physical Chemistry* **1993**, *97*, 815.
- (18) Dissanayake, D.; Rosynek, M. P.; Kharas, K. C. C.; Lunsford, J. H. *Journal of Catalysis* **1991**, *132*, 117.
- (19) Baerns, M.; Buyevskaya, O. *Catalysis Today* **1998**, *45*, 13.
- (20) Buyevskaya, O.; Wolf, D.; Baerns, M. *Catalysis Letters* **1994**, *29*, 249.
- (21) Mallens, E. P. J.; Hoebink, J. H. B. J.; Marin, G. B. *Journal of Catalysis* **1997**, *167*, 43.
- (22) Tulenin, Y. P.; Sinev, M. Y.; Savkin, V. V.; Korchak, V. N. *Catalysis Today* **2004**, *91-92*, 155.
- (23) Weng, W. Z.; Chena, M. S.; Yan, Q. G.; Wu, T. H.; Chaoa, Z. S.; Liao, Y. Y.; Wan, H. L. *Catalysis Today* **2000**, *63*, 317.
- (24) Yan, Q. G.; Wu, T. H.; Weng, W. Z.; Toghiani, H.; Toghiani, R. K.; Wan, H. L.; Pittman Jr., C. U. *Journal of Catalysis* **2004**, *226*, 247.
- (25) Wang, H. Y.; Ruckenstein, E. *Applied Catalysis A-General* **2000**, *204*, 143.
- (26) Otsuka, K.; Wang, Y.; Sunada, E.; Yamanaka, I. *Journal of Catalysis* **1998**, *175*, 152.
- (27) Zhu, J.; van Ommen, J. G.; Lefferts, L. *Journal of Catalysis* **2004**, *225*, 388.

- (28) Frusteri, F.; Arena, F.; Martra, G.; Coluccia, S.; Mezzapica, A.; Parmaliana, A. *Catalysis Today* **2001**, *64*, 97.
- (29) Beretta, A.; Forzatti, P. *Chemical Engineering Journal* **2004**, *99*, 219.
- (30) Berman, A.; Karn, R. K.; Epstein, M. *Applied Catalysis A-General* **2005**, *282*, 73.
- (31) Rostrup-Nielsen, J. R.; Bak Hansen, J. H. *Journal of Catalysis* **1993**, *144*, 38.
- (32) Praherso; Adesina, A. A.; Trimm, D. L.; Cant, N. W. *Chemical Engineering Journal* **2004**, *99*, 131.
- (33) Peri, J. B. *Journal of Physical Chemistry* **1965**, *69*, 211.
- (34) Grenoble, D. C.; Estadt, M. M.; Ollis, D. F. *Journal of Catalysis* **1981**, *67*, 90.
- (35) Amenomiya, Y.; Pleizier, G. *Journal of Catalysis* **1982**, *76*, 345.
- (36) Rhodes, C.; Hutchings, G. J.; Ward, A. M. *Catalysis Today* **1995**, *23*, 43.
- (37) Rofer-DePoorter, C. K. *Catalytic Conversions of Synthesis Gas and Alcohols to Chemicals*; Plenum: New York, 1984.
- (38) Lloyd, L.; Ridler, D. E.; Twigg, M. V. *Catalyst Handbook*, 2nd ed.; Wolfe: London, 1989.

Autothermal Reforming of Hexane over Ni, Pt and Rh Supported Metal Catalysts

Abstract

The activity of supported metal catalysts in the autothermal reforming of n-hexane in a fixed bed is presented. Reducible oxides, such as CeO₂, ZrO₂ and YSZ (yttrium-stabilized zirconia), as well as γ -Al₂O₃ were used as supports. Each oxide was impregnated with 1 wt% of Ni, Pt or Rh. Without metals the supports showed very low activity. Independently of the support, the activity of the catalysts increased following the sequence Ni < Pt < Rh. For Rh the sequence of activity was Rh/Al₂O₃ > Rh/ZrO₂, Rh/YSZ > Rh/CeO₂, with approaching thermodynamic equilibrium around 800°C. Hence, Rh supported on alumina seems to be the most promising catalyst for autothermal reforming of n-hexane.

3.1 Introduction

Hydrogen has been attracting great interest as a future clean fuel for combustion engines and fuel cells ^{1, 2}, the latter being developed for transportation, as well as for stationary and portable power generators. An efficient and compact process for hydrogen production has to be developed for such applications. Production of hydrogen based on water electrolysis with electricity originating from solar cells or hydropower has been regarded as the most clean and desirable method. However, these processes do not supply sufficient hydrogen at present stage. Other CO₂ neutral pathways to hydrogen are reforming of biofuels or other renewable carbon sources. On a route to such an ideal situation, intermediate solutions have to be explored that help to facilitate the transition to a hydrogen economy.

Decentralized or on board Reforming of liquid fuels combines in such a scenario the advantage of an easily adaptable fuel infrastructure and ease of refueling. Methanol, gasoline, and diesel are considered as liquid fuel sources for on-board hydrogen production ^{3, 4, 5, 6}. Methanol is easily stored and converted to hydrogen, although currently a methanol infrastructure is lacking. Thus, only gasoline or diesel fuels (hydrocarbons and/or oxygenate blends) offer the advantage of an existing infrastructure for distribution.

For the conversion of the primary fuel into a hydrogen-rich gas, three processes exist, *i.e.*, partial oxidation (POX), steam reforming (SR) or autothermal reforming (ATR) ⁴. Partial oxidation (POX) is an exothermic reaction ($\Delta H^\circ = -491.6$ kJ/mol for hexane), whereas steam reforming is endothermic ($\Delta H^\circ = +954.9$ kJ/mol for hexane). As partial oxidation in its essence is a combination of partial combustion and subsequent steam- and CO₂-reforming, it could be used on starting the engines by ignition, if necessary without the aid of a catalyst. However, the overall conversion efficiency is lowered if the released heat cannot be used in a way fully integrated into the fuel cell system. The overall efficiency can be improved by combining within one reactor endothermic steam reforming with exothermic partial oxidation. The resulting process is called autothermal reforming. Exothermic, endothermic and thermo-neutral conditions can be selected by choosing an appropriate ratio of hydrocarbons : oxygen : steam ^{2, 7, 8}.

Because of the high economic impact with respect to reforming at a large scale, investigations of catalytic processes has been focused mainly on steam reforming^{9, 10, 11, 12, 13} for a wide range of hydrocarbons. The, practically, more challenging processes of catalytic partial oxidation and autothermal reforming have been less broadly explored in the open literature and, when, within the published literature shows a strong focus on methane and light hydrocarbons. The literature addresses in most cases large scale applications.

Thus, especially for larger alkanes in fuels for automotive applications (e.g., diesel, aromatics) more information is needed for efficient hydrogen production on a small scale. The goal of the present study is to compare the performance of various supported metal catalyst based on three metals, i.e., Ni, Pt and Rh in autothermal reforming of hexane, as a model compound with the target of using the reformat as fuel for a solid oxide fuel cell (SOFC).

3.2 Experimental

3.2.1 Catalyst Preparation

Me/CeO₂

Ceria powder was prepared from 1M aqueous Ce(NO₃)₃-solution (*Sigma-Aldrich*) by addition of ammonium hydroxide (32%, extra pure, *Merck*). The obtained precipitate was filtrated, washed with bi-distilled water and dried at room temperature. The solid was calcined in flowing air, first at 500°C for 2h (heating rate 2 K·min⁻¹) and then at 900°C for 4h (heating rate 5 K·min⁻¹).

Subsequently, the metal (1 wt%) was deposited by wet impregnation using 1M Ni(NO₃)₂ (p.a., *Merck*), 0.155M Rh(NO₃)₃ (*Alfa Aesar*) and 0.144M H₂PtCl₆ (99%, *Stem Chemicals*) in addition with water. The slurries were dried over night at 70°C. Finally, the materials were calcined at 900°C for 4h (heating rate 5 K·min⁻¹).

Me/ZrO₂

Zirconia powder was prepared from an aqueous solution of ZrO(NO₃)₂ (*Fluka*) by addition of ammonium hydroxide (32%, extra pure, *Merck*). The final pH was 10. The obtained precipitate was filtrated, washed with bi-distilled water and dried at room temperature. It was calcined first at 500°C for 2h (heating rate 2 K min⁻¹) in flowing air and then at 900°C for 4h (heating rate 5 K min⁻¹).

Subsequently, the metal (1 wt%) was deposited by wet impregnation using 1M Ni(NO₃)₂, 0.155M Rh(NO₃)₃ or 0.144M H₂PtCl₆ in addition with water. The slurries were dried over night at 70°C. Finally, the materials were calcined at 900°C for 4h (heating rate 5 K min⁻¹).

Me/YSZ

Yttrium-stabilized zirconia particles (112-224 μm) were prepared by calcination up to 850°C (heating rate 3 K min⁻¹) of a commercial sample of mixed yttrium and zirconium hydroxides (8 mol% yttria, *Mel Chemicals*, XZ01012/01, 5020737, Batch No. 97/013).

Subsequently, the metal (1 wt%) was deposited by wet impregnation using 1M Ni(NO₃)₂, 0.155M Rh(NO₃)₃ or 0.144M H₂PtCl₆-solution. The slurries were freeze dried and the remainders calcined at 650°C for 15h (heating rate 3 K min⁻¹).

Me/ γ -Al₂O₃

Alumina particles (112-224 μm) were prepared by calcination up to 850°C (heating rate 3 K min⁻¹) of a commercial sample of aluminum hydroxide (Sasol Puralox SBa 200, Lot B9952).

Subsequently, the metal (1 wt%) was added by wet impregnation using a 1M Ni(NO₃)₂, 0.155M Rh(NO₃)₃ or 0.144M H₂PtCl₆-solution. The slurries were freeze dried and the remainders calcined at 900°C for 4h (heating rate 3 K min⁻¹).

Standard operations before utilization

All catalyst powders were isostatically pressed with 4 t·cm⁻² for 5 minutes, ground and sieved. The fraction 112-224 μm was used for catalytic tests and characterization.

3.2.2 Chemical and physical-chemical Characterization***Powder X-ray diffraction (XRD)***

Powder X-ray diffraction patterns were collected on a *Philips X'Pert-1* System diffractometer using Cu-K α radiation ($\lambda = 1.54186 \text{ \AA}$) to estimate the crystallinity and the structural changes of the synthesized materials. Data were collected in the 2θ range from 10 to 80° with a step size of 0.034° and a scan time per step of 20.32 s.

Atomic adsorption spectroscopy (AAS)

The metal content of the samples was determined by atomic absorption spectroscopy (AAS) using a *UNICAM 939 AA*-Spectrometer. All metal contents were determined to be 1 wt% \pm 0.05 wt%.

Specific surface area (BET)

Nitrogen adsorption measurements were performed at 77.4 K either with a *PMI Automated BET sorptometer 5.32* or with a *POROTEC Sorptomatic 1990*. The samples were outgassed at 400°C for 2 h prior to the adsorption measurements. The specific surface areas were calculated using the BET method.

Transmission electron microscopy (TEM)

For transmission electron microscopy (TEM) the samples were suspended in isopropanol and transferred to a carbon-coated copper grid. After drying in air overnight, the sample was placed inside the microscope (*JEOL 2010*, operated at 200 kV, LaB₆ electron source) equipped with a 1024-1024 pixel cooled slow-scan CCD-camera (*TVIPS*, Germany).

3.2.3 Catalytic Activity

The catalytic performance in autothermal reforming was determined at atmospheric pressure in a quartz tubular flow reactor with 4 mm internal diameter. A fixed bed consisting of 20 mg of catalyst particles (112-224 μm) diluted with 300 mg of SiC was placed in the isothermal zone of the oven and kept in place by quartz wool. The temperature at the top of the catalyst bed was measured with a thermocouple. The reactor is schematically depicted in the inset of Figure 3.1.

The hexane flow was regulated either by flowing Ar through an evaporator or by dosing hexane (and water) with an HPLC pump into the heated capillary lines ($T = 190^\circ\text{C}$) made in quartz.

Prior to the measurements the catalyst was reduced *in situ* with hydrogen at 800°C for 2 h.

The feed for autothermal reforming was a 200 ml/min mixture $\text{C}_6\text{H}_{14} : \text{O}_2 : \text{H}_2\text{O} : \text{Ar} = 1 : 3 : 7 : 29$ (equivalent to $\lambda = 0.32$ and S/C ratio of 1.17). This flow corresponds to a space velocity of 68000 h^{-1} calculated on the basis of the total volume of diluted catalyst bed. Fluid dynamics calculations (done with the software FEMLAB 3.0) showed that in the lines laminar flow existed, but that at the top of the catalytic bed the flow became turbulent and equivalent to plug flow conditions through the catalytic bed.

The reaction temperature was increased from 500 to 850°C in steps of 50°C , maintaining each reaction temperature for 1 h. After reaching 850°C , the temperature was decreased to 500°C , always in 50°C steps, in order to study the possible catalyst deactivation.

The reactor educts were analyzed with a Agilent 6890 Series gas chromatograph equipped with a Molecular Sieve 5A column and with a HP-Plot U

column (both columns: 30 m length and 0.53 mm inner diameter). Using argon as carrier gas, H₂ was detected besides O₂ and H₂O with a TCD. Hydrocarbons, CO and CO₂ (running through a methanizer) were detected with both TCD and FID, with the FID showing higher sensitivity. For some measurements a Balzers QMG 420 mass spectrometer was used as an additional analysis device (see Figure 3.1).

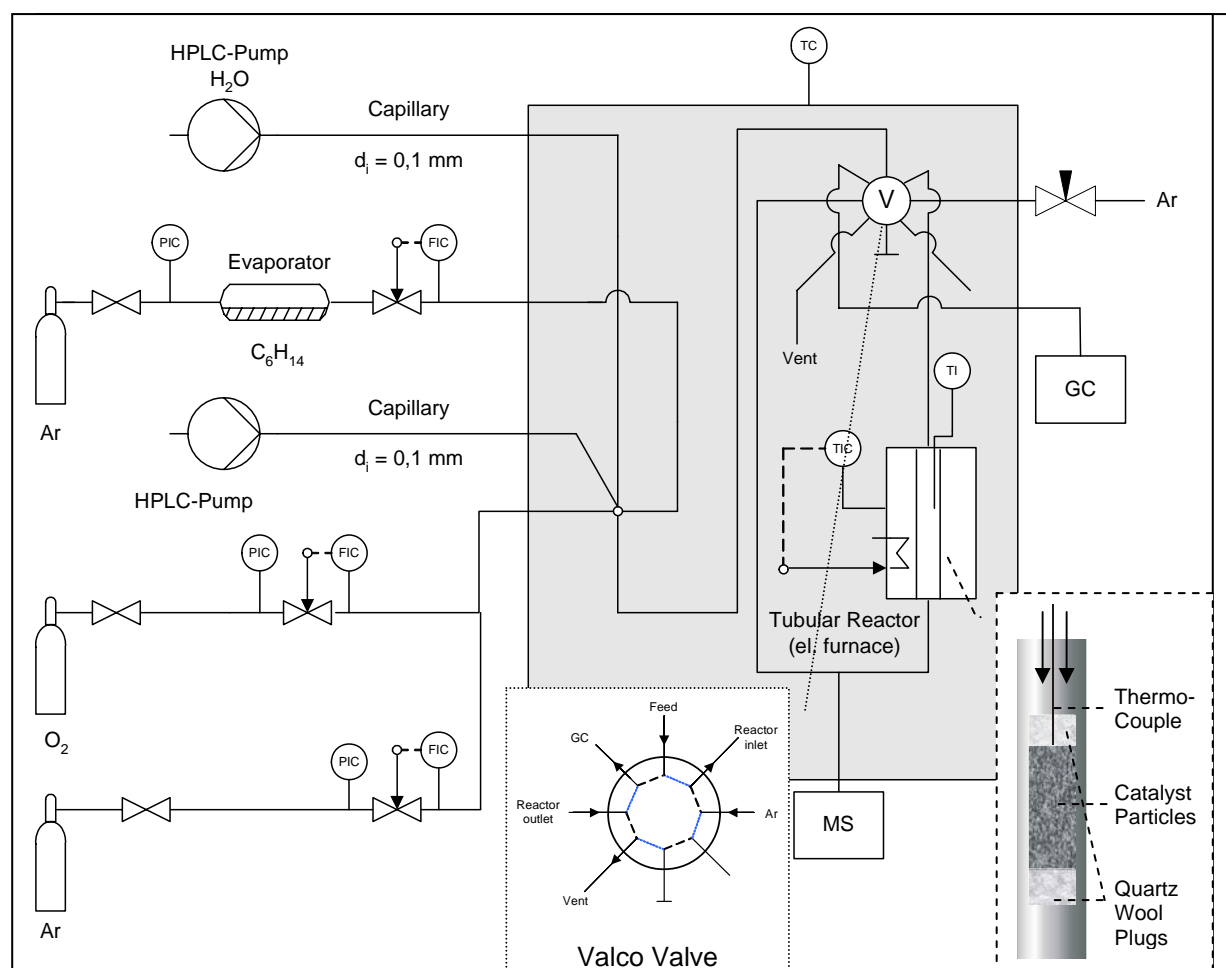


Figure 3.1: Scheme of the setup for catalyst testing.

Based on GC analysis data, the conversions and yields were calculated according to the following expressions:

$$X_{C_6H_{14}} = \left(1 - \frac{C_6H_{14}^{out}}{C_6H_{14}^{in}}\right) * 100 \quad X_{O_2} = \left(1 - \frac{O_2^{out}}{O_2^{in}}\right) * 100 \quad X_{H_2O} = \left(1 - \frac{H_2O^{out}}{H_2O^{in}}\right) * 100$$

$$Y_{\text{CH}_4} = \left(\frac{\text{CH}_4^{\text{out}}}{6\text{C}_6\text{H}_{14}^{\text{in}}} \right) * 100 \quad Y_{\text{H}_2} = \left(\frac{\text{H}_2^{\text{out}}}{7\text{C}_6\text{H}_{14}^{\text{in}}} \right) * 100 \quad Y_{\text{CO}_2} = \left(\frac{\text{CO}_2^{\text{out}}}{6\text{C}_6\text{H}_{14}^{\text{in}}} \right) * 100$$

$$Y_{\text{CO}} = \left(\frac{\text{CO}^{\text{out}}}{6\text{C}_6\text{H}_{14}^{\text{in}}} \right) * 100 \quad Y_{\text{C}_x\text{H}_y} = \left(\frac{\text{C}_x\text{H}_y^{\text{out}}}{\frac{6}{x}\text{C}_6\text{H}_{14}^{\text{in}}} \right) * 100$$

It should be noted that using these expressions the yield of hydrogen can exceed 100% because feed H_2O , besides C_6H_{14} , can be a source of hydrogen.

3.3 Results

3.3.1 Characterization

In Table 3.1 noble metal content, specific surface area and metal particle size of the different catalysts are compiled. The metal content of each material was 1 wt%.

Table 3.1: BET surface area and metal particle size of the fresh materials studied in autothermal reforming of hexane.

Material	BET Surface Area (m² g⁻¹)	Metal particle size (nm)
CeO ₂ (900°C) ^a	5.2	-
Ni/CeO ₂	4.3	3.0
Pt/CeO ₂	5.6	5.4
Rh/CeO ₂	29.4	2.0
ZrO ₂ (900°C) ^a	10.5	-
Ni/ZrO ₂	9.7	3.3
Pt/ZrO ₂	9.0	<1.0
Rh/ZrO ₂	9.1	5.3
YSZ (850°C) ^a	13.6	-
Ni/YSZ	6.5	1.9
Pt/YSZ	5.9	1.4
Rh/YSZ	11.2	<1.0
γ-Al ₂ O ₃ (850°C) ^a	137.2	-
Ni/γ-Al ₂ O ₃	129.9	4.5
Pt/γ-Al ₂ O ₃	123.2	<1.0
Rh/γ-Al ₂ O ₃	137.8	3.2

^a Calcination temperature

XRD

XRD pattern of the catalysts not reduced are shown in Fig. 3.2 and 3.3. For the noble metals supported on ceria, zirconia (monoclinic phase) and yttrium-stabilized zirconia (tetragonal phase) only the XRD features of the supports were observed. For γ -alumina supported metal catalysts, only in presence of platinum peaks characteristic of the noble metal (at 2θ 40°, 46.3° and 67.8°) were observed besides the reflections of the support. The absence of peaks corresponding to crystalline phases of the metals for all the other catalysts indicates that metal particles with very small size were formed.

The crystallinity of the supports was increased by higher calcination temperatures.

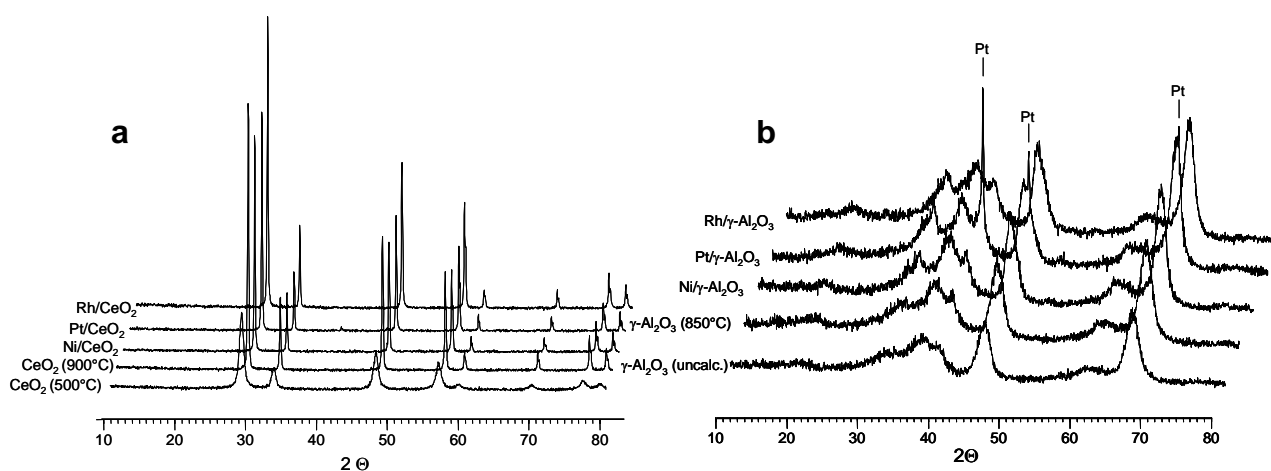


Figure 3.2: XRD pattern of noble metals supported on **a)** ceria or **b)** alumina before reduction.

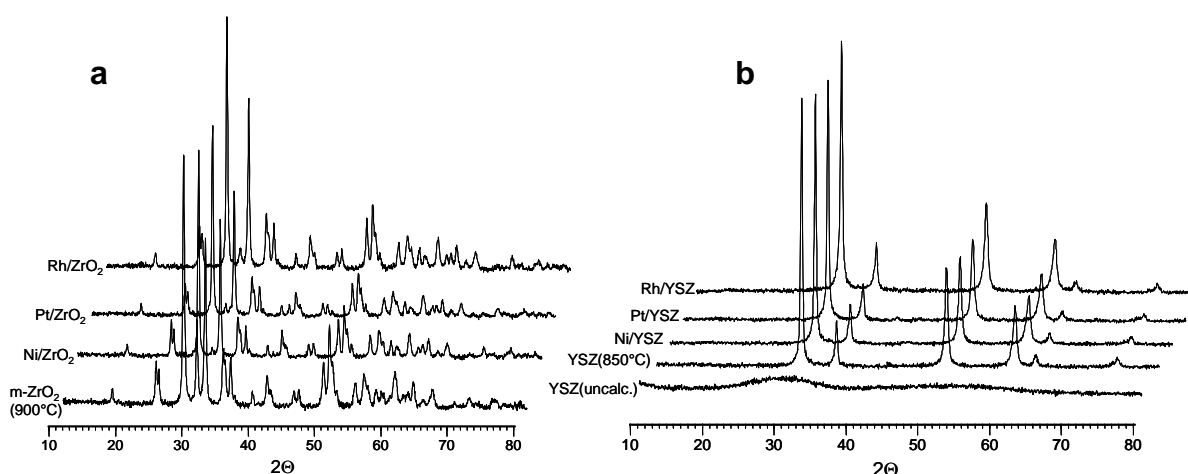


Figure 3.3: XRD pattern of noble metals supported on **a)** monoclinic zirconia or **b)** yttrium-stabilized zirconia before reduction.

3.3.2 Catalytic Activity

3.3.2.1 *Comparison of different metals supported on alumina*

Rhodium on alumina had a higher activity for converting hexane, oxygen and water into synthesis gas (Figures 3.4 a-h) compared to all other supported catalysts. At 500°C and a space velocity of 68,000 h⁻¹ 60% of hexane and 10% of H₂O were converted with full oxygen consumption producing yields of 60% H₂, 35% CO and 30% CO₂. At 700°C the conversions of hexane (100%), oxygen (100%) and water (48%) were close to the thermodynamic equilibrium with yields of 140% H₂, 59% CO and 41% CO₂. The yield of CH₄ decreased from 2% at 500°C to 1% at 700°C. CH₄ was the only hydrocarbon observed with Rh/Al₂O₃.

Ni and Pt showed a markedly different behavior with respect to converting hexane, water and oxygen at temperatures below 650°C. The conversion of hexane to CO₂ and H₂O was 20% at 500°C over Pt/Al₂O₃, while hexane was not converted below 600°C over Ni/Al₂O₃, although 10% of oxygen was consumed. Above 650°C conversion of hexane and the product distribution (H₂, CO, CO₂, CH₄ and C₂₊) was similar for Ni and Pt. Complete conversion of hexane was achieved at 800°C for both metals. The yield of CO increased almost linearly with temperature to 70% at 800°C, while the yield of H₂ increased first slowly up to 20% at 770°C and then steeply to approximately 70% at 800°C. The yield of CH₄ increased to 13% with increasing temperature. The yield of CO₂ (10%) did not change between 650°C and 800°C over Ni, while for Pt it passed through a minimum of 7% at 770°C. For both Ni and Pt the yield to cracking products (C₂₊, mainly ethylene) showed a trend with a common maximum (30%) at approximately 790°C.

Alumina did not convert hexane below 600°C. At 620°C the conversion of hexane and oxygen to CO, CO₂, CH₄ and cracking products started. With further temperature increase conversion and yields of all products increased. Full conversion was reached above 800°C with H₂, CO and CH₄ yields of 80%, 65% and 10%, respectively. In the whole temperature range water was one of the products (negative water conversion).

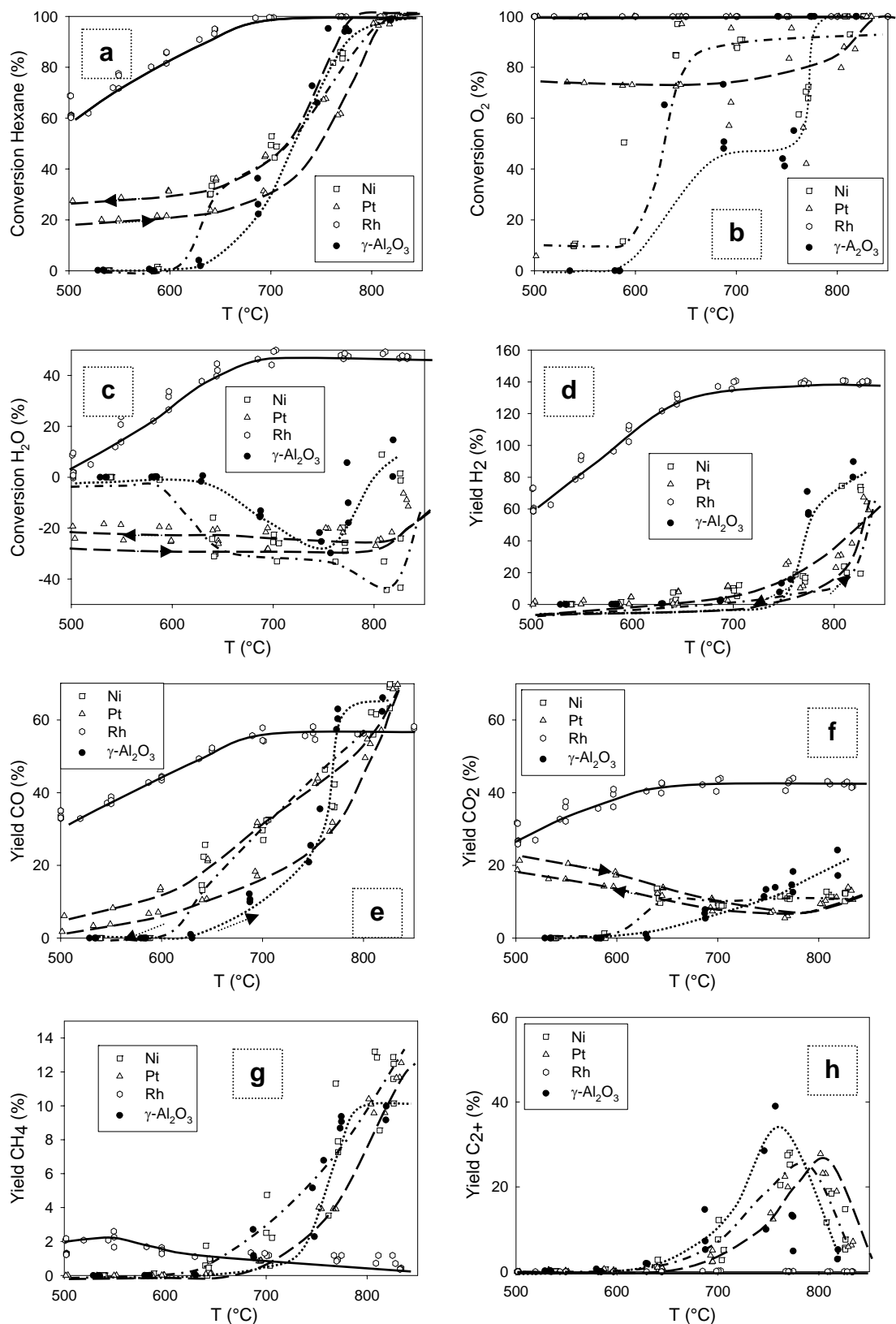


Figure 3.4: Conversion of a) hexane, b) oxygen, c) water and yields of d) hydrogen, e) carbon monoxide, f) carbon dioxide, g) methane and h) C_{2+} over alumina and metals supported on alumina.

During the catalytic test, the reaction temperature was increased from 500 to 850°C in steps of 50°C (“heating sequence”). After reaching 850°C, the temperature was decreased to 500°C, always in 50°C steps (“cooling sequence”). Each temperature was maintained for 1h. When Pt was supported on γ -Al₂O₃, a lower yield for CO and a higher yield for CO₂ were observed during the heating than during the cooling sequence. Additionally, a lower conversion of water was observed during the heating sequence than during the cooling sequence associated with lower H₂ yield.

3.3.2.2 Comparison of different metals supported on yttrium-stabilized zirconia

As for alumina-supported metal catalysts, also with yttrium-stabilized zirconia (YSZ) as support Rh was more active than Ni and Pt at low temperatures (Figures 3.5 a-h). Conversion of hexane increased with increasing temperature from 45% at 500°C up to full conversion at 780°C. Oxygen consumption was complete over the whole temperature range. With increasing hexane conversion, CO and H₂ production increased from 16% and 40% at 500°C to 58% and 130% at 830°C, respectively. The yield of CO₂ increased slightly from 30% at 500°C to 38% at 800°C. Simultaneously the conversion of water increased from -5% to 40%. Above 650°C CH₄ started to be produced increasing to around 5% at 830°C.

Over Pt/YSZ the conversion of hexane was stable at 40% until 600°C, increasing then to full conversion at 720°C. The oxygen conversion was complete over the whole temperature range. Water was one of the products. Its “yield” remaining negative and constant at about -30% between 500°C and 780°C, then it only slightly decreased above 780°C. The yield of H₂ was stable at 20% between 500°C and 650°C, afterwards it steeply increased over 140% for higher temperatures. CO and CH₄ yields increased exponentially with temperature to a level of 65% and 8% at 760°C, respectively. The formation of CH₄ started at 610°C. The yield of CO₂ linearly decreased with increasing temperatures. Cracking products, mainly ethylene, were observed between 610°C and 800°C, with a maximum at 700°C.

At 500°C less than 5% of hexane was converted over Ni/YSZ. The conversion of hexane increased with temperature to full conversion at 700°C. The product distribution⁹ CO₂, and cracking products (mainly ethylene) followed the same trend

observed for Pt. Interestingly, the consumption of oxygen was stable at 93% from 500°C to 800°C, when full consumption was attained.

On the support material itself (YSZ) hexane was converted at 620°C into its cracking products (displayed as C₂₊). When conversion of oxygen set in at 690°C, CO, CO₂ and H₂O as well as CH₄ were produced beside the cracking products, all increasing with increasing temperatures. Hydrogen was first observed in small amount (<5%) at 750°C, lifting off at temperatures higher than 820°C (30%). At this temperature the yield of cracking products decreased.

In the case of Pt/YSZ a hysteresis between heating and cooling sequence was observed. Unlike γ -Al₂O₃, only the yields of CO and CO₂ alter with heating or cooling sequences, the yield of CO₂ being higher during heating up (lower CO yield).

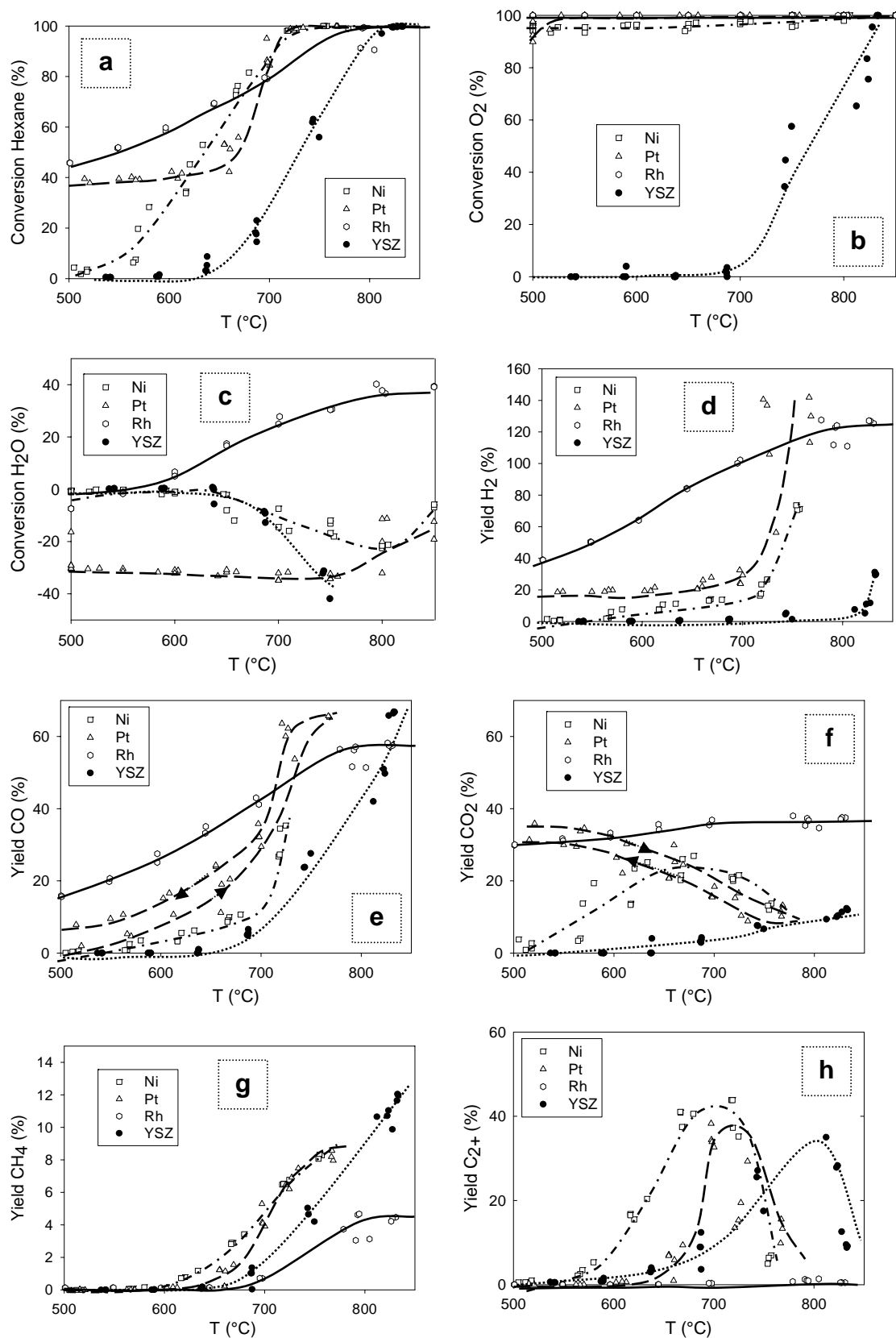


Figure 3.5: Conversion of **a)** hexane, **b)** oxygen, **c)** water and yields of **d)** hydrogen, **e)** carbon monoxide, **f)** carbon dioxide, **g)** methane and **h)** C₂₊ over YSZ and metals supported on YSZ.

3.3.2.3 Comparison of different metals supported on zirconia

In Figures 3.6 a-h the conversions and yields as a function of temperature for ZrO_2 and ZrO_2 -supported Ni, Pt and Rh are shown. Hexane and oxygen conversion was complete for all catalysts at temperatures above 730°C and 760°C , respectively.

As already for Al_2O_3 and YSZ supports, rhodium showed the highest activity in hexane and oxygen conversion over the whole temperature range investigated. At 500°C the conversion of hexane was 40% and increased exponentially to full conversion at 730°C . Oxygen consumption was complete over the whole temperature range. Water was produced below 600°C and consumed above 600°C , with a maximum conversion of around 40%, restricted by thermodynamic equilibrium. CO and H_2 yields exponentially increased with hexane conversion approaching the thermodynamic equilibrium (see Chapter 2) at full hexane conversion. CO_2 yield only slightly increased from 18% to 40% with the conversion of hexane. At temperatures above 650°C , unlike the thermodynamic prediction suggested, CH_4 increased to a maximum of 4%. Cracking products (C_{2+}) were observed only in traces. Until 780°C mainly ethylene was detected, while above 650°C propane was the main cracking product.

The conversion of hexane over Pt/ ZrO_2 was stable at 30% between 500°C and 615°C , and then it steeply increased to 100% at 730°C . Oxygen consumption was almost complete at 500°C (98%) and reached 100% at temperatures above 750°C . An excess of water was produced (conversion -30%) between 550°C and 780°C , while at higher temperatures water was consumed (conversion 10%). The yield of hydrogen was stable at 20% until 700°C and then increased towards the thermodynamic equilibrium. The CO yield showed a similar trend: it started at 5% at 500°C , slowly increased up to 650°C , and then increased steeper towards the thermodynamic equilibrium. Additionally, significant amounts of CH_4 (12% at 790°C) and cracking products (mainly ethylene with a maximum of 40% at around 700°C) were observed.

Ni/ ZrO_2 and pure ZrO_2 showed almost the same profile at temperatures between 500°C and 650°C . At low temperature ($< 600^\circ\text{C}$) only 5% of hexane was converted to short chain alkanes (C_{2+}). This was in correlation with low oxygen and water conversions and with traces of CO, CO_2 , CH_4 and H_2 . With increasing temperatures, the conversion of hexane to CO, CH_4 and C_{2+} -alkanes (maximum at 700°C) increased.

Over ZrO_2 a maximum yield of 70% of H_2 and 10% CO_2 was achieved even at high temperature, while for Ni/ZrO_2 the yields of CO_2 and H_2 increased to the level of Pt/ZrO_2 .

As observed already for $\text{Pt}/\gamma\text{-Al}_2\text{O}_3$ and Pt/YSZ a hysteresis between heating and cooling sequence in the case of Pt/ZrO_2 was observed. As for Pt/YSZ the yield to CO_2 was higher during the heating sequence.

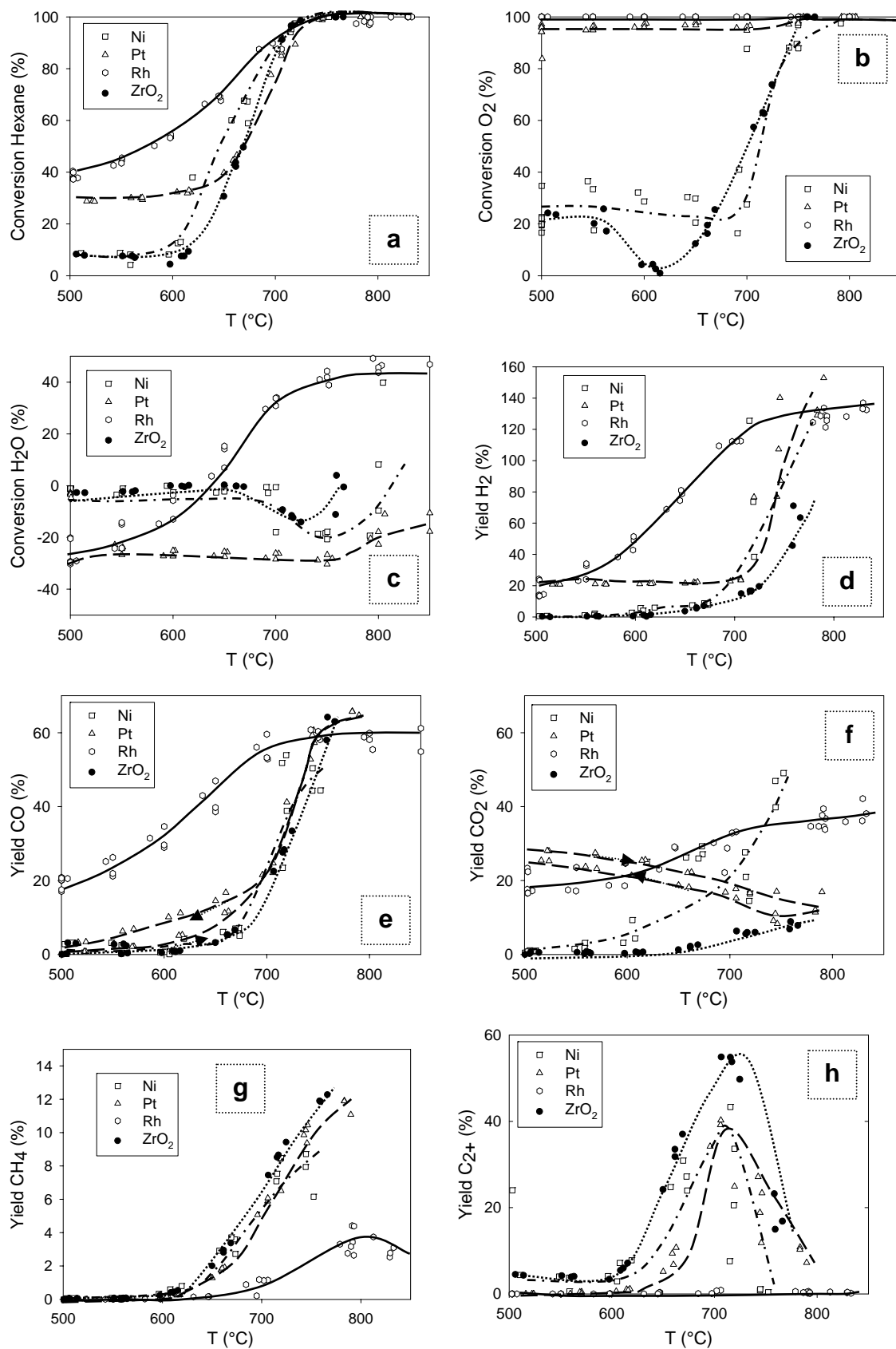


Figure 3.6: Conversion of **a)** hexane, **b)** oxygen, **c)** water and yields of **d)** hydrogen, **e)** carbon monoxide, **f)** carbon dioxide, **g)** methane and **h)** C₂₊ over zirconia and metals supported on zirconia.

3.3.2.4 Comparison of different metals supported on ceria

In Figures 3.7 a-h the catalytic performance of CeO₂ and CeO₂-supported Ni, Pt and Rh is compared.

At 500°C rhodium showed the highest activity with hexane conversion of 35% and complete consumption of O₂. The yields of H₂, CO and CO₂ were 10%, 10% and 25%, respectively. The conversion of hexane slowly increased to 100% at 800°C, being associated with increasing yields of H₂, CO and CO₂. At temperatures above 650°C the production of methane set in, in contrast to the thermodynamic equilibrium, as methane formation should decrease to zero, and traces of cracking products (ethylene, propane, C₄) were detected.

At 500°C platinum was more active than nickel in converting hexane (23%) and oxygen (full consumption). The conversion of hexane was almost constant until 700°C, CO₂ and H₂O being the main products. Simultaneously the yield to CO increased slowly from 2% to 10% and around 2% of lighter alkanes were produced. Above 700°C the conversion of hexane increased reaching 100% at 800°C. Simultaneously the yields of CO, CO₂, H₂ and CH₄ increased up to 50%, 35%, 100% and 9%, respectively. The cracking products showed a trend with a maximum peak (20%) at 780°C.

Ceria and Ni/CeO₂ did not convert hexane at temperatures below 550°C. However over Ni/CeO₂ approximately 10% of fed oxygen was converted already at temperature below 550°C. The conversion of hexane increased up to 100% at 720°C over both CeO₂ and Ni/CeO₂. CO and H₂ production set in at 650°C, increasing steeply with increasing temperature for Ni/CeO₂. The production of hydrogen started at 700°C and reached 80% at 750°C over ceria. A similar trend was observed for CO with a maximum yield of 60% at 750°C. Already at 600°C CO₂, CH₄ and C₂₊ alkanes were formed. At 750°C the amounts of CH₄ and CO₂ were 10% and 40%, respectively. A maximum of 30% for C₂₊ was observed at 650°C.

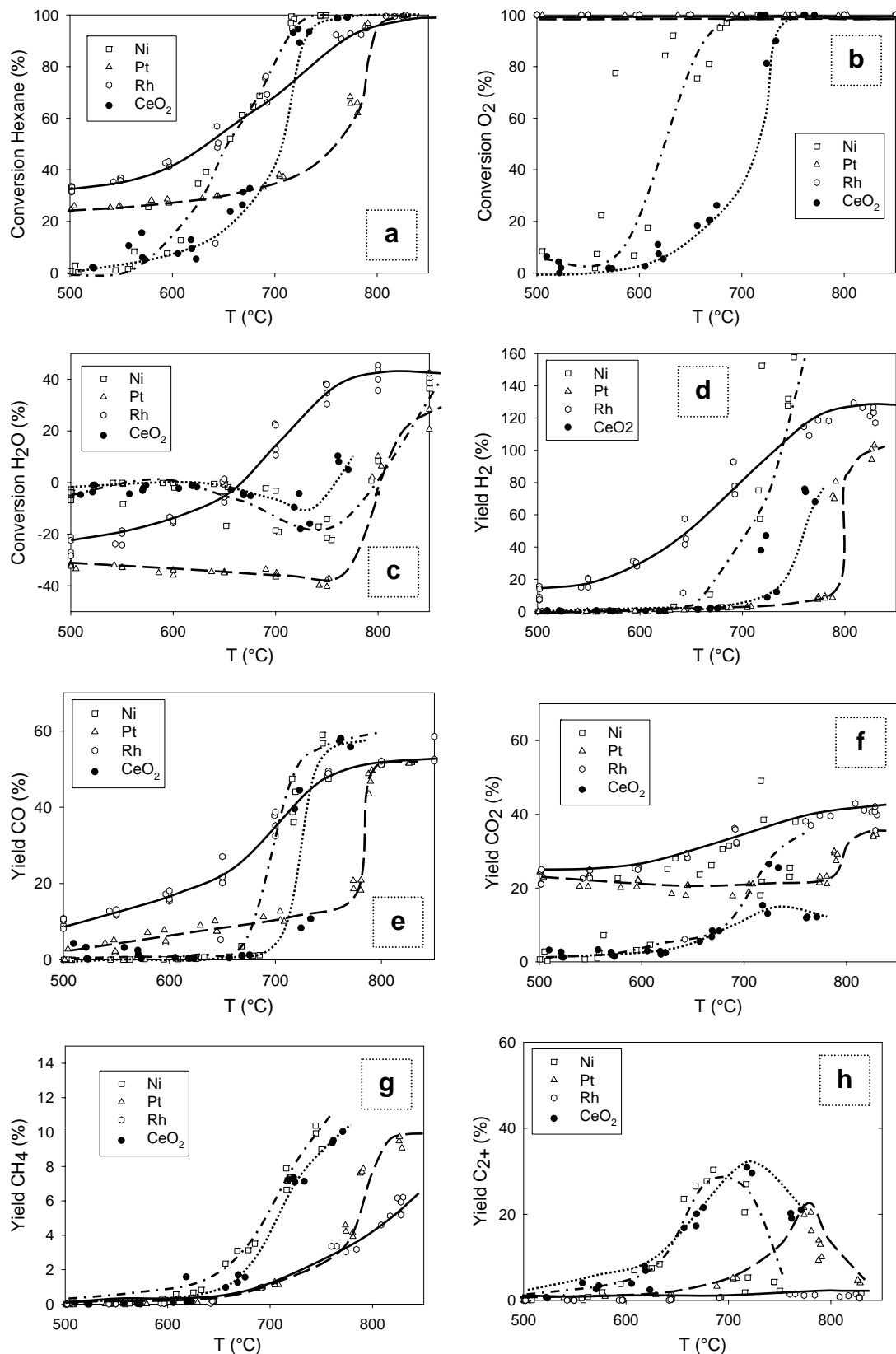


Figure 3.7: Conversion of a) hexane, b) oxygen, c) water and yields of d) hydrogen, e) carbon monoxide, f) carbon dioxide, g) methane and h) C₂₊ over ceria and metals supported on ceria.

3.4 Discussion

3.4.1 Effect of Noble Metal

The catalytic activity of Rh, Ni and Pt (1wt%) deposited on four supports (Al_2O_3 , YSZ, ZrO_2 and CeO_2) was tested in autothermal reforming of *n*-hexane at temperatures between 500 and 850°C. With the same support, the activity decreases in the sequence Rh>Pt>Ni. This sequence is in agreement with the results reported for steam reforming and ATR^{1, 14}.

For supported Ni catalysts high oxygen consumption was observed at low hexane conversion, while combustion products were not formed. Thus, the oxygen consumption is attributed to Ni oxidation. This suggests that with supported Ni catalysts two zones are present in the catalyst bed, one in which Ni is present in the form of oxide and a second with metallic Ni. The feature is well documented in literature for several Ni containing catalysts^{1, 15, 16} and in the following Chapter 4.

Thus, activity for converting hexane was low at low temperatures. At higher temperatures Ni catalysts produced a mixture of hydrocarbons C_{2+} with a maximum at around 700°C (790°C when alumina was used as support) and CH_4 . Syngas was produced at higher temperatures not reaching thermodynamic equilibrium. This could be an effect of oxidized Ni, as Ni^0 is known as good steam reforming catalyst.

Pt showed an intermediate activity between Ni and Rh at low temperature. Over supported Pt catalysts hexane was burned up to complete consumption of oxygen forming mainly H_2O , CO_2 and CO. Subsequently, the activity of the Pt catalysts to form H_2 and CO increased exhibiting similar results as supported Ni. Over Pt supported catalysts C_{2+} and CH_4 were formed likewise over Ni catalysts. Besides, a difference between the heating and cooling sequence were observed - most evident for Pt/ γ - Al_2O_3 . In this case the hexane conversion at 500°C increased from 20% to almost 30% after decreasing the reaction temperature from 850 to 500°C. The higher activity was associated with higher conversion of H_2O , higher yields in CO and H_2 and lower yield in CO_2 . The yields in CH_4 and C_{2+} remained unaffected. We speculate that carbonaceous deposits lower the activity in the heating sequence until at high temperature the deposits can be removed increasing the conversion in the cooling sequence. This would also explain that steam reforming and water-gas-shift reaction take place on the metal site.

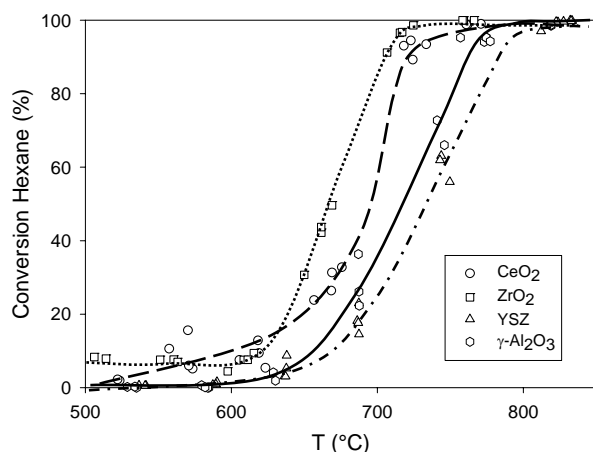
Rh supported catalysts showed the highest activity at low temperature with hexane conversions between 40 and 60% at 500°C forming H₂ and CO besides CO₂ and CH₄. Cracking products (C₂₊) were not observed, except in low amounts for the ceria support at temperatures above 750°C.

Apart from the support, the activity decreases in the sequence Rh>Pt>Ni. Pt supported on ZrO₂ and γ -Al₂O₃ had average metal particle size significantly smaller (by a factor 5 and 3, respectively) than that of Rh, while the molar content of Pt was only half of Rh. Therefore, the total number of surface active sites was higher for Pt than for Rh. The metal particle size of supported Ni was similar to that of Rh, and the molar amount of Ni was almost twice the amount of Rh. Therefore the number of surface active metal sites for Ni catalyst was even higher than that for Pt. Nevertheless Ni showed the lowest activity. These results suggest that the differences in the conversion observed over these catalysts are not related to the total number of accessible metal atoms. The different activities can be correlated with a different oxidation state of the metal (as in the case of Ni) and/or with different reaction mechanisms (due to different nature of adsorbed oxygen species¹⁷). Thus, over supported Rh catalysts the mechanism seems to be different from that operating on supported Pt and Ni as on Rh C₂₊ hydrocarbons were not detected as reaction products.

3.4.2 Effect of Support

The metal oxides used as supports were (partly) reducible (CeO₂, ZrO₂, and YSZ) and irreducible (γ -Al₂O₃). Ceria is easier to reduce than zirconia as reported from TPR experiments in literature^{18, 19}.

The supports themselves showed no activity to syngas or hydrogen production at temperatures below 600°C. However, ceria and zirconia showed some activity in the conversion of hexane (Fig. 3.8) at low temperatures (<600°C). Over ceria mainly combustion (CO₂) and over zirconia mainly cracking products (C₂₊) were observed. Probably CeO₂ – reducible support - delivered oxygen for hexane combustion from the lattice as more CO₂ was produced than oxygen from the gas phase consumed²⁰. Hydrogen production increased above 600°C probably due to gas phase reactions because all these supports do not possess significant activity for CO₂/H₂O reforming



or water-gas shift reaction ²¹. The main products were CH₄ and C₂₊ (cracking process) and CO, CO₂ and H₂O (combustion process).

Figure 3.8: Conversion of hexane over different supports.

The support can affect the activity of the metal catalyst through two mechanisms: (i) modification of the metal dispersion ¹⁸ and (ii) enhanced steam adsorption followed by “inverse spillover” ^{22, 23}. A direct correlation between metal dispersion and activity was found for Pt (γ -Al₂O₃, ZrO₂>YSZ>CeO₂) and Ni (YSZ>CeO₂, ZrO₂> γ -Al₂O₃) (see metal particle size in table 3.1). However for Rh the activity decreases in the sequence γ -Al₂O₃>YSZ>ZrO₂>CeO₂ (see Fig 3.9), while the

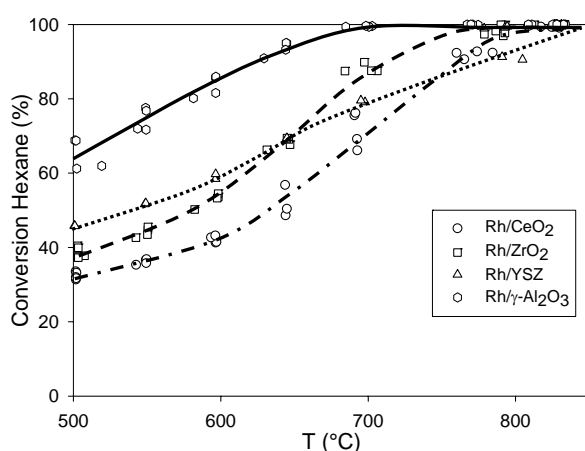


Figure 3.9: Conversion of hexane over Rh on different supports.

dispersion decrease in the sequence YSZ>CeO₂> γ -Al₂O₃>ZrO₂ (see table 3.1). Zhang *et al.* ²⁴ reported a similar sequence in Rh dispersion (YSZ> γ -Al₂O₃(>TiO₂>SiO₂) acting on the activity in CO₂ reforming of methane). For Rh catalysts probably the second mechanism (“inverse spillover”) plays the most important role. In this mechanism the catalyst support enhances the adsorption of steam, which is then transported or “spilled

over“ to the metal. The significant higher activity of Rh/ γ -Al₂O₃ compared to the other supports could be hence related to the higher surface area of γ -Al₂O₃. An evidence for the inverse spill over for Rh on γ -Al₂O₃ was found by Wang *et al.* ²³ in steam reforming of methane.

3.5 Conclusion

The activity and selectivity to CO and H₂ were found to increased in the sequence of noble metals Ni < Pt < Rh and for Rh-catalysts with support material in the sequence CeO₂ < YSZ ~ ZrO₂ < Al₂O₃.

At steady state conditions in autothermal reforming of hexane in the presence of oxygen and water, Ni could be present as metal oxide, while the more noble metals Pt and Rh can have oxide overlayers. Hexane conversion over an oxygen rich surface will primarily produce CO₂ and H₂O. After depletion of oxygen and reduction of the Ni and Pt surface, synthesis gas is produced via CO₂- and H₂O-reforming of the remaining hexane (see also Chapter 4).

Both Rh and Pt are active catalysts for the autothermal reforming of hexane, in line with the literature of light hydrocarbon partial oxidation and reforming or partial oxidation of methane ²⁵. Homogeneous reactions are known to play the most important role in the conversion of ethane and propane in Pt containing autothermal reactors. Highly dispersed Rh/Al₂O₃ seems to offer the possibility of circumventing the gas-phase process. CO and H₂ were produced selectively, even under conditions which favor the production of olefins. Direct evidence on C formation was not available over the Rh-based catalysts under the conditions used ($\lambda = 0.32$ and S/C ratio 1.2). This could depend on the especially high activity of the Rh-supported catalyst in indirect reactions such as steam reforming. With Rh high conversion and high selectivity to synthesis gas were achieved at low temperature.

Over ceria and zirconia hexane conversion started at temperatures below 600°C forming CO₂ and C₂₊, while over alumina and yttrium-stabilized zirconia temperatures higher than 600°C were needed. At temperatures above 600°C on all supports CO, CO₂, H₂O and H₂ were formed besides short chain alkanes formed trough thermal cracking.

3.6 References

- (1) Ayabe, S.; Omoto, H.; Utaka, T.; Kikuchi, R.; Sasaki, K.; Teraoka, Y.; Eguchi, K. *Applied Catalysis A-General* **2003**, *241*, 261.
- (2) Ahmed, S.; Krumpelt, M. *International Journal of Hydrogen Energy* **2001**, *26*, 291.
- (3) Trimm, D. L.; Önsan, Z. I. *Catalysis Reviews* **2001**, *43*, 31.
- (4) Springmann, S.; Eigenberger, G. *Chemie Ingenieur Technik* **2002**, *74*, 1454.
- (5) Pereira, C.; Wilkenhoener, R.; Ahmed, S.; M.Krumpelt. "Catalytic reforming of gasoline and diesel fuel"; AIChE Spring 2000 Meeting, 2000, Atlanta, GA.
- (6) Pacheco, M.; Sira, J.; Kopasz, J. *Applied Catalysis A-General* **2003**, *250*, 161.
- (7) Moon, D. J.; Sreekumar, K.; Lee, S. D.; Lee, B. G.; Kim, H. S. *Applied Catalysis A-General* **2001**, *215*, 1.
- (8) Choudhary, V. R.; Uphade, B. S.; Mamman, A. S. *Microporous and Mesoporous Materials* **1998**, *23*, 61.
- (9) Achenbach, E.; Riensche, E. *Journal of Power Sources* **1994**, *52*, 283.
- (10) Asprey, S. P.; Wojciechowski, B. W.; Peppley, B. A. *Applied Catalysis A-General* **1999**, *179*, 51.
- (11) Dicks, A. L. *Journal of Power Sources* **1996**, *61*, 113.
- (12) Garcia, L.; French, R.; Czernik, S.; Chornet, E. *Applied Catalysis A-General* **2000**, *201*, 225.
- (13) Wiese, W.; Emonts, B.; Peters, R. *Journal of Power Sources* **1999**, *84*, 187.
- (14) Ehwald, H.; Kürschner, U.; Smejkal, Q.; Lieske, H. "Investigation of Different Catalysts for Autothermal Reforming of i-Octane (Poster)"; Innovation in the Manufacture and Use of Hydrogen, 2003, Dresden.
- (15) Swaan, H. M.; Rouanet, R.; Widyananda, P.; Mirodatos, C. *Studies in Surface Science Catalysis* **1997**, *107*, 447.
- (16) Santos, A.; Menendez, M.; Monzon, A.; Santamaria, J.; Miro, E. E.; Lombardo, E. A. *Journal of Catalysis* **1996**, *158*, 83.
- (17) Mallens, E. P. J.; Hoebink, J. H. B. J.; Marin, G. B. *Journal of Catalysis* **1997**, *167*, 43.
- (18) Wang, H. Y.; Ruckenstein, E. *Applied Catalysis A-General* **2000**, *204*, 143.
- (19) Diagne, C.; Idriss, H.; Kiennemann, A. *Catalysis Communications* **2002**, *3*, 565.
- (20) Fathi, M.; Bjorgum, E.; Viig, T.; Rokstad, O. A. *Catalysis Today* **2000**, *63*, 489.
- (21) Steghuis, A. G. Catalyzed partial oxidation of methane to synthesis gas. PhD-Thesis, University of Twente, 1998.
- (22) Rostrup-Nielsen, J. R. Catalytic steam reforming. In *Catalysis Science and Technology*; Boudart, M., Ed.; Springer, 1984.
- (23) Wang, D.; Dewaele, O.; Groote, A. M. D.; Froment, G. F. *Journal of Catalysis* **1996**, *159*, 418.
- (24) Zhang, Z. L.; Tsipouriari, V. A.; Efstathiou, A. M.; Verykios, X. E. *Journal of Catalysis* **1996**, *158*, 51.
- (25) Beretta, A.; Forzatti, P. *Chemical Engineering Journal* **2004**, *99*, 219.

Autothermal Reforming of n-Hexane over Structured Catalysts

Abstract

In this chapter the autothermal reforming of n-hexane over Ni, Pt and Rh supported on alumina monoliths was investigated. The influence of feed composition on the catalytic activity and stability at 775 °C was studied. The activity and stability were found to decrease in the sequence Rh > Pt > Ni. Ni can be deactivated by re-oxidation and carbon deposition, while on Pt only carbon deposition can occur. None of these effects was observed over the Rh catalyst. In the temperature range from 500 °C to 800 °C only Al₂O₃-supported Rh and Pt catalysts were investigated at a constant hexane : oxygen : water ratio of 1 : 3 : 7 (with Ar as diluent). The performance of these catalysts was compared with that of a typical commercial catalyst (Umicore A-Type).

4.1 Introduction

In Chapter 3 the catalytic performance in the autothermal reforming of n-hexane was investigated on powder catalysts tested in a fixed bed reactor. This has the disadvantage of high pressure drops and inefficient heat exchange. These drawbacks can be overcome by using a fluidized bed. Fluidized bed reactors are discussed in literature ¹ for partial oxidation and steam reforming for fuel cell stationary applications ⁵. Nonetheless they can not be used for mobile applications. As alternative monolithic catalysts that are well known in the field of automotive exhaust gas treatment, offer the advantage of a low pressure drop.

In this chapter the autothermal reforming of n-hexane over Ni, Pt and Rh supported on monoliths was investigated. Only γ -Al₂O₃ was used as washcoat layer of the monoliths because, as shown in Chapter 3, the chemical nature of the support influences the catalytic performance only slightly.

Carbon deposition is the major cause of catalyst deactivation in autothermal reforming ⁵. In particular, carbon deposition is a more serious problem when using heavy hydrocarbons than when using methane. Although the reaction condition for carbon deposition can be estimated from the thermodynamic equilibrium, the real deposition conditions are rather complex. Thus, we have directly studied the reaction conditions affecting the catalytic activity and stability of Ni, Pt and Rh supported on monoliths.

4.2 Experimental

4.2.1 Impregnation of monolithic catalysts

Alumina monoliths from Sasol ["24-Loch Extrudat", mean diameter 5.7 mm, corresponding to a cell density of 600 triangular cpsi (channel per square inch); Fig. 4.1] were washcoated by dipping into a slurry of γ -Al₂O₃. The excess slurry was removed by gently blowing the monolith channels slurry free. The washcoated monoliths were freeze dried and calcined at 500 °C for 2h (heating rate 5 °C min⁻¹). Subsequently, the washcoated monoliths were impregnated with 1M Ni(NO₃)₂, 0.155M Rh(NO₃)₃, or 0.144M Pt(NH₃)₄(NO₃)₂. After contacting the



Fig. 4.1: Monolith from Sasol with triangular channels.

monoliths with the solution for 1 h, they were withdrawn and the channels were gently blown free from excess liquid following the preparation procedure published by Vergunst *et al.*⁶. Then, the samples were freeze dried and calcined at 900 °C for 4h (heating ramp 3 °C min⁻¹).

The noble metal content was determined by AAS (UNICAM 939 AA-Spectrometer, see Chapter 3).

4.2.2 Characterization techniques

Chemisorption

Chemisorption measurements were performed by static volumetric analysis using the set-up represented in Figure 4.2. The catalyst already reduced *ex situ* at 800 °C for 2h, was activated *in situ* at 400 °C (maximum temperature of the set-up) for 2h in flowing hydrogen. Finally, the activated catalyst was cooled down to room temperature in flowing helium. The volume of the sample holder (between valves 1 and 6) and of overall system (between valves 6, 5 and 3, with valves 4 and 2 open) were determined by introduction (after evacuation) of a known volume of helium (from the flask). After evacuating the system, a known volume of hydrogen (from flask) was introduced at room temperature in the volume between valve 6-5-4-3 and allowed to equilibrate for at least 5h. Desorption of physisorbed hydrogen was carried out by evacuating the volume between valve 1 and 3 (valve 4 open) and reopening valve 1 after valve 3 was closed. This procedure (evacuation/opening of valve 1) was repeated several times up to constant pressure.

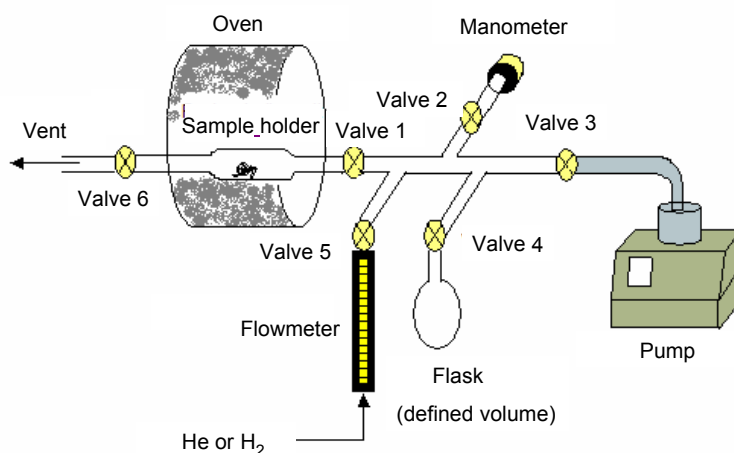


Figure 4.2: Chemisorption set-up.

Temperature programmed oxidation (TPO)

Temperature programmed oxidation (TPO) was performed in a flow system consisting of a tubular quartz reactor heated uniformly by a furnace. 200 mg of catalyst after autothermal reforming were oxidized with 5 % O₂ in He (total flow 60 ml/min) during temperature increase from 30 to 850 °C with heating rate 10°C/min. A fraction of the gases from the reactor outlet was directed *via* a heated stainless steel capillary into a mass spectrometer (*Balzers QMG 420*), where the partial pressure of the reactants was continuously monitored. Carbon deposition was calculated from the area of the CO₂ peak while the H/C ratio was determined from the water peak. These peaks were calibrated by thermal decomposition of NaHCO₃.

Temperature programmed desorption (TPD)

Temperature programmed desorption (TPD) of ammonia was used for determining the concentrations of acid sites in the samples. Prior to the TPD measurement, the sample (~25 mg) was first degassed by evacuating to 10⁻³ mbar, then heated for 1 h at 450 °C (increment 10 C min⁻¹). After cooling to 150 °C, the sample was equilibrated with 1 mbar of ammonia for 60 min. After evacuation for 60 min, the TPD measurement was started by heating the samples to 800 °C at a rate of 10 °C min⁻¹. During this procedure, mass spectra of the gas phase were collected at 5 °C intervals using a *Balzers QMG 420* mass spectrometer to determine the rate of ammonia evolving.

X-ray diffraction (TPD), transmission electron microscopy (TEM), atomic adsorption spectroscopy (AAS) and surface area measurement

Powder X-ray diffraction, transmission electron microscopy, atomic adsorption spectroscopy, and specific surface area measurements are described in Chapter 3.

4.2.3 Catalytic experiments

Autothermal reforming tests were performed in the setup described in Chapter 3, using a fixed bed tubular reactor made in quartz (inner diameter 6 mm, outer diameter 8 mm). The monoliths were placed in the reaction zone between two quartz wool plugs. The industrial catalyst (Umicore A-Type AC 009 - EXP, with a cell

density of 600 cpsj, quadratic channels) was cut to fit into the quartz tube. Prior to catalytic test the catalysts were reduced *in situ* at 800 °C for 2 h.

The stream entering the reactor contained hexane, oxygen, water and argon as diluents. The **effect of the feed composition** was investigated through two series of experiments, both performed at 775 °C (furnace temperature 800 °C) with approximately 400 mg of monolithic catalyst (corresponding to 4 pieces of Sasol extrudates). In all these experiments the total flow and the hexane flow were maintained constant at 200 ml/min and 5 ml/min, respectively. In the first sequence of tests the ratio oxygen/hexane was changed ($O_2/C_6H_{14} = 3:1, 4.5:1$ or $1.5:1$) keeping the water/hexane ratio constant at 7:1. In the second one the ratio water/hexane was changed ($H_2O/C_6H_{14} = 10:1$ or $4:1$) keeping the oxygen/hexane ratio constant at 3:1. A summary of the investigated feed compositions is depicted in Table 4.1.

Only for the Ni catalyst the same experiments were also performed separately with fresh catalyst instead that in the sequence indicated in Table 4.1. From the comparison of the corresponding results it was possible to point out under which conditions and why the Ni catalyst deactivates.

Table 4.1: Sequence of experiments with different molar ratios $C_6H_{14}/O_2/H_2O$. During this sequence of experiment the catalyst was never removed from the reactor.

experiment sequence	hexane	oxygen	water
1	1	3	7
2	1	4.5	7
3	1	1.5	7
4	1	3	10
5	1	3	4

For studying the **effect of the reaction temperature** the ratio of hexane : oxygen : water : argon was set to 1 : 3 : 7 : 29 (steam/carbon ratio = 1.2 and oxygen/carbon ratio = 1) with a total flow of 200 ml/min. This flow is equivalent to a weight hourly space velocity (WHSV) of 2.7 ($g_{C_6H_{14}}/h$)/ $g_{monolith}$. The reaction temperature in autothermal reforming was decreased from 800 °C to 500 °C in steps of 50 °C, keeping each temperature for 1.5 h. The temperature was then increased to 800 °C always in steps of 50 °C for testing the eventual catalyst deactivation. The

values calculated for the Reynolds number (Re) suggests a laminar flow in each channel:

$$\text{Re} = \frac{W}{A\varepsilon} \cdot \frac{d_{ch}}{\mu}$$

with W total flow, d_{ch} hydraulic diameter of a channel, A frontal area, ε open frontal area, μ gas viscosity of the mixture at reaction temperature T . Simulations with the software FEMLAB 3.0 considering the geometry of the monolith and the inner diameter of the quartz tube showed turbulences at the top of the monolith.

The exit stream from the reactor was analyzed by gas chromatography as described in Chapter 3. The areas of the peaks were corrected with response factors obtained by calibration. Conversion and selectivity (with respect to hexane) were calculated according to the formula described in Chapter 3.

4.3 Results

4.3.1 Characterization

XRD patterns of the catalysts before and after reduction are shown in Fig. 4.3 and 4.4, respectively. In addition to the reflections typical for γ -alumina (cubic phase), the XRD pattern of the unreduced catalysts exhibited reflection peaks characteristic for Pt^0 (cubic) at 2θ values of 39.5° , 46.2° and 67.5° and for NiAl_2O_4 (cubic) at 40.0° , 45.1° , and 65.5° (the reflex at 59.6 was below detection limit). Peaks corresponding to metallic Rh or other Rh-species were not observed, which suggests highly dispersed Rh precursor species.

After reduction at 800°C for 2 h, the XRD peaks corresponding to cubic NiAl_2O_4 disappeared. The sole presence of the diffraction peaks of γ -alumina indicated that Ni is well dispersed. The reduction treatment did not affect the profile of the X-ray diffractogram recorded for the Pt catalyst. For supported Rh, XRD diffraction peaks characteristic for Rh^0 (cubic) appeared at 2θ 41.2° , 47.8° and 70.0° . The intensity of these peaks was lower than that corresponding to cubic Pt.

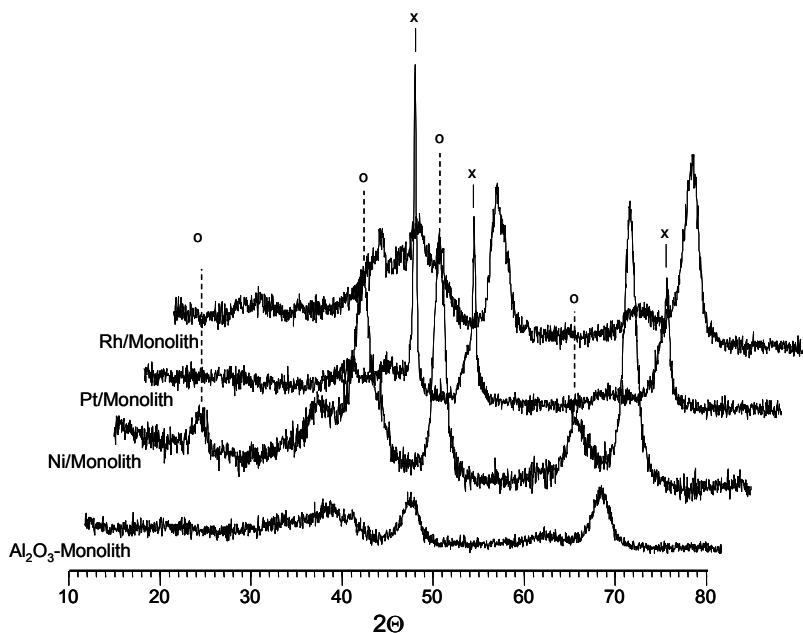


Figure 4.3: XRD pattern of Ni, Pt and Rh supported on Al_2O_3 -monolith before reduction. (x) cubic Pt; (o) cubic NiAl_2O_4 .

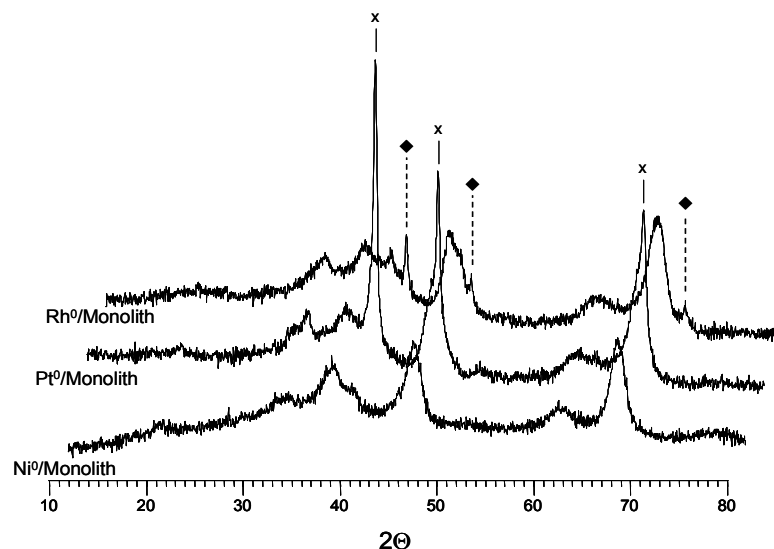


Figure 4.4: XRD pattern of Ni, Pt, Rh supported on Al_2O_3 -monolith after reduction. (x) cubic Pt; (◆) cubic Rh.

The results of AAS, BET, TPD, TEM and H₂ chemisorption are compiled in table 4.2.

Table 4.2: Specific surface area, noble metal content and metal dispersion of the monolithic catalysts.

Material	Noble metal content [wt%]	Specific Surface Area [m ² g ⁻¹]	Acid Site Concentration ¹ [mmol g ⁻¹]	Metal Particle Size (TEM) [nm]	Metal Dispersion ² [%]	Metal Particle size ² [nm]	Metal Surface Area [m ² g ⁻¹]
Monolith	-	201	0.207	-	-	-	-
Ni/ γ -Al ₂ O ₃	4.8	142	0.033 (unred) 0.147 (red. ³)	4 (red. ³)	5	21	31
Pt/ γ -Al ₂ O ₃	4.2	126	0.046 (unred) 0.176 (red. ³)	31 (unred.) 43 (red. ³)	2	44	6
Rh/ γ -Al ₂ O ₃	1.7	140	0.052 (unred) 0.064 (red. ³)	7 (unred.) 7 (red. ³)	17	7	75
Umicore A-Type	Rh: 0.1 to 2 [Rh:Pt 20:1 to 2:1 (wt:wt)] ⁷	46	n.d. ⁴	n.d.	n.d.	n.d.	n. d.

¹ From ammonia TPD.

² Calculated from chemisorption according to Literature (7) .

³ red.: reduced at 800°C for 2 h under H₂.

⁴ not determined

Transmission electron micrographs (Fig. 4.5) show Pt formed clusters with an average diameter of 31 nm in the unreduced material. After reduction at 800 °C for 2 h in H₂ the Pt particles sintered slightly the average size increasing to 43 nm. The average dimension of the Rh particles (7 nm) was essentially unaffected by reduction treatment. The smallest particle size (4 nm) was observed for reduced Ni. In the corresponding unreduced catalyst Ni was present as NiAl₂O₄. The particle size of Ni calculated from H₂-chemisorption for the reduced catalyst was more than five times larger (21 nm) than observed by TEM. This strong discrepancy between the two methods for the Ni catalyst could be attributed to the smaller portion of material observed by TEM with respect to that analyzed by H₂-chemisorption. Thus, with TEM the fraction observed may not have been representative of the overall sample. The results suggest that few large particles were not detected in the TEM analysis and could so lead to an underestimation of the particle size.

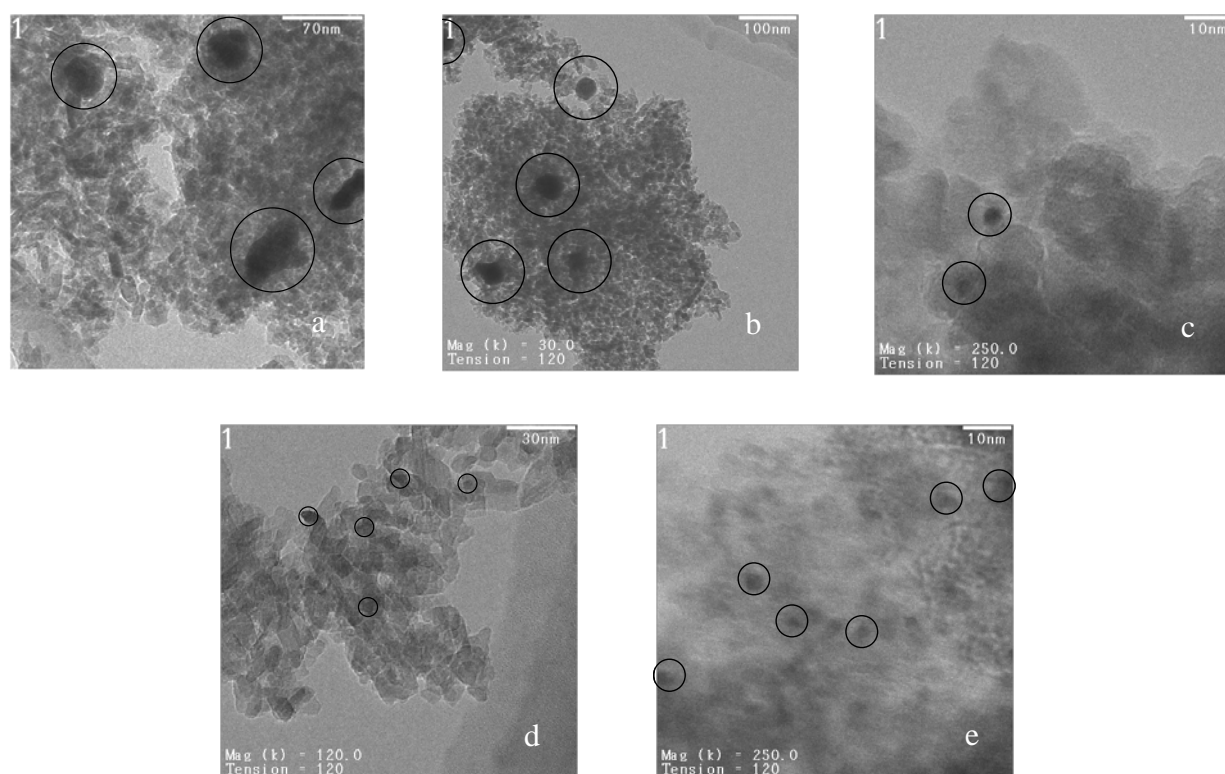


Figure 4.5: TEM pictures of **a)** unreduced Pt/monolith, **b)** reduced Pt/monolith, **c)** reduced Ni/monolith, **d)** unreduced Rh/monolith, and **e)** reduced Rh/monolith.

It is interesting to note that the concentration of acid sites correlated with the dispersion of noble metal (see Table 4.2). For the Rh-supported catalyst the concentration of acid site was essentially unaffected by reduction treatment, while for

Ni and Pt based materials the acid site concentration increased after reduction due to metal particle sintering.

4.3.2 Catalytic activity at 775°C - Effect of feed composition

The catalytic tests were performed at 775 °C, by feeding hexane : oxygen : water with ratio 1:3:7. The hourly space velocity was 2.7 (g_{C6H14}/h)/g_{monolith}. In a series of experiments also the effect of feed composition was investigated by varying either the hexane to water or the hexane to oxygen ratio, while keeping the other parameters constant.

When feeding the mixture C₆H₁₄ / O₂ / H₂O / Ar 1:3:7:29, hexane and oxygen were fully consumed for all three catalysts (Ni, Pt and Rh supported on Al₂O₃ monoliths). As displayed in Figure 4.6, the selectivity of all components (calculated with respect to hexane) and the conversion of water (not displayed) were constant over time for Rh [Conv(H₂O) = 29%] and Pt [Conv(H₂O) = 25%]. The ratio CO/CO₂ was higher for Pt (57/43) than for Rh (50/50), while the selectivity to H₂ was slightly lower for Pt (130%) than for Rh (140%). Note that H₂ can be formed from steam reforming of hexane as well as by partial oxidation of hexane (and the water gas shift reaction). Thus, if the H₂ yield is defined only in respect to n-hexane dissociation (see page 38), the H₂ yield can exceed 100 %. With supported Pt and Rh catalysts, methane or higher hydrocarbons were not observed at 775 °C. Ni, however, showed initially a high selectivity (30%) to C₂₊ products, which markedly decreased after 15 minutes TOS. After 90 minutes the production of CO, starting at 35%, reached a maximum of 60%. The equilibrium composition was reached after 320 minutes with a selectivity of 120% H₂, 50% of CO₂, 45.5% CO and 4.5% CH₄. The conversion of water (not shown) was in the beginning negative (formation of water) and increased with TOS to an equilibrium value of 25.6% conversion. These results seem to suggest that at the beginning of the catalytic reaction nickel, being present as at least partially unreduced (NiAlO₄), underwent reduction. In order to prove this hypothesis, the Ni catalyst was reduced before the catalytic test *in situ* for 5h instead of 2h. As shown in Fig. 4.7, the equilibrium composition was reached after a shorter time (30 min instead of 230 min). This was accompanied by higher H₂ and CO₂ selectivities (145.5% and 58.2%, respectively), and lower CO selectivity (41.6%). These features are in agreement with a lower initial consumption of H₂ due to a better degree of reduction of the metal. The higher amount of H₂ associated with the absence of water

produced by metal reduction, justifies the minor extent of the water gas shift reaction and therefore the higher initial ratio CO_2/CO .

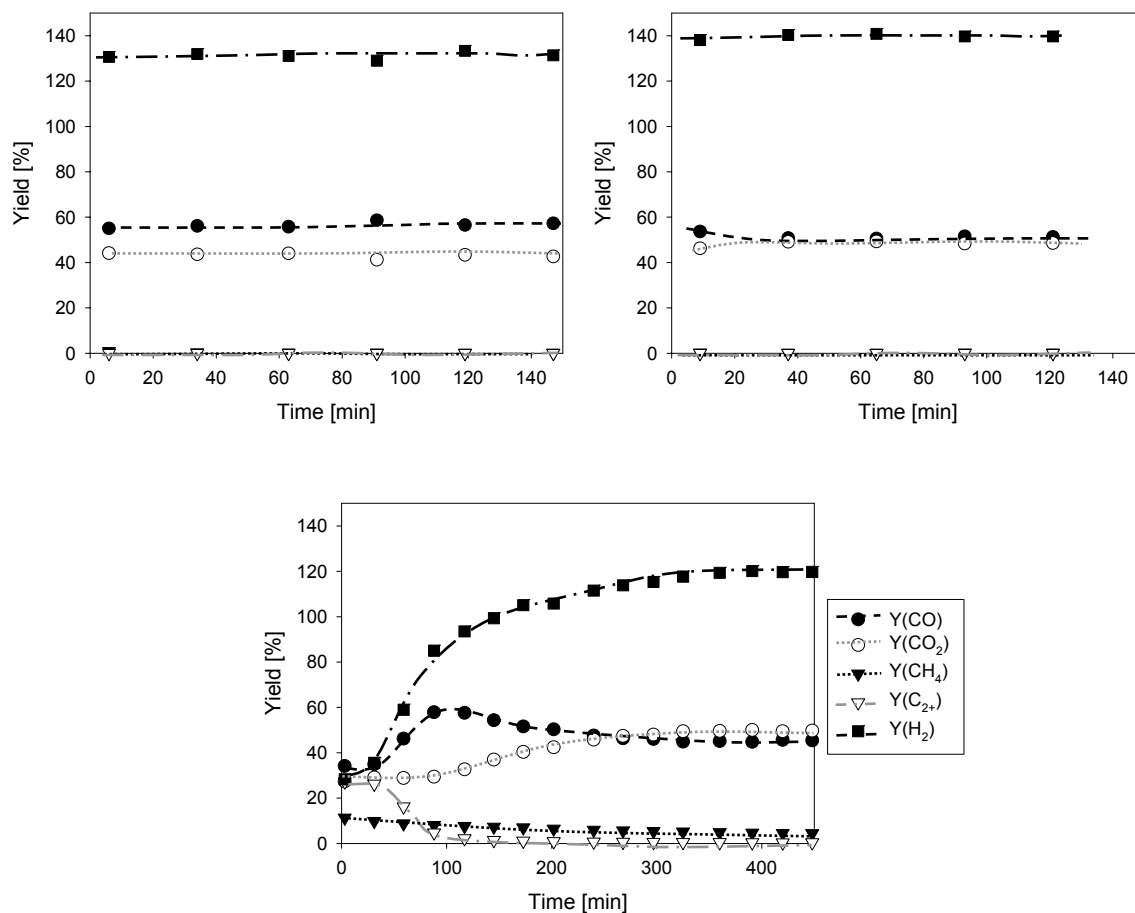


Figure 4.6: Catalytic activity of Pt, Rh and Ni supported on Al_2O_3 monoliths vs. time (775°C , $\text{WHSV } 2.7 \text{ h}^{-1}$, $\text{C}_6\text{H}_{14}/\text{O}_2/\text{H}_2\text{O}/\text{Ar} = 1/3/7/29$, total flow 200 ml/min). The catalysts were pre-reduced *in situ* at 800°C for 2h.

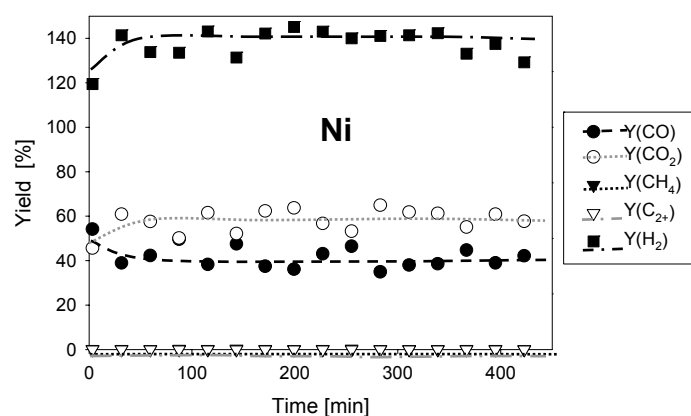


Figure 4.7: Catalytic activity of Ni supported on Al_2O_3 monoliths after 5 h *in situ* reduction vs. reaction time (775°C , $\text{WHSV } 2.7 \text{ h}^{-1}$, $\text{C}_6\text{H}_{14}/\text{O}_2/\text{H}_2\text{O}/\text{Ar} = 1/3/7/29$, total flow 200 ml/min).

The effect of the oxygen/hexane and water/hexane ratios on the catalytic performance is shown in Fig. 4.8 and 4.9, respectively. Under all conditions full

conversion of hexane was achieved over rhodium in agreement with thermodynamic equilibrium. With lower oxygen concentration more H₂ and CO (less combustion products: CO₂ and H₂O) were produced and *vice versa*. Adding more water shifted the equilibrium composition to more H₂ and CO₂ and less CO and H₂O (lower conversion).

Over the Pt based catalyst full conversion of hexane was not achieved at low oxygen concentration (95.5% conversion at an oxygen/hexane ratio of 1.5). This led to much lower yields in hydrogen and carbon monoxide. Additionally, CH₄ (6% yield) and C₂₊ (7.7% yield, not shown) products were observed. At low water concentration (ratio water/hexane of 4) low yields of CH₄ (1.3%) and C₂₊ (0.6%) were obtained, while the hexane conversion was almost complete (99.7%). The uncompleted conversion of hexane with a feed poor in oxygen, but rich in water (C₆H₁₄/O₂/H₂O = 1/1.5/7) may be tentatively attributed to Pt deactivation by coke deposition. The quasi-complete conversion of hexane with a feed rich in oxygen but poor in water (C₆H₁₄/O₂/H₂O = 1/3/4) suggests that the presence of oxygen is more crucial than that of water for maintaining high activity. Increasing the water/C₆H₁₄ ratio from 7 to 10 and the oxygen/C₆H₁₄ ratio from 1.5 to 3 (experiment n°4 of Table 4.1) led to full activity of Pt again. Thus, it was deduced that the deactivation of the catalyst observed for a water lean feed (H₂O/C₆H₁₄=4) was not due to the eventual effect of the sequence followed in performing these experiments (sequence of feed changed according to Table 4.1). Feeding mixtures simultaneously rich in water and oxygen (H₂O/C₆H₁₄ ≥ 7 for C₆H₁₄/O₂ = 1/3 and O₂/C₆H₁₄ ≥ 3 for C₆H₁₄/H₂O = 1/7), the product distribution was similar for Pt and Rh supported on Al₂O₃ monoliths. Only a slightly higher hydrogen yield was observed with Rh at equal C₆H₁₄/H₂O ratios.

For the Ni catalyst the reaction conditions had a strong influence on the catalytic activity. The highest activity was achieved at C₆H₁₄/O₂/H₂O/Ar 1/3/7/29 with 37.6% H₂O conversion and yields of 120% H₂, 45.5% CO and 4.5% CH₄. The yield to higher hydrocarbons was 0.4% (not shown). Higher oxygen concentration deactivated the catalyst by oxidizing Ni. Water was observed, as Ni²⁺ does not exhibit steam reforming activity and hexane was combusted. A dramatic decrease of the H₂ yield (45.5%) and slight increase of CO (52.3%), CH₄ (7.4%) and C₂₊ (4%) yield were observed in consequence.

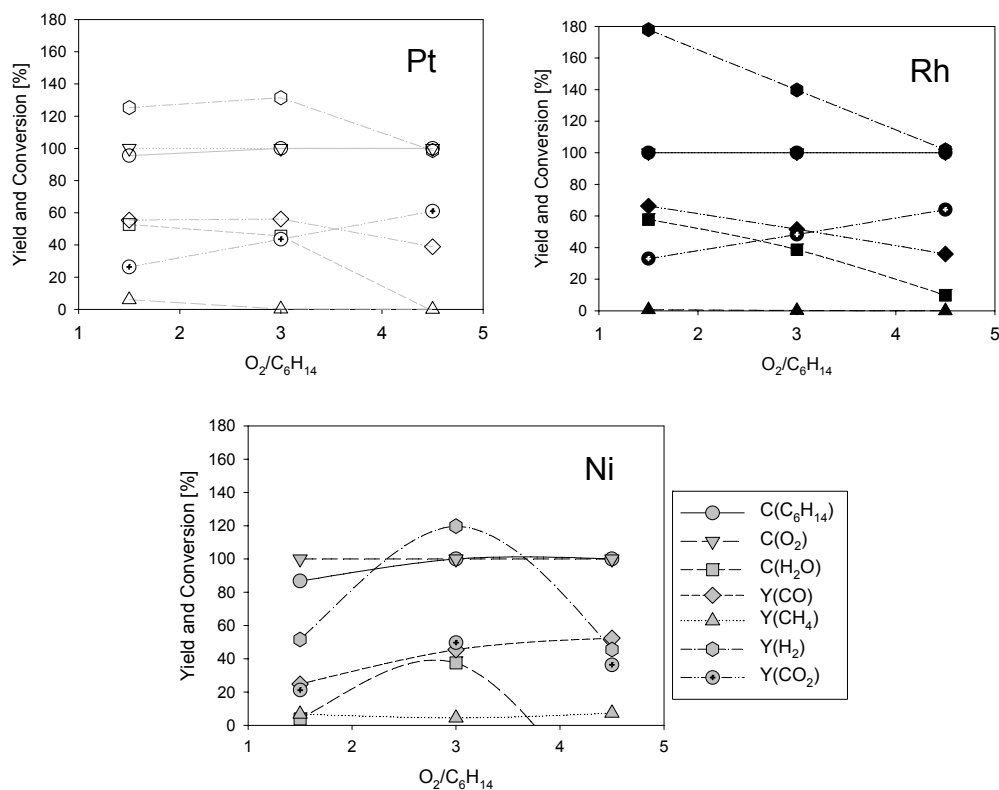


Figure 4.8: Conversions and yields as function of O_2/C_6H_{14} ratio for Pt, Rh and Ni supported on Al_2O_3 monoliths ($800^\circ C$, $C_6H_{14}/H_2O = 1/7$, WHSV of $2.7 h^{-1}$, total flow 200 ml/min).

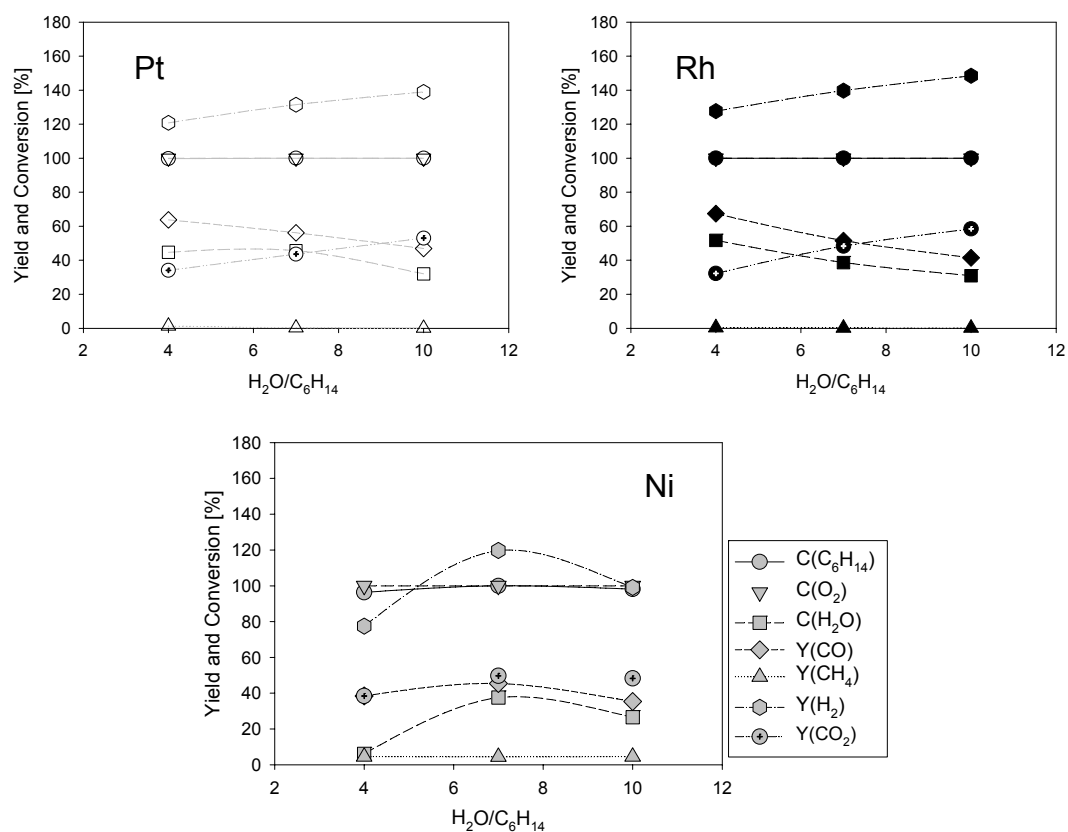


Figure 4.9: Conversions and yields as function of H_2O/C_6H_{14} ratio for Pt, Rh and Ni supported on Al_2O_3 monoliths ($775^\circ C$, $C_6H_{14}/O_2 = 1/3$, WHSV of $2.7 h^{-1}$, total flow 200 ml/min).

Lowering the oxygen concentration ($C_6H_{14} / O_2 = 1/1.5$) in the following step was expected to increase the yield of hydrogen (shift of the thermodynamic equilibrium) and therefore to lead to nickel re-reduction. In contrast to these expectations, the hexane conversion decreased to 87% producing a high amount of a hydrocarbon mixture (34% yield of C_{2+} - not shown) besides yields of 24.8% CO, 21.2% CO_2 , 6.8% CH_4 and 51.6% H_2 .

This is speculated to be an effect of both nickel in the oxidized state and coke deposition on the surface. Oxidation (oxygen/ C_6H_{14} ratio 4.5) first leads to inactive Ni^{2+} , then promotes formation of carbonaceous deposits in the following experiment of the sequence depicted in Table 4.1. Increasing the water/ C_6H_{14} ratio from 7 to 10 (and the O_2/C_6H_{14} ratio from 1.5 back to 3) improved the activity of the nickel catalyst again. At a hexane conversion of 98.2% the yields of H_2 (99.1%) and CO_2 (48.3%) increased, while the yield of C_{2+} decreased to 10% and CH_4 yield (4.5%) was equal to that observed for the initial conditions. Decreasing the water to hexane ratio to 4 led to a slight decrease in hexane conversion (96.3%) and an increase of C_{2+} hydrocarbons yield (15%). It is interesting to note that despite the increase in the conversion of water (after changing the water/ C_6H_{14} ratio from 10 to 4) the yield of H_2 decreased to 77.5%.

In order to prove that Ni supported on Al_2O_3 monoliths is partially oxidized by a feed rich in oxygen ($C_6H_{14} / O_2 / H_2O = 1 / 4.5 / 7$), a separate catalytic test was performed in which the activity and product distribution were monitored during 5h time-on-stream (TOS). The results (see Fig. 4.10) show that steady state was reached after 165 min TOS, i.e., after a time span longer than that normally elapsing between change of the feed composition and analysis of the reaction stream. Before reaching the steady state, the H_2 yield increased from 60% to 106% and the CO_2 yield from 40% to 68%. This trend is attributed to the preferential oxidation of metallic nickel to Ni^{2+} ($NiAl_2O_4$). The color of the catalyst after the test confirmed this interpretation, the first third of the catalytic bed in the direction of the flow had the typical blue color associated with $NiAl_2O_4$ while the remainder was still grey.

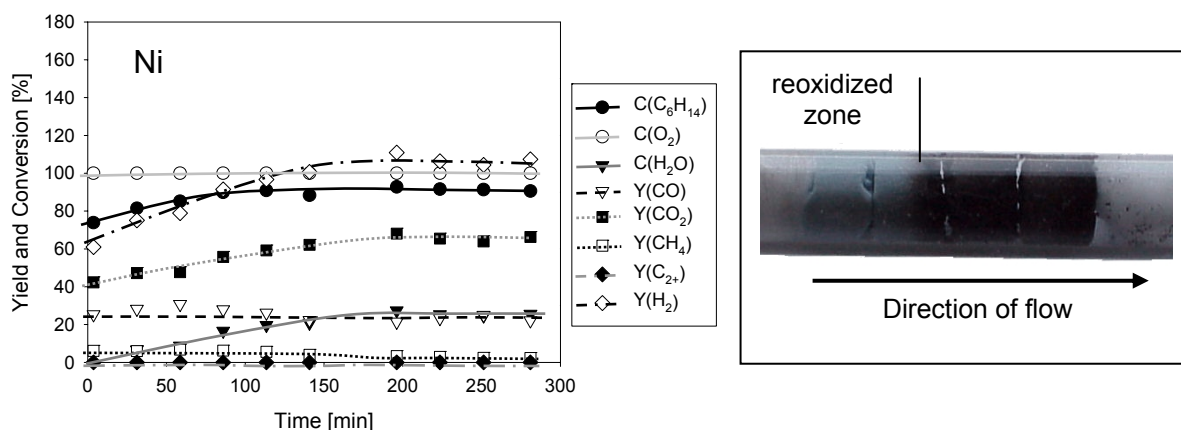


Figure 4.10: a) Catalytic activity of Ni supported on Al₂O₃ monoliths vs. time at C₆H₁₄/O₂/H₂O = 1/4.5/7 (775°C, WHSV 2.7 h⁻¹, total flow 200 ml/min). b) View of the same catalyst after 5h time-on-steam.

Figures 4.11a and b show the reactivity results after performing separately the same experiments summarized in Table 4.1 with fresh portions for the Ni catalyst (reduced *in situ* at 800°C for 2h). Except for C₆H₁₄/O₂/H₂O = 1/4.5/7 (as previously discussed), all reactions were in steady state right from the beginning. The trends observed resemble those for Rh catalyst and follow the thermodynamic equilibrium. However incomplete conversion of hexane (97.7%) was observed also for the lowest H₂O/C₆H₁₄ ratio explored (H₂O/C₆H₁₄ = 4). Simultaneously, methane was detected (yield 0.9%). A possible explanation for incomplete conversion of hexane could be the deposition of carbonaceous deposits on the active sites. This hypothesis was confirmed by TPO measurements (Table 4.3). Around 4 wt% of C was deposited on the catalyst.

With the rhodium catalyst the formation of carbonaceous deposits was not observed even for oxygen or water-lean conditions. On platinum only a small amount of carbonaceous deposits with H/C ratio of around 3 was detected (CH₃-species, possibly remaining from hexane dissociation (α -scission)). These deposits could be easily oxidized at temperature between 270 and 670 °C. In contrast on Ni/Al₂O₃ (after the sequential change of feed composition) a significant amount of deposits (2.9 wt%) was observed. These species were characterized by a low H/C ratio (about 1) and were removed at relatively high temperatures (400-800 °C). After performing the changes in feed composition separately in single experiments on fresh Ni-Al₂O₃, carbon deposition was observed after 5 h TOS only for H₂O/C₆H₁₄ ratio 4. In this

case only carbon was formed. It was removed in oxygen/helium atmosphere between 600 °C and 770 °C.

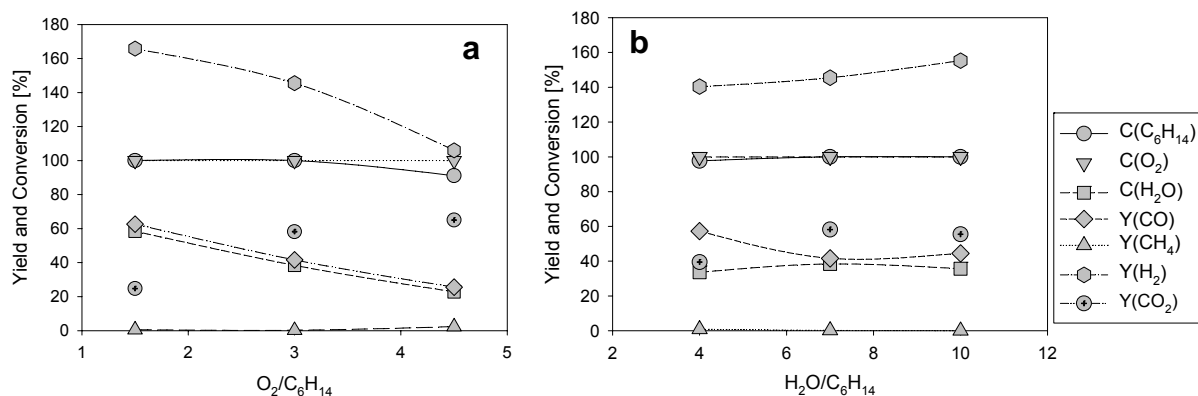


Figure 4.11: Catalytic activity of Ni supported on Al₂O₃ monoliths depending on **a)** O₂/C₆H₁₄ ratio (C₆H₁₄/H₂O = 1/7) and **b)** H₂O/C₆H₁₄ ratio (C₆H₁₄/O₂ = 1:3). (T=775°C, WHSV 2.7 h⁻¹). For each feed composition a portion of fresh catalyst was used. The data are referring to 5h time-on-stream.

Table 4.3: Carbon deposition during reaction calculated from TPO experiments.

Catalyst	Carbon deposited [wt%]	H/C ratio	TPO temperature interval [°C]
Ni/γ-Al ₂ O ₃	2.88	1.06/1.00	400-800
Ni/γ-Al ₂ O ₃ ^a	4.09	Only C	600-770
Pt/γ-Al ₂ O ₃	0.84	2.93/1.00	270-670 (2 peaks)
Rh/γ-Al ₂ O ₃	-	-	-

^a Single experiment performed on fresh catalyst with C₆H₁₄ : O₂ : H₂O = 1:3:4.

4.3.3 Effect of reaction temperature on catalytic activity (ratio hexane/oxygen/water=1/3/7)

The effect of decreasing reaction temperature (T≤800 °C) on the catalytic performance in autothermal reforming was investigated only on Pt and Rh supported on Al₂O₃ monoliths. The behavior of the corresponding Ni catalyst was not further studied due to its strong deactivation (by oxidation and carbonaceous deposit formation) observed at 775 °C.

With Pt/Al₂O₃ the conversion of hexane (Fig. 4.12a) started from 40% at 500 °C and increased with temperature to full conversion above 750 °C. Water conversion started above 680 °C, at temperature below water was macroscopically produced (conversion ~40% at 500 °C). Oxygen, in contrast, was fully consumed over the whole temperature range. High selectivity (Fig. 4.12c) towards cracking products (a mixture of C₂ and higher hydrocarbons) was observed with a maximum of 20% at 650 °C. Only traces of methane, however, were produced at low temperatures. The selectivity towards hydrogen increased exponentially with increasing temperature from 2.2% to 132 %, at 500 °C and 800 °C, respectively. The same trend was observed for carbon monoxide, increasing from 5.3 % at 500 °C to 55% at 800 °C. On the other hand, CO₂ selectivity decreased from 90% at 500 °C to 45% at 800 °C.

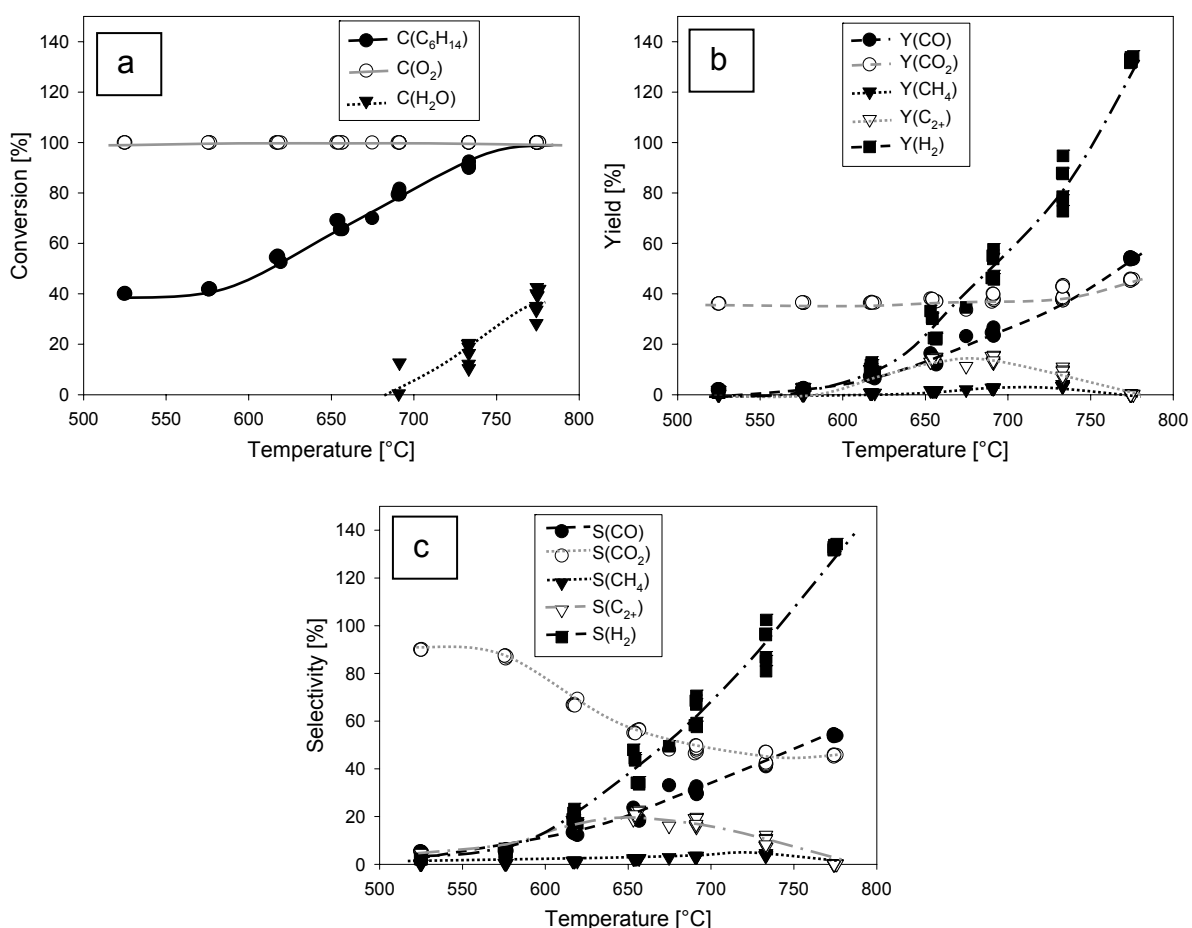


Figure 4.12: (a) Conversions of hexane, water and oxygen: (b) yields and (c) selectivity vs. reaction temperature on Pt supported on Al₂O₃ monoliths (C₆H₁₄ : O₂ : H₂O : Ar = 1:3:7:29, WHSV of 2.7 h⁻¹, total flow 200 ml/min).

The rhodium based catalyst showed very high activity for hexane and water conversion (Fig. 4.13a) and high selectivity to H₂ (Fig. 4.13c). Full conversion of

hexane was achieved above 550 °C, starting from 95% at 530 °C. The conversion of oxygen was complete over the whole temperature range. The conversion of water started from around 15% at 530 °C, increased to 40% until 650 °C and then decreased again to 35% at 800 °C (limited by thermodynamic constraints). The yields and selectivities observed corresponded to the thermodynamic equilibrium with a maximum yield of hydrogen at 650 °C (140%). The production of methane decreased from 22% at 530 °C to 0% at temperatures above 650 °C. Cracking products were not observed.

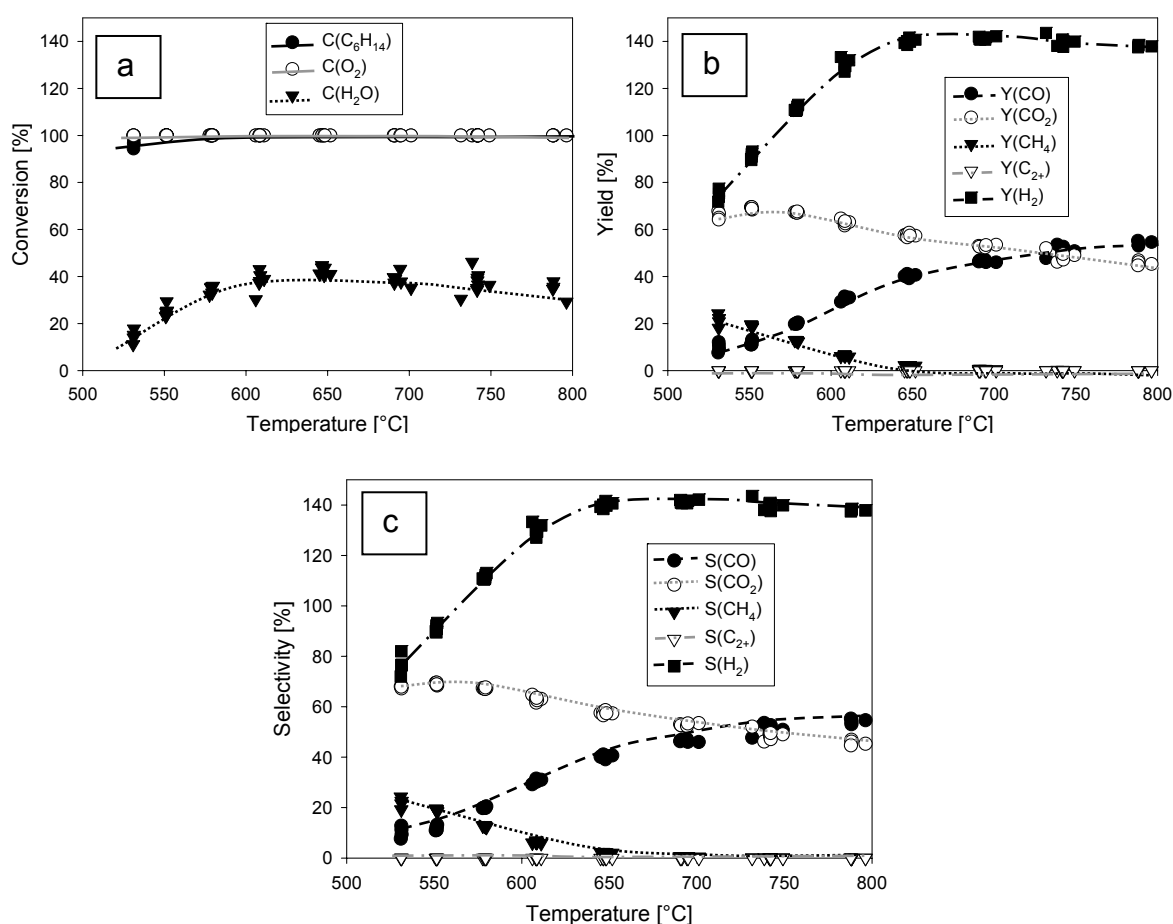


Figure 4.13: (a) Conversions of hexane, water and oxygen; (b) yields and (c) selectivity vs. reaction temperature on Rh supported on Al₂O₃ monoliths (C₆H₁₄: O₂: H₂O : Ar = 1:3:7:29, WHSV of 2.7 h⁻¹, total flow 200 ml/min).

The effect of reaction temperature was also investigated for an industrial catalyst that, according to the patent literature ⁷, contains mainly Rh as noble metal (ratio Rh/Pt from 20/1 to 2/1 wt/wt). As expected, the commercial catalyst showed a

behavior similar to that of the Rh catalyst prepared in this study, *i.e.*, high activity in hexane and water conversion (Fig. 4.14a) and high selectivity to hydrogen (Fig. 4.14c). Full conversion of hexane was achieved above 550 °C, starting from 50% at 510°C. Conversion of oxygen was complete over the whole temperature range. The conversion of water started from around -12% at 510 °C, increased until 600 °C to 40% and decreased again to 30% at 800°C. This trend was close to the thermodynamic equilibrium at temperatures above 550°C. At 500 °C the catalyst showed a high selectivity to combustion products as water was produced and CO₂ selectivity reached 77%. In the temperature range from 530 °C to 620 °C a plateau in CO₂ selectivity (60%) was observed. CO selectivity decreased slightly while CH₄ selectivity (maximum 10% at 565 °C) increased. Above 620°C yields and selectivities followed thermodynamic calculations showing a maximum yield of hydrogen at approximately 650 °C. Cracking products were not observed.

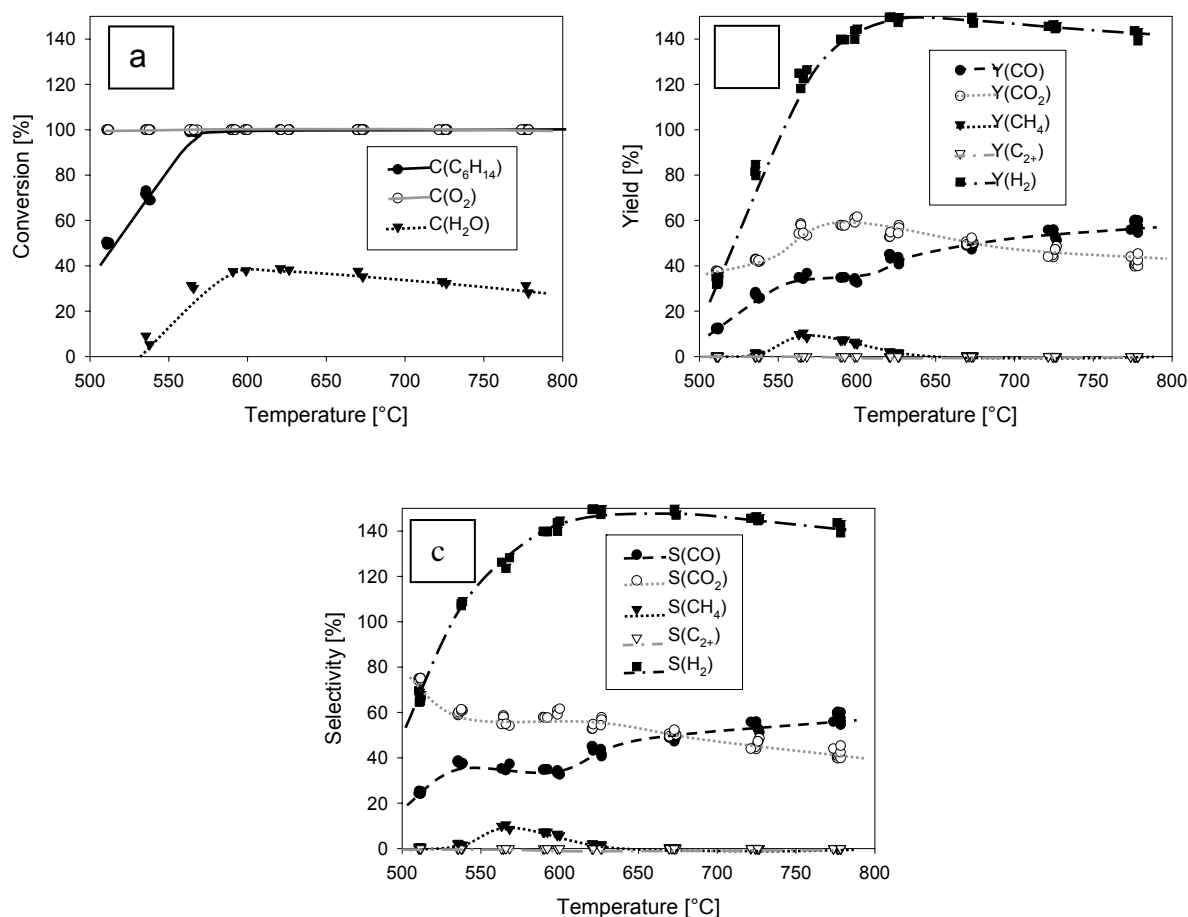


Figure 4.14: (a) Conversions of hexane, water and oxygen; (b) Yields and (c) selectivity vs. reaction temperature on the industrial catalyst Umicore A-Type ($C_6H_{14} : O_2 : H_2O : Ar = 1 : 3 : 7 : 29$, WHSV of 2.7 h^{-1} , total flow 200 ml/min).

4.4 Discussion

Under the standard reaction conditions for autothermal reforming chosen in this study (775°C, hexane : oxygen : water : argon = 1:3:7:29, total flow 200 ml/min), the catalytic performance of Pt and Rh supported on γ -Al₂O₃ monolith was stable after short time on stream (not more than 10 minutes). On the other hand Ni supported on γ -Al₂O₃ monolith needed around 300 minutes to reach stable product distribution. This behaviour is attributed to slow changes in the oxidation state of nickel from Ni²⁺ to Ni⁰ under reaction conditions. This seems at first not possible, as after *ex situ* reduction, the XDR peak corresponding to the precursor NiAl₂O₃ disappeared. However, indirect evidence strongly points to the presence of Ni²⁺ we collected other evidences for the presence of Ni²⁺ in the reduced catalyst. First of all, during the induction period the yield of hydrogen increased continuously. Second, we observed a strong effect of the duration of the *in situ* reduction (reduction within the reforming reactor) on the catalytic performance, i.e., when the *in situ* reduction was extended from 2 hours to 5 hours, the initial transient period decreased from 230 minutes to 30 minutes.

The oxidation state of Ni was a decisive factor in determining the product distribution. Thus, during the initial induction period, the presence of Ni²⁺ induced high selectivity towards cracking products and low CO₂ selectivity. As the reduction from Ni²⁺ to Ni⁰ proceeded, the yield of cracking products decreased. The opposite trend was observed for CO₂. Finally, when Ni was completely reduced (steady state), the yield of hydrogen increased to the thermodynamic equilibrium, while the cracking products are not observed.

Under oxygen rich conditions (C₆H₁₄/O₂ = 1/4.5) Ni deactivates due to re-oxidation to Ni²⁺. Similar results are reported in literature^{8,9,10}. The deactivation manifests itself by the drastic decrease of the hydrogen yield and the formation of combustion and cracking products. Once Ni is oxidized, formation of (mainly olefinic) cracking products leads to carbon deposition (shown by TPO) further accelerating deactivation. Deactivation by coke occurs also with Pt in oxygen lean conditions (C₆H₁₄/O₂ = 1/1.5) again with cracking products being the coke precursors.

Unlike Pt and Ni, Rh/Al₂O₃ tends not to form carbonaceous deposits as reported¹¹ and proven by TPO analysis of the used catalysts. An option to reduce the carbon deposition on Ni could be the addition of alkali metal. Additionally it has

been reported that the controlled passivation of the catalyst with sulfur can reduce the carbon deposition¹².

The effect of the reaction temperature on product distribution in presence of Pt and Rh catalysts was more evident, when these metals were supported on Al₂O₃ monolith instead that on Al₂O₃ powder. Although the Pt content (4.2 wt%) was more than twice that of Rh (1.7 wt%) (molar ratio per g catalyst Pt / Rh = 1.3), for Pt the conversion of hexane and water was much lower. However it is to note that Pt sintered slightly during reduction at 800°C (for 2 h) forming particles with an average diameter of 44 nm (from TEM and H₂-chemisorption analysis) and resulting in low dispersion (2.3%). This is in agreement with the report of van den Brink *et al.*¹³. The authors show that the dispersion of a 2 wt% Pt/ γ -Al₂O₃ decreased progressively with increasing calcination temperature from 47% at 500 °C to 20% at 600 °C, reaching 7.3% at 700 °C and finally to 3.2% at 800 °C.

On the contrast the supported Rh catalyst was resistant to sintering during reduction, thus, maintains an average particle size of about 7 nm, corresponding to 17% dispersion. However the difference in particle size does not seem to be the major cause for the lower activity over Pt (40% conversion of n-hexane) compared to Rh (95% conversion) under the same reaction conditions (500°C, C₆H₁₄/O₂/H₂O = 1/3/7). In fact in Chapter 3 it has been shown that even though Pt has had a smaller particle size than Rh (<1 nm for Pt, 3.2 nm for Rh) and the content of the metal is the same (1wt% over γ -Al₂O₃ powder, resulting in comparable dispersion), Pt exhibited a much lower activity at 500°C. Therefore the nature of the metal and not just the extent of the accessible metal surface seems to be the feature determining factor for high activity.

Pt enhances combustion below 800°C and shows low activity in steam reforming. Thermal and catalytic cracking are observed as side reactions. While the catalyst based on supported Pt converts hexane fully above 750°C its activity was much lower than that of Rh/Al₂O₃. The activity of Pt strongly depends on the feed gas composition. High activity was obtained for oxygen/hexane ratio higher than 1.5 and a water/hexane ratio higher 4. At oxygen/hexane ratio 1.5 and water/hexane ratio 4 the conversion of hexane dropped below 100% enhancing the production of methane and C₂₊. This easily led to carbonaceous deposition (H/C ratio of around 3) on the catalyst proved after the experiment (see Table 4.1).

Large differences are also observed in the ability to convert water, which indicates that Rh is more active for steam reforming than Pt. The product distribution over Rh follows the thermodynamic limitation. Thus, the presented results suggest that Rh is the preferred catalyst component for the autothermal reforming of hexane. This conclusion is supported by the relatively high selectivity of Pt based materials towards cracking and combustion products ¹⁴, which in turn accelerates catalyst deactivation.

The industrial ATR catalyst showed nearly the same results as Rh/ γ -Al₂O₃. This was not surprising as the main noble metal component of the industrial catalyst seems to be Rh. The additional presence of minor amount of Pt seems not have effect at high temperatures (thermodynamic regime). However at low temperatures (500°C) the selectivity towards combustion products was higher compared to Rh/ γ -Al₂O₃. The plateau in CO₂ selectivity observed between 530°C and 620°C seems to be related to the presence of Pt.

4.5 Conclusions

Rhodium supported on γ -Al₂O₃ monoliths has the highest activity and selectivity to synthesis gas. Moreover, its performance is stable even when the feed was oxygen- or water-lean. Pt supported on γ -Al₂O₃ monoliths is also active but more sensitive to low oxygen/hexane ratios. Under these conditions the activity decreases, leading to lower H₂ production and some carbonaceous deposits. Ni supported on γ -Al₂O₃ monoliths is easily deactivated by oxidation under oxygen rich conditions and shows severe coke deposition. Moreover, the Ni catalyst needs longer reduction time - compared to Rh and Pt - to minimize the time required to reach steady hexane conversion. Therefore, Ni supported on γ -Al₂O₃ monoliths is concluded to be not a suitable for mobile application. Rh exhibited excellent performance in the autothermal reforming of hexane over the whole temperature range investigated (500-800 °C). At temperatures lower than 750 °C Rh and the industrial catalyst (Umicore A-Type) were more active than Pt with higher selectivity towards H₂ and CO. Over Pt mainly combustion took place at low temperatures (<570 °C). At intermediate temperatures (570 - 750°C) cracking products were observed, that easily could deactivate the catalyst. A further drawback of the Pt catalyst is the low metal dispersion (Pt clusters of 44 nm) after reduction at high temperatures. Therefore, among the metal studied (Pt, Rh, Ni) Rh proved to be the most suitable noble metal for steam reforming in the presence of oxygen (autothermal reforming conditions).

4.6 References

- (1) Opoku-Gyamfi, K.; Adesina, A. A. *Applied Catalysis A-General* **1999**, *180*, 113.
- (2) Matsuo, Y.; Yoshinaga, Y.; Sekine, Y.; Tomishige, K.; Fujimoto, K. *Catalysis Today* **2000**, *63*, 439.
- (3) Courson, C.; Magaka, E.; Petit, C.; Kiennemann, A. *Catalysis Today* **2000**, *63*, 427.
- (4) Asadullah, M.; Ito, S.; Kunimori, K.; Tomishige, K. *Industrial Engineering and Chemical Research* **2002**, *41*, 4567.
- (5) Pena, M. A.; Gomez, J. P.; Fierro, J. L. G. *Applied Catalysis A-General* **1996**, *144*, 7.
- (6) Vergunst, T.; Kapteijn, F.; Moulijn, J. A. *Applied Catalysis A-General* **2001**, *213*, 179.
- (7) Ahlborn, R.; Baumann, F.; Wieland, S. Verfahren zur autothermen, katalytischen Dampfreformierung von Kohlenwasserstoffen. In *Patent EP 1157968*; OMG AG & Co. KG, Hanau, 2001.
- (8) Dissanayake, D.; Rosynek, M. P.; Kharas, K. C. C.; Lunsford, J. H. *Journal of Catalysis* **1991**, *132*, 117.
- (9) Huszar, K.; Racz, G.; Szekely, G. *Acta Chimica Acad. Sci. Hung.* **1971**, *70*, 287.
- (10) Torniainen, P.; Chu, X.; Schmidt, L. D. *J. Catal.* **1994**, *146*, 1.
- (11) Clarke, S. H.; Dicks, A. L.; Pointon, K.; Smith, T. A.; Swann, A. *Catalysis Today* **1997**, *38*, 411.
- (12) Rostrup-Nielsen, J. R. *Catalysis Today* **1993**, *18*, 305.
- (13) van den Brink, R. W.; Krzan, M.; Feijen-Jeurissen, M. M. R.; Louw, R.; Mulder, P. *Applied Catalysis B-Environmental* **2000**, *24*, 255.
- (14) Ehwald, H.; Kürschner, U.; Smejkal, Q.; Lieske, H. "Investigation of Different Catalysts for Autothermal Reforming of i-Octane (Poster)"; Innovation in the Manufacture and Use of Hydrogen, 2003, Dresden.

Kinetic parameters for the autothermal reforming of n-hexane on Al₂O₃-supported Rh catalysts

Abstract

The autothermal reforming of n-hexane was studied over three Al₂O₃-supported Rh catalysts: 1 wt% Rh/ γ -Al₂O₃ powder, 1.7 wt% Rh/ γ -Al₂O₃ monoliths and an industrial catalyst containing also Pt. The influence of the hexane flow rate in a temperature range of 500-800 °C and the effect of steam/hexane and oxygen/hexane ratios at selected temperatures were studied. An attempt has been made to classify the products in primary, secondary and tertiary products.

Additionally, hydrogenolysis of n-hexane was investigated as an option to increase the methane content in the off-gas of the reformer for SOFC application.

5.1 Introduction

As shown in Chapter 4 (pages 72-74), under the standard conditions ($C_6H_{14} : O_2 : H_2O : Ar = 1 : 3 : 7 : 29$, $WHSV=2.7 \text{ g}_{C_6H_{14}}/h \cdot g$) a temperature of $550 \text{ }^\circ\text{C}$ is already sufficient to obtain full n-hexane conversion in autothermal reforming over Rh-containing Al_2O_3 monolithic catalysts.

However, higher temperatures seem to be desirable for the following reasons. First, in order to reduce the volume of the catalyst used in the reformer for fuel cell mobile application, it can be convenient to perform the reforming at temperatures above $550 \text{ }^\circ\text{C}$, also accepting a not complete n-hexane conversion. Second, the reformer could be operated at a temperature close to that of the SOFC ($\sim 800 \text{ }^\circ\text{C}$), thus simplifying the heat management of the entire system (reformer and fuel cell treated as a so-called “hot box”). Additionally, based on the experimental results described in Chapter 4 (pages 73/74), the maximum yield of hydrogen was attained at $650 \text{ }^\circ\text{C}$. On the contrary, temperatures lower than $650 \text{ }^\circ\text{C}$ would be preferred to produce more CH_4 . By closely coupling the endothermic methane steam reforming and the exothermic electrochemical oxidation within the fuel cell (SOFC), the quantity of air needed to maintain the fuel cell at $800 \text{ }^\circ\text{C}$ can so be reduced. If desired, the methane yield could be increased by hydrogenolysis of small amount of n-hexane added to the off-gas from the autothermal reformer. This reaction (hydrogenolysis of hexane) could be catalyzed by the same Al_2O_3 -supported Rh catalyst used for autothermal reforming.

Based on the above considerations, we tested Rh- Al_2O_3 - catalysts in n-hexane autothermal reforming in the temperature range $500\text{-}850 \text{ }^\circ\text{C}$. The main difficulty for obtaining kinetic parameters was the high n-hexane conversion observed also in absence of catalyst in this temperature range (between 10 and 100% depending on residence time). Pant *et al.*¹ reported a similar observation for pyrolysis of n-heptane and methylcyclohexane at temperatures between 680 and $800 \text{ }^\circ\text{C}$.

The basic kinetic equations for hydrocarbon autothermal reforming were published by Pacheco *et al.*² studying isooctane reforming on Pt/ CeO_2 in a packed micro-reactor. These authors reported that a Langmuir Hinshelwood-Hougen-Watson approach

$$r = \frac{k_A P_{C_nH_m}}{(1 + (k_A / k_r K_W)(P_{H_2} / P_{H_2O}) P_{C_nH_m} + K_{H_2O}(P_{H_2O} / P_{H_2}) + \sqrt{K_{H_2} P_{H_2}})^2} \quad (5.1)$$

where P_i is the partial pressure of the species i , $K_{\text{H}_2\text{O}}$ the dissociative adsorption constant of water, K_{H_2} the adsorption constant for hydrogen, k_A the reaction rate constant for the hydrocarbon chemisorption, and k_r the reaction rate constant for the reaction between adsorbed C1-species and chemisorbed oxygen produced from water dissociation describes adequately the observed conversion and yields. This equation ² was based on the mechanism proposed by Rostrup-Nielsen ³ for steam reforming. A basic assumption leading to an important simplification in this mechanism was a sequence of α -scissions of the carbon-carbon bonds resulting only in C₁-species. Another important assumption was the implicit enhanced adsorption of steam due to the inverse spillover from the support to the active metal site (see Chapter 2 section 2.4.3). Therefore the surface of the active metal was may be covered by water ² because of the possibly strong metal-support interaction and/or the direct activation of steam by the active metal. Furthermore, to derive equation 5.1 it was assumed that the surface concentration of heavier hydrocarbons chemisorbed on dual sites ($\text{C}_n\text{H}_z\text{-}^*2$, in our case * represents Rh) and the reversibility of all the reactions involving hydrocarbons were negligible. Activated oxygen (O-^*) was assumed to be the most abundant reaction intermediate.

Keiski and coworkers ^{4,5} developed the following rate expression (power-law type) for the water-gas-shift (WGS) reaction:

$$r_{\text{WGS}} = k_{\text{WGS}} C_{\text{CO}}^n C_{\text{H}_2\text{O}}^m C_{\text{CO}_2}^p C_{\text{H}_2}^q (1 - \beta_{\text{WGS}}) \quad (5.2)$$

where C_i is the molar concentration of species i and β_{WGS} is the reversibility factor that accounts for the approach to chemical equilibrium:

$$\beta_{\text{WGS}} = \frac{C_{\text{CO}_2} C_{\text{H}_2}}{K_{\text{T}} C_{\text{CO}} C_{\text{H}_2\text{O}}} \quad (5.3)$$

K_{T} is the equilibrium constant. The reaction kinetics for the WGS reaction has been studied for a wide range of catalysts and temperatures ^{4,5}. Depending on the temperature range and catalyst used the kinetic parameters and reaction orders of reactants and products in Eq. (5.2) change.

5.2 Catalytic Experiments

Three Rh-containing catalysts were tested in autothermal reforming of n-hexane. Two of these catalysts were prepared in our laboratory using $\gamma\text{-Al}_2\text{O}_3$ powder or monoliths as support (see Chapter 3, page 35 and Chapter 4, page 57). The third catalyst was provided by Umicore. It contains Pt and Rh, supported on Al_2O_3

monoliths (Umicore A-Type “AC 009 – EXP”, cell density of 600 cpsi, quadratic channels). The properties of these catalysts are compiled in Table 5.1.

Before reaction the catalysts were reduced *in situ* at 800 °C for 2h.

The reactivity tests on the Rh catalyst supported on γ -Al₂O₃ powder were performed in a quartz tubular micro reactor with an inner diameter of 4 mm (outer diameter 6 mm) using the setup described in Chapter 3 (pages 36 and 37). The laboratory catalyst supported on Al₂O₃ monoliths was tested in a quartz tubular reactor with an inner diameter of 6 mm (outer diameter 8 mm). The industrial catalyst was cut to fit into this reactor.

The stream entering the reactor contained n-hexane, oxygen, water and argon (as diluent). The total flow was kept constant at 200 ml/min unless otherwise specified. The effect of the ratios oxygen/hexane and water/hexane as well as the effect of the hexane flow rate were studied one by one.

The performance of powder and monolithic catalysts was studied at different weight hourly space velocities (WHSV in h⁻¹), calculated according to the following formula:

$$\text{WHSV} = \frac{\text{Hexane[g]}}{\text{Catalyst[g]} \cdot \text{Time[h]}}$$

The reaction products were analyzed by on-line chromatography as described in Chapter 3 (pages 36 and 37). A mass spectrometer was used to detect hexane (m/z = 57), H₂O (m/z = 18 and 17), O₂ (m/z = 32), CO (m/z = 28), CO₂ (m/z = 44), CH₄ (m/z = 14 to 16), H₂ (m/z = 2) and Ar (m/z = 40).

Table 5.1: Characterization of Al₂O₃-supported Rh catalysts.

Material	Noble metal content [wt%]	Specific Surface Area [m² g⁻¹]	Acid Site Concentration^a [mmol g⁻¹]	Metal Particle Size (TEM) [nm]	Metal Dispersion^b [%]	Metal Particle size^b [nm]	Metal Surface Area [m² g_{Rh}⁻¹]
Rh/γ-Al ₂ O ₃ (P) ^c	1	138	0.016	3 (red.)	34	3	151
Rh/γ-Al ₂ O ₃ (M) ^d	1.7	140	0.064	7 (red.)	17	7	75
Umicore A-Type	Rh: 0.1 to 2 [Rh:Pt 20:1 to 2:1 (wt:wt)] ⁶	46	n.d.	n.d.	n.d.	n.d.	n. d.

^a From ammonia TPD

^b Calculated from chemisorption according to literature (ref 5)

^c Al₂O₃ powder

^d Al₂O₃ monoliths

5.3 Results and Interpretation

Preliminary reactivity tests were performed in order to study the thermal conversion of n-hexane in the temperature range 500 – 800 °C. A mixture hexane/oxygen/water/argon with molar ratio 1 : 3: 7 : 29 and total flow 160 ml/min was fed into the reactor filled with crashed quartz or kept completely empty. These two arrangements were devised to produce a shorter and a longer residence time of the feed, respectively. The results are represented in Fig. 5.1 and Fig 5.2.

In absence of catalyst, already at the lowest temperature investigated (500 °C) hexane was partially converted. For short residence times and temperatures between 500 and around 630 °C only thermal cracking of hexane (10% conversion) occurred leading a mixture of short chain hydrocarbons, mainly C₃ and C₄. For longer residence time, already at 500 °C n-hexane was converted (50% conversion) not only to cracking products (selectivity to C₂₊ fraction 70% up to approximately 600 °C) but also to CO (20%), CO₂ (10%) and small amount of H₂ (1%) and CH₄ (0.5%).

For short residence time the conversion of n-hexane increased to full conversion at 750 °C. Simultaneously O₂ conversion increased up to 100% and water was produced (negative conversion -20%), the main products being CO, C₂₊, H₂, CH₄ and CO₂ with selectivity at 800°C of 58, 23, 25, 15 and 5%, respectively. The selectivity towards cracking products slightly decreased to 95% at 680°C and then it dropped to 20% at 800°C, with ethylene as main hydrocarbon besides ethane and some longer chain hydrocarbons. Also for longer residence times the conversion of hexane increased with temperature from 50% at 500 °C up to full conversion at 650 °C, resulting in the same product distribution observed for short residence time.

These experiments show that, under the chosen temperature and flow conditions, in presence of the catalyst it is not possible to perform the reaction in differential regime (hexane conversion lower than 10%), which is necessary for a rigorous kinetic study. Nonetheless, it is important to get kinetic parameters for scale-up the catalytic autothermal reforming process that works at thermodynamic equilibrium⁷.

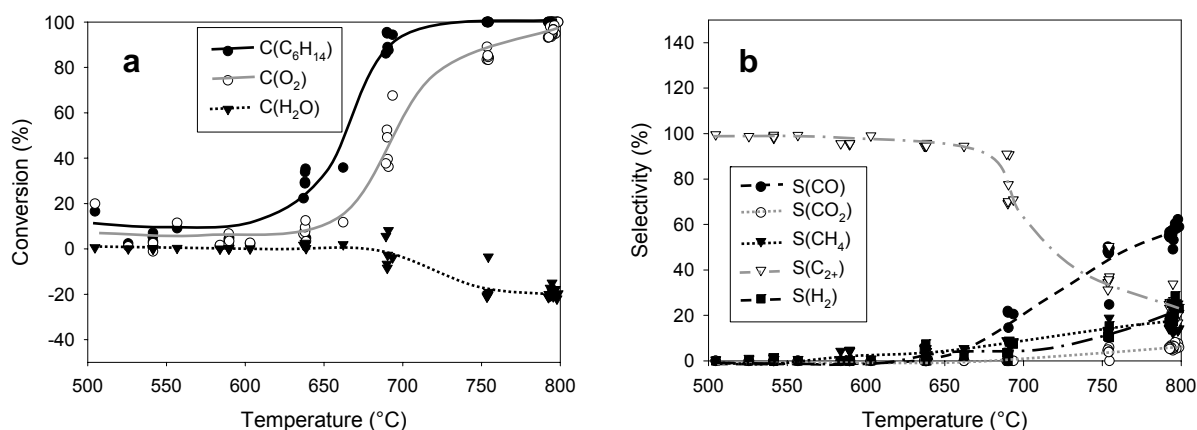


Figure 5.1: Conversion (a) and selectivity (b) in non-catalytic n-hexane autothermal reforming vs. reaction temperature (Reactor filled with crashed quartz; feed $C_6H_{14}/O_2/H_2O/Ar = 1:3:7:29$, total flow 160 ml/min, $P = 1$ bar).

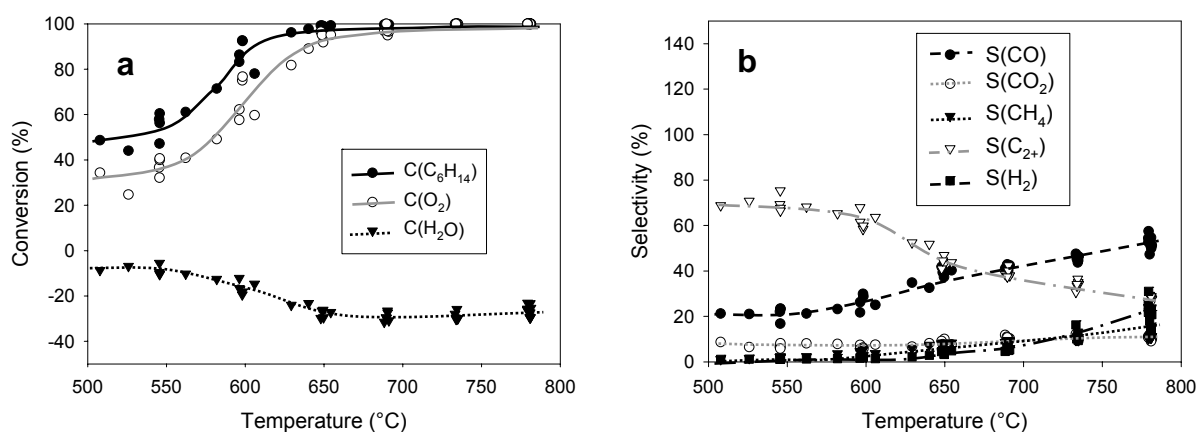


Figure 5.2: Conversion (a), and selectivity (b) in non-catalytic n-hexane autothermal reforming vs. reaction temperature (Empty reactor; feed $C_6H_{14}/O_2/H_2O/Ar = 1:3:7:29$, total flow 160 ml/min, $P = 1$ bar).

5.3.1 Variation of WHSV

When the reformer has to be coupled with a fuel cell for mobile application, its volume should be quite small and the catalyst should be able to work in a wide range of space velocities. The effect of different space velocities on the reforming catalyst has to be investigated with respect to the two main parameters that can affect the overall performance of the reformer/fuel cell system that is the n-hexane conversion and the product composition. Additionally, changes in product selectivity with space velocity allow gaining insight into reaction mechanism by classifying the products in kinetically primary, secondary and tertiary products. This in turn is a requirement for implementing the reaction in simulation programs.

5.3.1.1. *Rh/γ-Al₂O₃ (M)*

The influence of the catalyst bed length for Rh/γ-Al₂O₃ (M) was investigated at constant flow and composition of the feed (200 ml/min, molar ratio C₆H₁₄/O₂/H₂O/Ar 1:3:7:29) in the temperature range 500-850 °C. Over the whole temperature range investigated and for all catalyst bed lengths the oxygen conversion was 100% and no C₂₊ species were observed.

As shown Fig. 5.3, at temperatures between 500 and 620 °C, the higher the catalyst amount the higher was the hexane conversion. At around 500 °C, it increased from 85% for a reactor length of 0.57 cm (86.2 mg) to 95% for a reactor length of at least 1.40 cm (223.8 mg). In this temperature interval (500-620 °C), the selectivities to H₂ (~110%), CO (~27%) and CH₄ (~12%) were not influenced markedly by the reactor length in the range 0.57-1.40 cm. The selectivity to CO₂ (61%) and the conversion of water (20%) - not shown - were constant. Only at a reactor length of 2.09 cm (389 mg) - and therefore longer contact time - a significant change was observed. The H₂ and CO selectivities decreased to 70% and 10%, respectively, while the selectivities of CH₄ and CO₂ increased to 20% and 68%, respectively. These values and the lower conversion of water (10%) correspond to thermodynamic equilibrium values. In spite of the reactor length, at temperatures higher than 620 °C the hexane conversion and the selectivity of all compounds converged to the thermodynamic equilibrium values (see Chapter 2, page 20).

In Fig. 5.4 the n-hexane conversion and the selectivities to the main products are displayed vs. WHSV at 650°C. Only slight changes were observed, i.e., H₂ and CO selectivities increased, whereas the selectivity to CO₂ decreased and CH₄ was found to be constant.

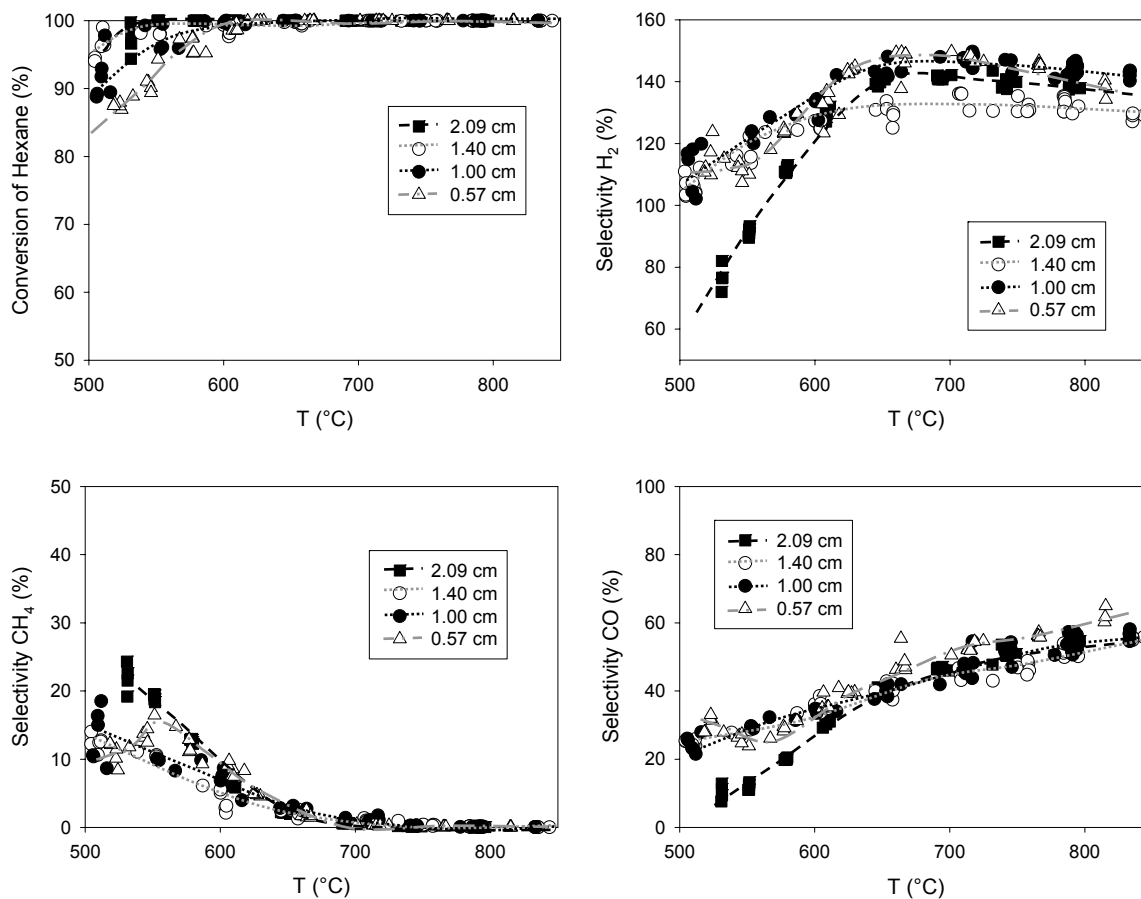


Figure 5.3: Rh/ γ -Al₂O₃ (M): conversion of hexane and selectivities to H₂, CH₄ and CO at different catalyst bed lengths (corresponding SV 20300 h⁻¹, 30300 h⁻¹, 42400 h⁻¹, 74500 h⁻¹) vs. reaction temperature (feed: total flow 200 ml/min, molar ratio C₆H₁₄/O₂/H₂O/Ar 1:3:7:29).

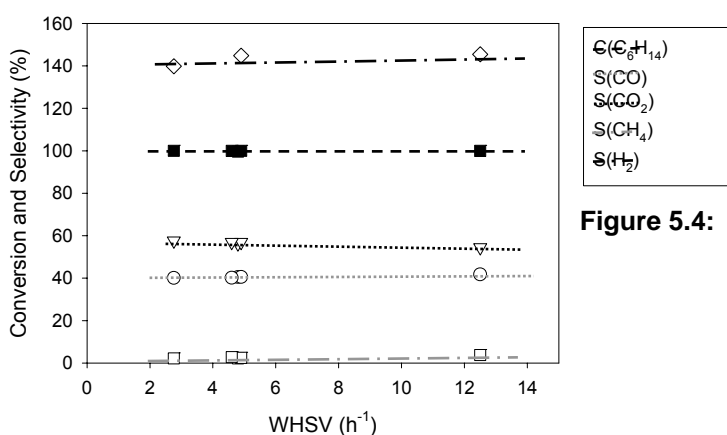


Figure 5.4: Rh/ γ -Al₂O₃ (M): conversion of hexane and selectivity to CO, CO₂, CH₄ and H₂ at a reactor inlet temperature of ~650°C for different WHSV (feed: total flow 200 ml/min, molar ratio C₆H₁₄/O₂/H₂O/Ar 1:3:7:29).

5.3.1.2 Umicore A-Type

The influence of the reactor length on the performance of the industrial monolithic catalyst was investigated under the same conditions employed for the laboratory catalyst (feed: 200 ml/min, molar ratio $C_6H_{14}/O_2/H_2O/Ar$ 1:3:7:29). Oxygen consumption was complete over the whole temperature range (500 - 850 °C). At 500 °C (reactor inlet temperature) a non-uniform trend in the conversion of hexane was observed (see Fig. 5.5). In fact the n-hexane conversion first increased from 62 to 80% when the reactor length increased from 0.89 to 1.50 cm (from 94.7 to 188.7 mg), then it decreased to 52% for a further increase of the reactor length (3.55 cm corresponding to 396.5 mg). At 500 °C for 3.55 cm bed catalyst length the conversion of hexane was unexpectedly low. In this context it should be mentioned that in the corresponding experiment we were obliged to set a furnace temperature much lower than that normally used for similar experiments in order to keep the temperature of the top of the catalyst bed at 500°C. We speculate that, for reason still not clarified, exothermic reactions (combustion) occurred to a larger extent at the inlet of the catalyst. In the range 550-650 °C the conversion of hexane clearly depends on the catalyst amount: the longer the monolith, the higher the conversion. Above 650 °C hexane conversion was always complete.

With the exception of the 1.50 cm catalyst bed length, the selectivity to H_2 (Fig. 5.5) followed almost the thermodynamic equilibrium in the temperature range 500-850 °C. It started at ~80% at 500 °C, increased to a maximum of ~150% at 675 °C and then decreased slightly to 140%. For the catalyst bed length of 1.50 cm the H_2 selectivity started from 105% at 500°C and did not further increase until 570 °C. Then it reached the thermodynamic equilibrium value at 610 °C.

For all reactor lengths the CH_4 selectivity (Fig. 5.5) passed through a maximum shifting from 560°C (long contact time) to 590 °C (short contact time). The corresponding values of the maximum were 18% and 7%, respectively. On the contrary the CO selectivity (Fig. 5.5) passed through a minimum shifting from 560 °C (23%, long contact time) to 650 °C (50%, short contact time). At temperatures higher than 650 °C the thermodynamic equilibrium was reached. Only C_{2+} traces could be detected at low temperature (<650 °C).

In Fig. 5.6 the n-hexane conversion and selectivities to the main products are displayed vs. different WHSV, obtained by changing the mass of the catalyst at

constant hexane flow (Fig. 5.6a) or by changing the hexane flow at constant catalyst amount (Fig. 5.6b).

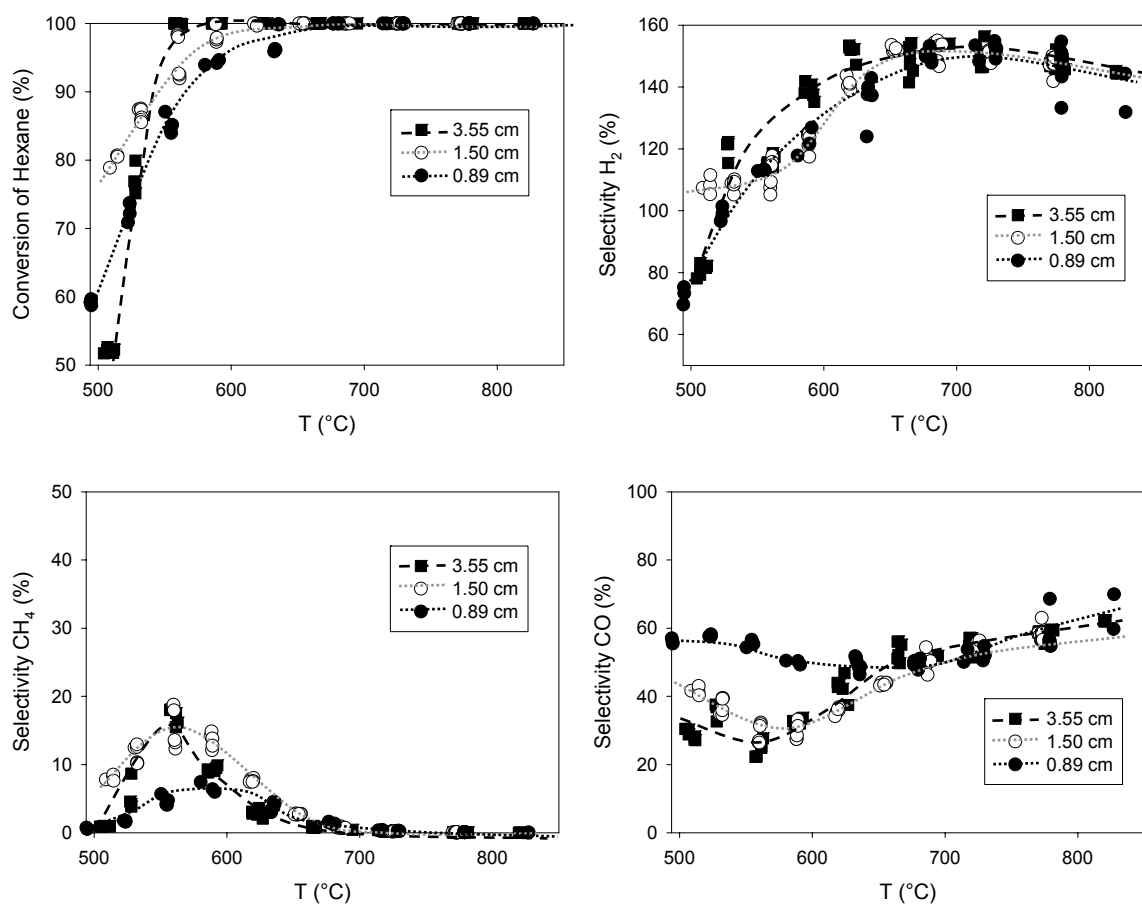


Figure 5.5: Umicore A-Type catalyst: conversion of hexane and selectivities to H₂, CH₄ and CO at different catalyst bed lengths (corresponding SV 12000 h⁻¹, 28300 h⁻¹, 47700 h⁻¹) vs. reaction temperature (feed: total flow 200 ml/min, molar ratio C₆H₁₄/O₂/H₂O/Ar 1:3:7:29).

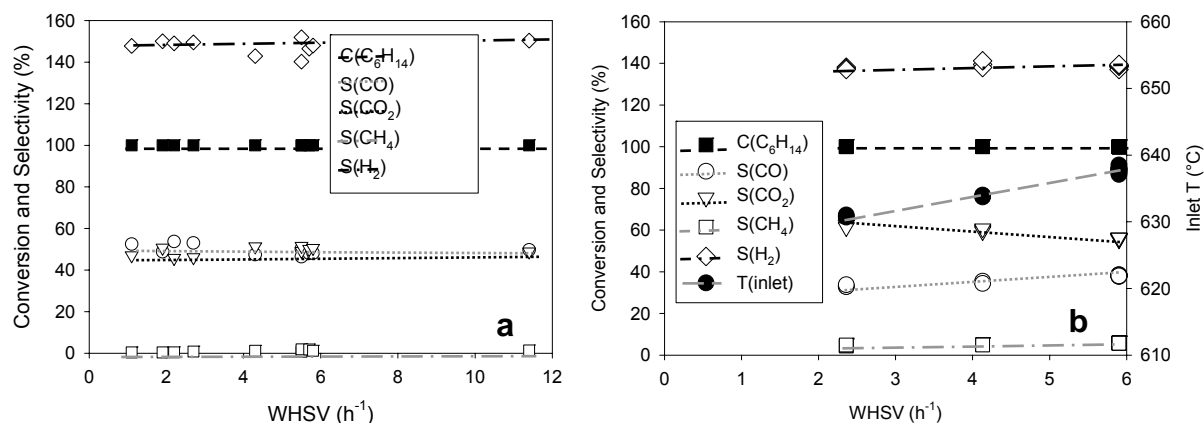


Figure 5.6: Umicore A-Type catalyst: conversion of hexane and selectivities to CO, CO₂, CH₄ and H₂ for different WHSV: **a)** reactor inlet temperature ~680°C, constant hexane flow, variable catalyst bed length and **b)** constant catalyst bed length, variable hexane flow (furnace temperature 650°C). For all experiments the molar ratio C₆H₁₄/O₂/H₂O/Ar was 1:3:7:29.

At 680°C the product distribution was not affected by changes of WHSV (obtained by variation of the catalyst bed length at constant feed flow; Fig. 5.6a). However, when different WHSV were obtained by variation of the hexane flow (at constant feed composition and at constant catalyst length), the product distribution changed (Fig. 5.6b). This can be explained by the increase of the catalyst temperature (at parity of furnace temperature), with increasing feed flow, as shown in Fig. 5.6b for the temperature at the top of the catalytic bed. Thus, higher temperatures shifted the product distribution according to the expected thermodynamic equilibrium. The increase of the temperature with increasing hexane flow is due to the exothermicity of the overall reaction.

The autothermal reforming could be shifted from exothermic to endothermic or thermo-neutral conditions by changing either the ratio of hexane/oxygen or the ratio hexane/steam. In both cases the selectivities to CH₄, H₂ and CO will change. If the stream leaving the autothermal reformed has to be fed to a SOFC, all these three products can undergo reactions at the anode. However, as already discussed in Chapter 2 (pages 19 to 20), the total number of electron produced in the anodic reactions per mol of hexane converted in the ATR, is constant only if the ratio hexane/oxygen remains constant. On the other hand changes of temperature and of water/hexane ratio do not affect the energy output of the SOFC.

5.3.1.2.1 Partial poisoning with sulfur (hexane containing 10 ppm S)

The effect of sulfur containing hydrocarbons was tested on the industrial catalyst from Umicore by adding thiophene to fed hexane up to 10 ppm sulfur. The initial idea behind this experiment was to partially poison the catalyst to reduce hexane conversion enabling kinetic measurements (without carbonaceous deposits⁸). However it was not possible to reach this goal due to the non-catalytic reaction (see paragraph 5.3). Nevertheless, the results obtained from the experiment performed with thiophene are important as in the real feed it is realistic to assume the presence of at least 10 ppm sulfur to be present.

Fig. 5.7 compares the catalytic performance in presence and absence of sulfur at around 780 °C versus time-on-stream. Under the chosen conditions, oxygen and hexane were fully converted. While for pure hexane the product distribution corresponded to the thermodynamic equilibrium, the addition of sulfur led to a different distribution. During the first 80 min time-on-stream the H₂ selectivity decreased linearly from 150% to 110%, while CH₄ selectivity increased from 0% to 10%. The CO and CO₂ selectivity changed from 43% and 57% to 47% and 43%, respectively. Afterwards this product distribution remained unchanged. These results show that sulfur blocked some of the noble metal sites.

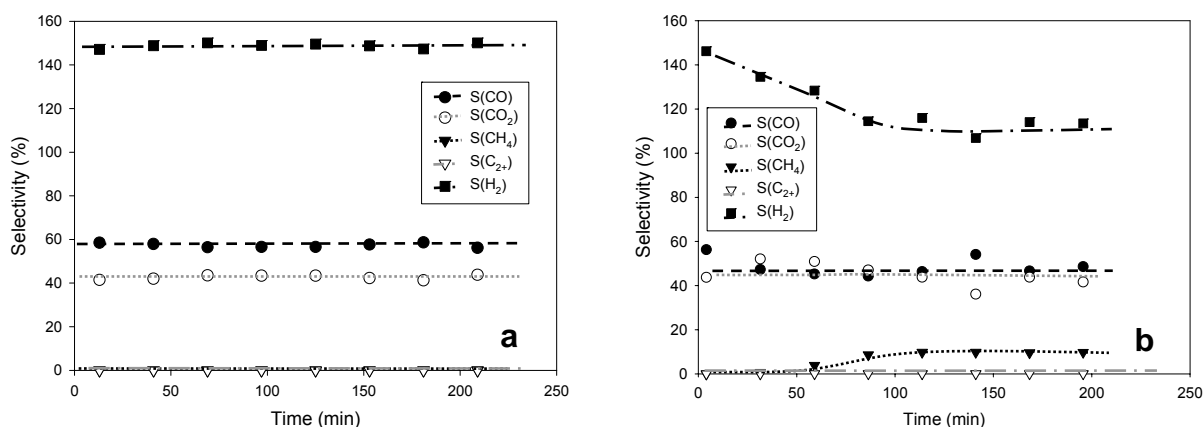


Figure 5.7: Product selectivity for Umicore A-Type catalyst vs. time on stream **a)** hexane without S, temperature 770°C and **b)** hexane containing 10 ppm S, temperature 790°C. WHSV: 5.5 h⁻¹; C₆H₁₄/O₂/H₂O/Ar 1:3:7:29. The conversion of C₆H₁₄ was complete.

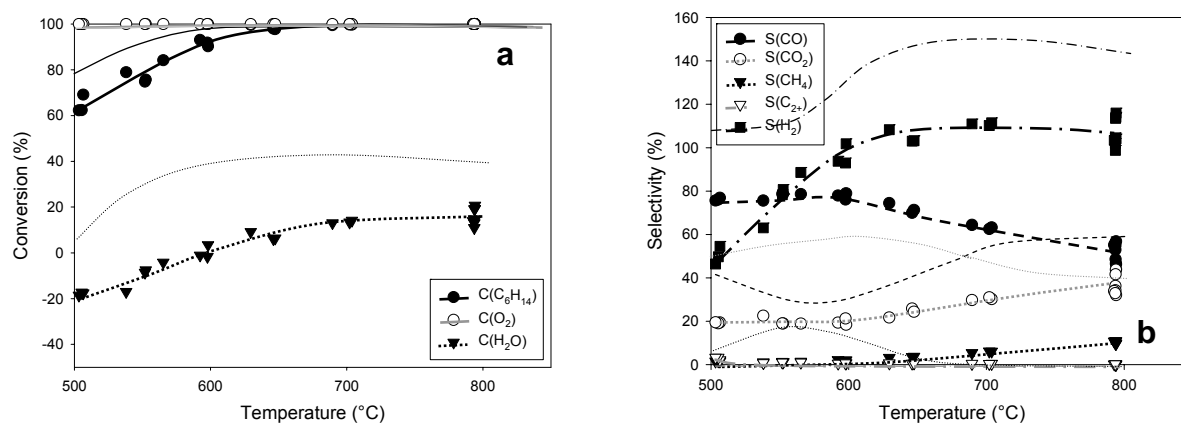


Figure 5.8: a) Conversion and b) product selectivity for Umicore A-Type catalyst vs. temperature in presence of sulfur (thick lines, 10ppm S in hexane) or in absence of sulfur (thin lines).

WHSV: 5.5 h⁻¹, C₆H₁₄/O₂/H₂O/Ar 1:3:7:29.

The effect of sulfur was also investigated at different reaction temperatures by keeping constant the other reaction conditions (WHSV = 5.5 h⁻¹, total flow= 200 ml, molar ratio C₆H₁₄/O₂/H₂O/Ar 1:3:7:29). As shown in Fig. 5.8, in presence of sulfur the conversion of hexane at 500 °C was 60% instead of 80% and the full hexane conversion was reached at higher temperature, i.e., at 660 °C instead of 600 °C. While the conversion of oxygen was not affected by poisoning with sulfur, the ability of the catalyst to convert water was strongly reduced and water was produced (negative conversion) until 600 °C. Even at higher temperatures (800 °C) the conversion of water was lower than 20%. As a consequence the H₂ selectivity was much lower in presence of sulfur. On the other hand the selectivity to CO was higher with value close to 80% between 500 °C and 600 °C. At higher temperatures the CO selectivity decreased even if from the thermodynamic equilibrium and measurements without sulfur the opposite trend of increasing CO selectivity was observed. An unexpected trend was also observed for CO₂ and CH₄, those selectivities increased with increasing temperature. Besides at 500 °C a mixture of higher hydrocarbons species (C₂₊) was detected (up to 3.3% selectivity).

5.3.1.3 Rh/γ-Al₂O₃ (P)

As the monolithic catalysts (1.7wt% Rh/γ-Al₂O₃ M and Umicore A-Type) cannot be cut into shorter pieces (as they would easily break) and it was not possible to increase the total flow (the maximum WHSV reached was 14 h⁻¹), the shortest

contact time achieved was 0.0755 s. Under so long contact time probably it, is not possible to detect the first intermediate products (primary products). Therefore to gain insight into the reaction mechanism a powdered catalyst with lower Rh amount (1wt% Rh/ γ -Al₂O₃ (P)) was tested in autothermal reforming of n-hexane at 650 °C under high space velocities (10 and ~50 times higher than those tested for monolithic catalysts). As shown in Table 5.2, the WHSV ($g_{C_6H_{14}}/g_{cat} \cdot h$) was changed from the standard value of 53.7 h⁻¹ by changing, one by one, the catalyst amount or the hexane flow. The composition of the feed was kept constant (molar ratio C₆H₁₄/O₂/H₂O/Ar 1:3:7:29). The effect of WHSV on catalytic performance is shown in Fig. 5.9. An influence of mass transfer on secondary and primary reaction was tested by changing the catalyst loading and keeping the gas flow constant. As the results did not exhibit variations in the rate or selectivity an influence of mass transfer on secondary and primary reaction products is excluded.

Table 5.2: Weight hourly space velocity (WHSV = $g_{C_6H_{14}}/g_{cat} \cdot h$) in autothermal reforming on Rh/ γ -Al₂O₃ (P) (constant bed height: 14 mm).

WHSV (h ⁻¹)	Catalyst amount (mg)	SiC (mg)	Flow rate of hexane (mL/min)	Total flow rate (mL/min)
53.7	20.0	300	5.0	200
256	4.2	315	5.0	200
537	20.1	300	50.0	2000

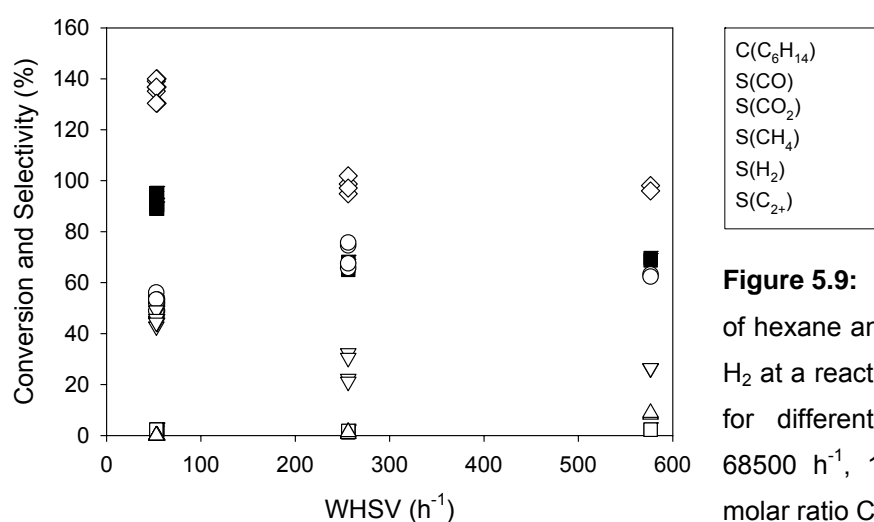


Figure 5.9: Rh/ γ -Al₂O₃ (P): conversion of hexane and yields of CO, CO₂, CH₄ and H₂ at a reactor inlet temperature of ~650 °C for different WHSV (corresponding SV 68500 h⁻¹, 142000 h⁻¹, 685000 h⁻¹, feed molar ratio C₆H₁₄/O₂/H₂O/Ar 1:3:7:29).

In both experiment corresponding to high WHSV (256 and 537 h⁻¹) the conversion of hexane decreased significantly from 95% to approximately 65%. The

H₂ and CO₂ selectivities decreased from 140 to 100% and from 50 to 30%, respectively, while the CO selectivity increased. CH₄ increased slightly from 1% (WHSV of 53.7 h⁻¹) to 1.5% (WHSV of 256 h⁻¹) and 2.3% (WHSV of 537 h⁻¹). C₂₊ was not detected for a WHSV of 53.7 h⁻¹, but its selectivity increased from 1.0% at WHSV 256 h⁻¹ to 8.6% at WHSV 537 h⁻¹. This trend can be interpreted considering C₂₊ and CH₄ as primary products. C₂₊ and CH₄ selectivities were much lower compared to non-catalytic experiments (see Fig. 5.1 and 5.2), while CO, H₂ and CO₂ selectivities were higher.

5.3.2 Variation of O₂/C₆H₁₄ and H₂O/C₆H₁₄

The effect of feed composition was studied at three different temperatures (500 °C, 650 °C and 700 °C) for the three Al₂O₃-supported Rh-containing catalysts (Rh/γ-Al₂O₃ (P), Rh/γ-Al₂O₃ (M) and Umicore A-Type). For each temperature three sets of catalytic tests were performed and in each experiment the total flow was kept constant at 200 ml/min balancing it with Ar. In the first set of experiments the O₂/C₆H₁₄ ratio was changed from the standard value 3/1 keeping constant at 7/1 the H₂O/C₆H₁₄ ratio while in the second one the ratio O₂/C₆H₁₄ was maintained constant at 3/1 and the ratio H₂O/C₆H₁₄ changed. In both of these two series of experiments the C₆H₁₄ flow was maintained constant at 5ml/min corresponding to a WHSV of 53.5h⁻¹. With these experiments we also tested the stability of the catalysts under steam reforming (no oxygen fed) and partial oxidation conditions (no steam fed), each set of reaction conditions being maintained for 2h time-on-stream. In the last series of experiments the flows of oxygen and water were kept constant to 15 and 35 ml/min, respectively, while the C₆H₁₄ flow was changed from the standard value of 5 ml/min thus obtaining different WHSV. For every set of catalytic experiments, the first test was always performed under our standard conditions (C₆H₁₄/O₂/H₂O/Ar =1:3:7:29, 5ml/min C₆H₁₄) then the highest ratio respect to standard conditions was set. Finally, this ratio was progressively lowered up to pure partial oxidation or pure steam reforming conditions. The typical product distribution obtained from these tests is depicted in Fig. 5.10 for Rh/γ-Al₂O₃(P) (reaction temperature 650 °C). For the other two catalysts, Rh/γ-Al₂O₃(M) and Umicore A-Type, similar trends in the product distribution were observed, while the activity was higher.

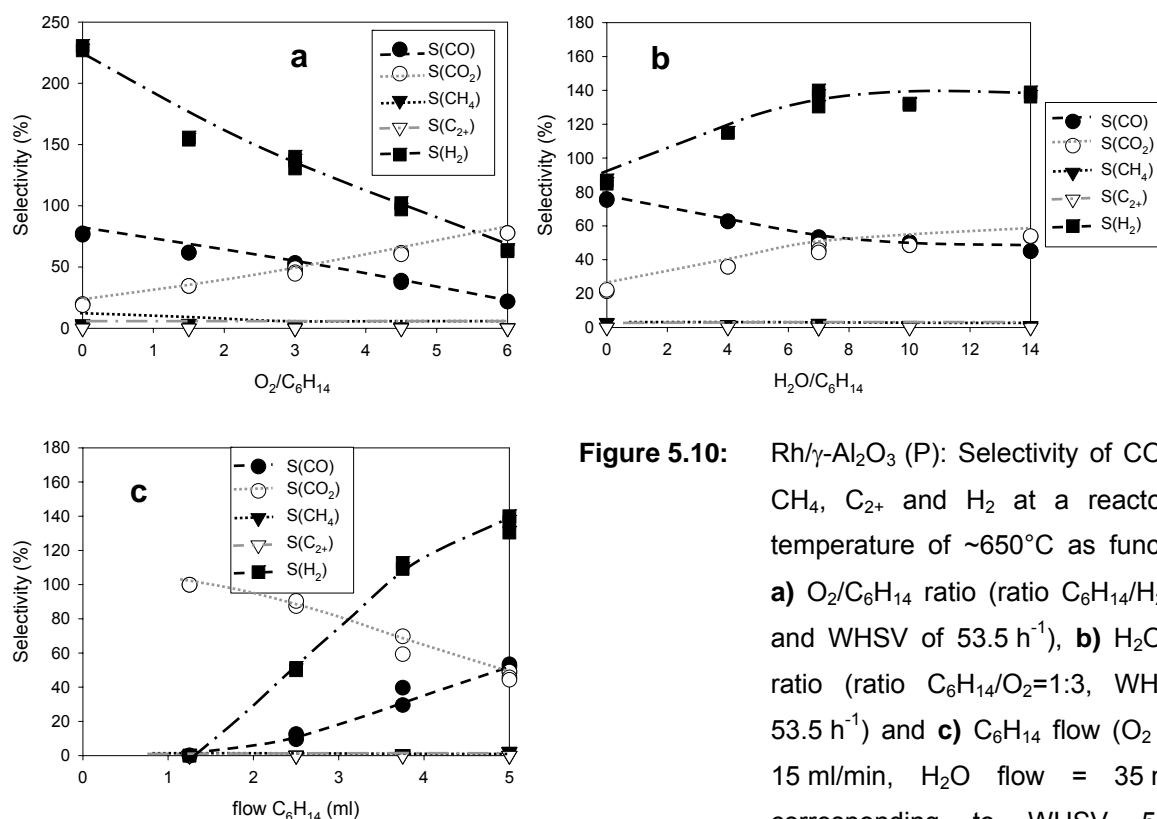


Figure 5.10: Rh/ γ -Al₂O₃ (P): Selectivity of CO, CO₂, CH₄, C₂₊ and H₂ at a reactor inlet temperature of $\sim 650^\circ\text{C}$ as function of **a)** O₂/C₆H₁₄ ratio (ratio C₆H₁₄/H₂O=1:7 and WHSV of 53.5 h⁻¹), **b)** H₂O/C₆H₁₄ ratio (ratio C₆H₁₄/O₂=1:3, WHSV of 53.5 h⁻¹) and **c)** C₆H₁₄ flow (O₂ flow = 15 ml/min, H₂O flow = 35 ml/min) corresponding to WHSV 53.5 h⁻¹, 40.1 h⁻¹, 26.8 h⁻¹ and 13.4 h⁻¹.

The selectivity of all products changes linearly with the O₂/C₆H₁₄ ratio as expected from thermodynamic calculations (see Chapter 2). The lower the oxygen/hexane ratio the higher the selectivity to H₂, CO and CH₄. With the decreasing of the H₂O/C₆H₁₄ ratio starting from 7, the selectivities to H₂ and CO₂ linearly decreased, while the CO selectivity increased. For H₂O/C₆H₁₄ higher than 7 no remarkable changes on selectivities were observed. Deactivation due to variation of the ratios H₂O/C₆H₁₄ and O₂/C₆H₁₄ with respect to the standard conditions (H₂O/C₆H₁₄ = 7 and O₂/C₆H₁₄ = 3) was not observed. Lowering the hexane ratio shifted the equilibrium to the combustion products CO₂ and water (not shown). The selectivities to H₂ and CH₄ selectivity decreased to zero for a hexane ratio of 0.25.

The reaction order in n-hexane was determined at three different temperatures (500 °C, 600 °C and 650 °C) for the three catalysts (Rh/ γ -Al₂O₃ (P), Rh/ γ -Al₂O₃ (M) and Umicore A-Type) (see Table 5.3). The apparent rate constants with respect to n-

hexane or water were calculated for a temperature range of 500 °C to 650°C and various reaction conditions as:

$$k_i = \frac{F}{W} \cdot \ln \left[\frac{1}{\left(1 - \frac{X_i}{X_{i,eq}}\right)} \right] \quad (5.4)$$

where F is the flow rate of i (mol min^{-1}), W the catalyst mass (g), X the conversion of i and X_{eq} the equilibrium conversion of i . The apparent activation energies were calculated from the Arrhenius form as

$$k_i = k_{i,0} \cdot \exp\left(\frac{-E_{a,i}}{RT}\right) \quad (5.5)$$

Table 5.3: Reaction orders for C_6H_{14} , O_2 and H_2O

Catalyst	E_a (kJ mol^{-1}) ^a		T (°C)	Reaction order
	C_6H_{14}	H_2O		C_6H_{14} ^b
1 wt% Rh/ γ - Al_2O_3 (P)	33	29	500	1
	to	to	600	1
	50	160	650	1
1.7 wt% Rh/ γ - Al_2O_3 (M)	29	3	500	1
	to	to	600	1
	160	20	650	1
Umicore A-Type	55	12	500	1
	to	to	600	1
	172	36	650	1

^a The activation energy was invariant with changes in the feed composition, but varied with the retention time.

^b Reaction order for the hexane consumption.

5.3.3 Oscillations during autothermal reforming

During autothermal reforming of hexane, at temperatures between 500 and 800 °C and for different hexane/oxygen/water ratios, oscillations in product

concentration were observed in the MS signals of the off-gas. In Figure 5.11 is reported a representative example of oscillations observed over the Umicore A-Type catalyst at around 640 °C for a ratio hexane/oxygen/water 1/3/7. Over Rh/ γ -Al₂O₃ (M) the same phenomenon was observed. In general, peaks of CO and CH₄ correspond to minima in H₂, CO₂ and H₂O. Simultaneously the temperature increases. The amplitudes of the oscillation increased with increasing WHSV, but did not alter with temperature. The amplitudes of H₂ and CO₂ peaks changed with the steam/hexane and oxygen/hexane ratio in the same manner as the product selectivity changed. The lower the oxygen/hexane ratio for example the higher the amplitude of the hydrogen oscillation.

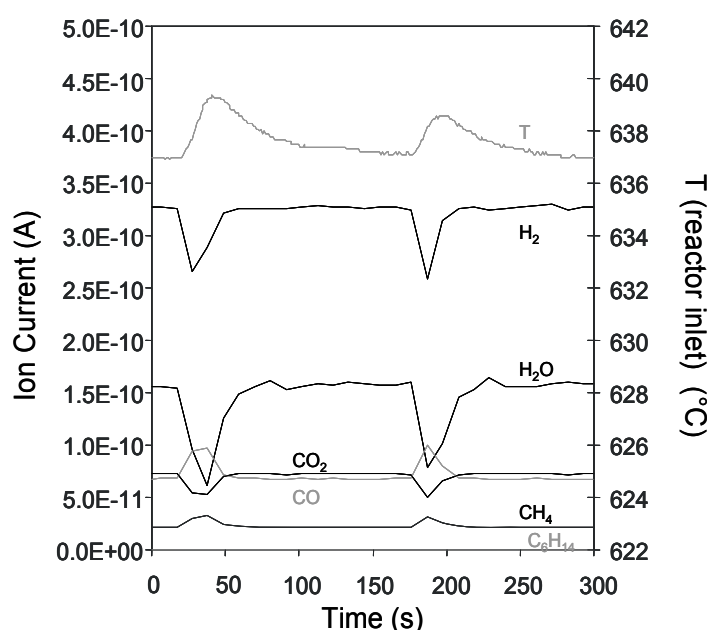


Figure 5.11: Oscillations over Umicore A-Type catalyst: WHSV of 5.9 h⁻¹, S/C = 1.2 and O/C = 1 (time resolution 10 s).

Oscillation phenomenon is mainly reported for CO oxidation in literature (e.g. ⁹, ¹⁰, ¹¹) and explained with cyclic changes in the oxidation state of the surface. Oscillations were also observed and explained for methanol oxidation over copper/oxygen systems ¹² and partial oxidation of methane over Pd⁰ (foils and wires) or Ni foils ^{13,14}. In general oscillations are not always fully understood. Here, it should be only mentioned that this phenomenon was observed but no attempt was made to get a complete explanation.

5.3.4 Discussion

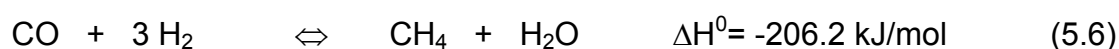
For the autothermal reforming of hexane several generic reaction pathways have to be considered including catalytic and thermal cracking, partial

oxidation, steam reforming and many side reactions described in detail in Chapter 2 (pages 13-16). Two reaction schemes have been proposed to explain partial oxidation of a hydrocarbon to CO and H₂. Some authors consider that hydrocarbon undergoes combustion followed by both steam reforming and carbon dioxide reforming. The other mechanism is based on the catalytic pyrolysis of the hydrocarbon followed by hydrogen desorption and carbon oxidation^{2, 15}. Combustion route can be assumed if a relatively high amount of CO₂ is present in the reformat in the early stages of the reaction. Primary and secondary reaction products were distinguished by variation of catalyst loadings at a constant gas flow. Generally the occurrence of CO and H₂ before all oxygen is converted is considered an indication of direct partial oxidation¹⁸.

From the non-catalytic experiments described at page 84 and 85 it is evident that already at low temperature gas phase reactions of hexane, i.e., cracking and combustion are possible. Complete conversion of hexane can be attained without catalyst at high temperatures (above 750 °C). Thus, it can be concluded that over catalysts only mass transfer limitation of n-hexane dominates at temperatures above 750 °C. Hydrogen, methane, carbon monoxide and carbon dioxide were already present as products of gas-phase reactions in significant concentrations at temperatures above 650 °C. As the selectivity of these products increased over Rh catalysts, and water was converted, these catalysts seem to play a major role on the kinetics of steam reforming and water-gas-shift reaction. The oxidation reactions, which can occur simultaneously in the gas phase and on the catalyst surface, are considered to be very fast compared to the reforming reactions.

The variation in product selectivity with catalyst bed length (and therefore with space velocity) at low temperatures (500-650 °C) for monolithic catalysts (Rh/γ-Al₂O₃ (M)) allows to conclude that CO and H₂ from partial oxidation of hexane and from steam reforming are primary product with respect to CO₂ and CH₄. The results for the low temperature region (500-550 °C) are compared in Table 5.4 with the Umicore catalyst including the experiment with sulfur-containing feed. However, it has to be noted that for practical reasons the experiments with monolithic catalysts were carried out at relatively low space velocities (WHSV not higher than 14h⁻¹). On the contrary for powdered catalyst (Rh/γ-Al₂O₃ (P)) it was possible to reach much higher space velocities. At 650°C and WSHV higher than 53.7 h⁻¹ (see Fig. 5.9) cracking

products were observed indicating that the first step of the reaction is pyrolysis and/or cracking with C_{2+} species as fast reacting intermediates and therefore not rate limiting (see also the results for determination of reaction orders). Over Rh/ γ -Al₂O₃ (M) (Fig. 5.4) and Umicore A-Type (Fig. 5.6) the WHSV was much lower (longer contact time) and traces of C_{2+} species were hardly observed. Based on the result from Rh/ γ -Al₂O₃ (P) we tentatively conclude that CH₄ and C_{2+} olefins and alkanes are kinetically primary products, CO a secondary product, and CO₂ and H₂ are tertiary products. note that methane could also be formed as a tertiary product, through the (reversible) reactions 5.4. and 5.5.



The increasing selectivity of CO₂ and decreasing conversion of H₂O are in agreement with both reactions. Thus a part of H₂O is also a tertiary product formed through methanation. CO₂ possibly originate as well from WGS reaction.

Blocking the metal sites partially with sulfur prevents these tertiary reactions and confirms that reactions 5.4 and 5.5 take place on the metal (Rh). Additionally the water-gas shift reaction was inhibited as water was produced and CO selectivity was much higher compared to the results without sulphur. Thus the possibility of CO formation from fast CO₂ reforming and reverse water-gas shift reaction can be excluded (compare ¹⁸).

Over the Umicore A-Type catalyst the mechanism was slightly different: in general the CO selectivity was higher together with lower CO₂ and CH₄ selectivity. This can be related to Pt inhibiting methanation reaction or a lower amount of Rh (the exact amount of noble metal on the industrial catalyst was not specified).

With increasing temperature the tertiary reactions become slower as the endothermic reactions were favored. The changes in selectivity at 650 °C and 680 °C (see Fig. 5.4 and 5.6a) become less significant – e.g. 1.5% in CH₄ and 6% in H₂ - with increasing WHSV (decreasing contact time). The experiment with sulfur partially blocking the metal sites showed that pyrolysis played a role as CH₄ can be assigned as primary product and C_{2+} unexpected from thermodynamic at temperatures higher than 650°C. Thus, the kinetic model of Rostrup-Nielsen ³ assuming successive α -scissions of the carbon cannot be applied to our data for the powdered catalyst.

However this model can be used for monolithic Rh catalysts, because C_{2+} species were only observed for short contact time. Thus, as already Rostrup-Nielsen³ showed, experimental data for light and heavy hydrocarbons can be explained by using a Langmuir-type mechanism to describe the adsorption and reaction of reactants and product on the catalyst active sites (e.g. Rh). This mechanism type and rate expressions were described in detail for the corresponding methane reactions (POX and SR)^{15, 19}.

The catalytic activity of monolithic catalysts, Rh/Al₂O₃ (M) and Umicore A-Type, was not affected by the feed composition. The reaction of hexane conversion was found to be first order in hexane. From literature it is known that the reaction order in water may become positive or negative³. A temperature dependence of the reaction orders is also possible. For instance, reaction orders in water are reported³ to decrease with increasing temperature during steam reforming. Negative orders in water are reported for methane^{20, 21} and ethane²² steam reforming. The oscillation occurring over the catalysts and the partial poisoning experiment of the Umicore A-Type catalyst with S point at an inhibiting effect of water. The apparent activation energy of around 40 kJ mol⁻¹ (± 10 kJ mol⁻¹) for hexane implied that the rate is affected by internal diffusion on the powdered catalyst. Pore diffusion and heat transfer limitations can be also assumed for the monolithic catalysts as the apparent activation energy for hexane strongly varied depending on the contribution of limitation at different retention times. For comparison, the intrinsic activation energy for n-heptane steam reforming without diffusional limitation was found to be 67.8 kJ mol⁻¹²³ over a Ni/MgO catalyst. The simplest overall reaction representing the autothermal reforming of n-hexane can be written as:



Predominantly power rate laws were applied for the SR of higher aliphatic hydrocarbons (e.g. Tracz et al.²⁴) alternatively to Langmuir-Hinshelwood rate expressions. As the reaction is irreversible the overall reaction rate can be written as:

$$r = k \cdot p(C_6H_{14}) \cdot p(H_2O)^a \quad \text{with } a \geq 0 \text{ or } a < 0 \quad (5.9)$$

Table 5.4: Comparison of conversion and selectivity for Rh catalysts and Umicore A-Type catalyst (S/C = 1.2 and $\lambda = 0.32$).

Catalyst (reactor inlet temperature)	C(C ₆ H ₁₄) (%)	C(H ₂ O) (%)	S(H ₂) (%)	S(CO) (%)	S(CO ₂) (%)	S(CH ₄) (%)	S(C ₂₊) (%)	Reactor Length (cm)
1.7 wt% Rh/ γ -Al ₂ O ₃ (500°C)	85	19	110	27	61	12	0	0.57
	90	19	110	26	62	12	0	1.00
	95	19	110	27	61	12	0	1.40
	95	10	70	12	68	20	0	2.09
Umicore A-Type (550°C)	85	4	113	55.3	40	4.7	0	0.89
	95	35	116	29	55	16	0	1.50
	100	35	116	22.3	59.6	18	0	3.55
Umicore A-Type (500°C) (550°C) 10 ppm S	62	-20	48	76	19	1.6	3.3	~1.4
	75	-8	80	78.6	19	1.3	1.1	

Note: Selectivity was based on hexane.

5.4 Hydrogenolysis

The heat generated during operation of the SOFC requires an efficient cooling system. Thus, large amounts of air (e.g., for a power of 12 kW_{el} around 2200 L/min) are needed to maintain a stable temperature inside a typical SOFC. To reduce this amount of air the intrinsically exothermic oxidation processes of the fuel cell can be combined with the endothermic steam reforming of methane. Thus a combined feed of hydrogen and methane would be conceptually ideal for the heat-balanced operation of a SOFC.

This can be thermodynamically achieved by incomplete autothermal reforming of light alkanes over noble metal catalysts. Another option to increase the methane content in the fuel cell is to add a hydrocarbon, such as hexane, to the off-gas of the reformer. This hydrocarbon will undergo hydrogenolysis, generating methane:



Here the main results of catalytic activity in hexane hydrogenolysis over supported Rh catalysts (Rh/ γ -Al₂O₃ (M) and Umicore A-Type) are briefly reported.

Thermodynamic calculations for hydrogenolysis

Fig. 5.12 shows the effect of the temperature on the calculated equilibrium composition obtained from a mixture C₆H₁₄/H₂ (molar ratio 1/30). In the temperature range investigated (300 – 750 °C) the conversion of C₆H₁₄ was complete. When considering coke (C) beside CH₄ as product, the yield of methane decreased with increasing temperature and above 400 °C H₂ was one of the products (negative conversion). The yield of carbon reached 100% above 700 °C.

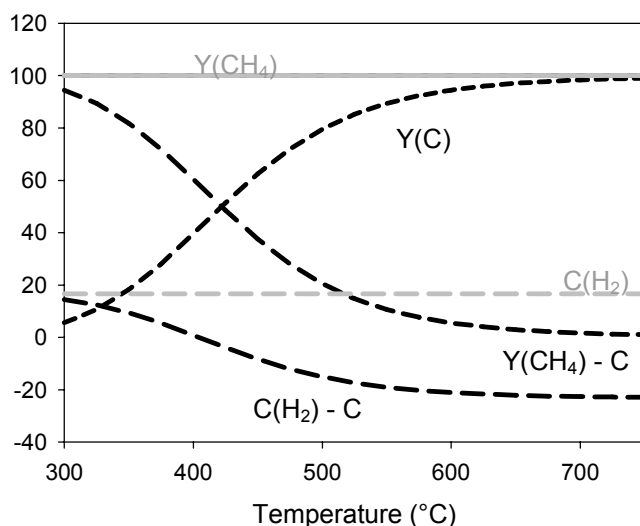


Figure 5.12: Conversions of hexane and hydrogen and the yield of methane for a C₆H₁₄ to H₂ ratio of 1:30 vs. temperature calculated from thermodynamic equilibrium (black: considering C and grey: without C).

With the real composition of the off-gas of the reformer (including CO, CO₂, H₂O and possibly CH₄, besides H₂) the situation is more complicated. However, thermodynamic calculations show that also under these conditions the methane content can be increased. For example, the addition of 30 mol of n-hexane per mole of hydrogen to the off-gas of an ATR unit operating at 650°C, increases by a factor of 1.27 the amount of methane (1.27 = mol CH_{4,out} / mol CH_{4,in}), which corresponds to a factor of 1.135 between molar percentages (mol% CH_{4,out} / mol% CH_{4,in}).

The activity of Rh/ γ -Al₂O₃ (M) in hydrogenolysis was tested at several temperatures, WHSVs and C₆H₁₄/H₂ ratios. Representative results are summarized in Fig. 5.13. The experiments were performed following the same order indicated in the legend. As a general trend, it was observed that the conversion of hexane increased for lower hexane to hydrogen ratios. The catalyst slightly deactivated with time-on-stream probably in consequence of carbon deposition. The lower the WHSV, the higher was the conversion. Additionally, higher temperatures are advantageous for obtaining lower carbon deposition. However, it should be emphasized that under all conditions measured the rate of formation of higher alkenes and alkanes were extremely small posing no threat for a stable operation of the SOFC.

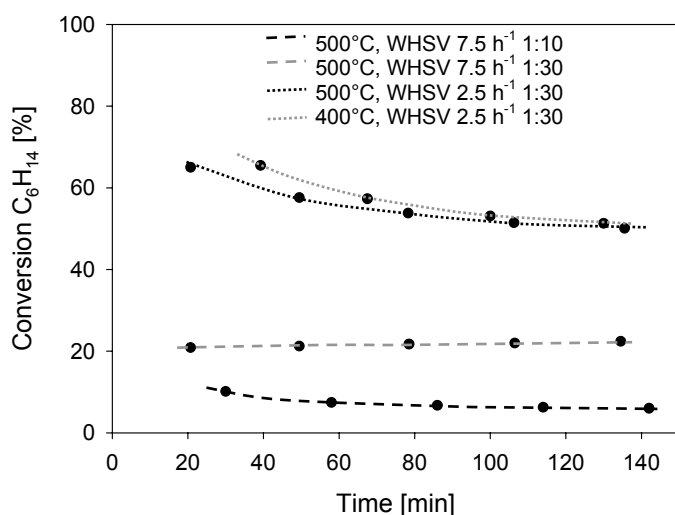


Figure 5.13: Conversion of hexane vs. TOS at different reaction conditions (temperature, WHSV and hexane/hydrogen ratio) over Rh/ γ -Al₂O₃ (M)

The catalytic activities of Rh/ γ -Al₂O₃ (M) and Umicore A-Type catalyst were compared with respect to hexane hydrogenolysis performed in excess hydrogen (molar ratio hexane/hydrogen 1:30). Conversions of hexane and hydrogen and product yield are represented in Fig. 5.14 a (Rh/ γ -Al₂O₃ (M)) and b (Umicore A-Type). The performance of the two catalysts was quite similar. At temperatures above

500 °C hexane was fully converted to methane and the activity was stable with time-on-stream. At lower temperature the conversion was reduced (88% at 450 °C) and the catalyst deactivated with time-on-stream.

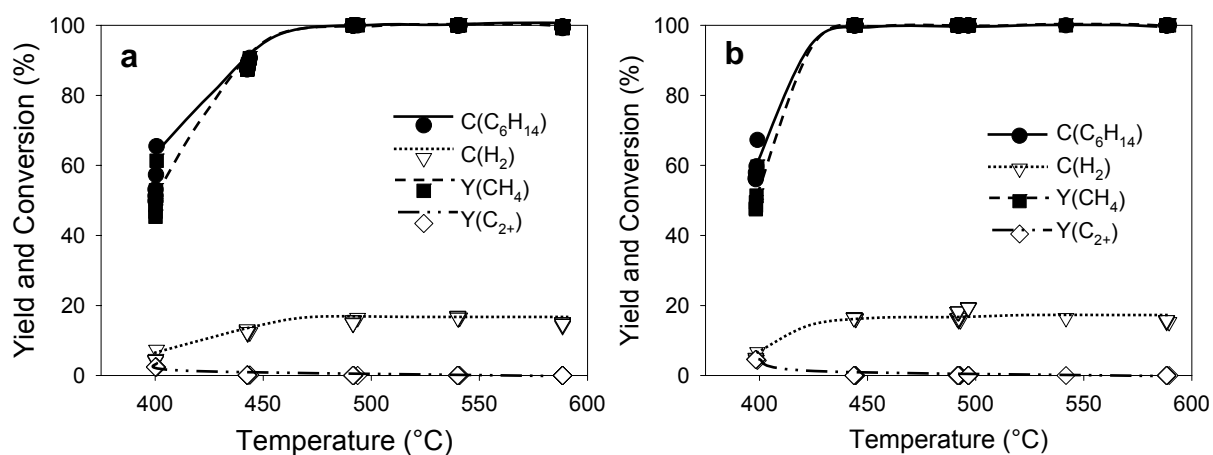


Figure 5.14: Conversions of hexane and hydrogen and yield of methane and C₂₊ vs. temperature over **a)** the Rh/ γ -Al₂O₃ (M) catalyst (WHSV 3.1 h⁻¹) and **b)** the Umicore A-Type catalyst (WHSV 3.2 h⁻¹) at a C₆H₁₄ to H₂ ratio of 1:30.

5.5 Conclusions

From the variation in the flow rate, it can be concluded that CO and H₂ were primary products through direct partial oxidation and steam reforming reaction. CH₄ was a secondary product at low temperature produced in the methanation reaction from CO or CO₂ and hydrogen or a primary product at high temperatures due to α -scissions of C-C bonds on metal sites. Variations in the steam to hexane and the oxygen to hexane ratios showed that the catalysts are stable for at least 2h under conditions only allowing partial oxidation or steam reforming. The overall reaction was found to be first order in hexane. The values of the apparent activation energies indicated diffusion and heat transfer limitations.

Two options can be considered to increase CH₄ yield. First, the reaction temperature of the autothermal reforming unit could be reduced. However this solution will imply that full n-hexane conversion could be attained only with more catalyst. This option is inappropriate for mobile application due to the limited space. A further disadvantage could be the complicate heat management if a SOFC operating at around 800 °C followed the reforming unit. The second option is to add another reaction step after the autothermal reforming unit, in which small amounts of n-hexane are added to the off stream from the reformer and are converted in a hydrogenolysis step to methane. The hydrogenolysis can be catalyzed by the same Rh/Al₂O₃ catalyst used in the reformer.

5.6 References

- (1) Pant, K. K.; Kunzru, D. *Journal of Analytical and Applied Pyrolysis* **1996**, *36*, 103.
- (2) Pacheco, M.; Sira, J.; Kopasz, J. *Applied Catalysis A-General* **2003**, *250*, 161.
- (3) Rostrup-Nielsen, J. R. Catalytic steam reforming. In *Catalysis Science and Technology*; Anderson, J., Boudart, M., Eds.; Springer, 1984.
- (4) Keiski, R.; Salmi, T.; Pohjola, V. *Chemical Engineering Journal* **1992**, *48*, 17.
- (5) Keiski, R.; Desponds, O.; Chang, Y.; Somorjai, G. *Applied Catalysis A - General* **1993**, *101*, 317.
- (6) Ahlborn, R.; Baumann, F.; Wieland, S. Verfahren zur autothermen, katalytischen Dampfreformierung von Kohlenwasserstoffen. In *Patent EP 1157968*; OMG AG & Co. KG, Hanau, 2001.
- (7) Rostrup-Nielsen, J. R. *Journal of Molecular Catalysis A* **2000**, *163*, 157.
- (8) Rostrup-Nielsen, J. R. *Catalysis Today* **1993**, *18*, 305.
- (9) Hendriksen, B. L. M.; Bobaru, S. C.; Frenken, J. W. M. *Catalysis Today* **2005**, *105*, 234.
- (10) Hendriksen, B. L. M.; Bobaru, S. C.; Frenken, J. W. M. *Surface Science* **2004**, *552*, 229.
- (11) Ioannides, T.; Efstathiou, A. M.; Zhang, Z. L.; Verykios, X. E. *Journal of Catalysis* **1995**, *156*, 265.
- (12) Werner, H.; Herein, D.; Schulz, G.; Wild, U.; Schlögl, R. *Catalysis Letters* **1997**, *49*, 109.
- (13) Zhang, X.; Lee, C. S.-M.; Mingos, D. M. P.; Hayward, D. O. *Applied Catalysis A-General* **2003**, *240*, 183.
- (14) Zhang, X.; Hayward, D. O.; Mingos, D. M. P. *Catalysis Letters* **2002**, *83*, 149.
- (15) Jin, W.; Gu, X.; Li, S.; Huang, P.; Xu, N.; Shi, J. *Chemical Engineering Science* **2000**, *55*, 2617.
- (16) Hickman, D. A.; Schmidt, L. D. *Journal of Catalysis* **1992**, *138*, 267.
- (17) Hickman, D. A.; Schmidt, L. D. *AIChE Journal* **1993**, *39*, 1164.
- (18) Steghuis, A. G. Catalyzed partial oxidation of methane to synthesis gas. PhD-Thesis, University of Twente, 1998.
- (19) Xu, J.; Froment, G. *AIChE Journal* **1989**, *35*, 97.
- (20) Ma, L.; Trimm, D. L. *Applied Catalysis A-General*. **1996**, *138*, 265.
- (21) Hayes, R. E.; Kolaczkowski, S. T.; Li, P. K. C.; Awdry, S. *Chemical Engineering Science* **2001**, *56*, 4815.
- (22) Rostrup-Nielsen, J. R. *Journal of Catalysis* **1973**, *31*.
- (23) Jennings, J. R.; Twigg, M. V. *Selected Developments in Catalysis*; Blackwell Science: Oxford, 1985; Vol. 12, Chapter 4.
- (24) Tracz, E.; Scholz, T.; Borowiecki, T. *Applied Catalysis A - General* **1990**, *66*, 133.

Chapter 6

Summary

The worldwide capacity of crude oil is decreasing and the price for fuels is dramatically increasing. Therefore the call for alternatives to fossil fuels is becoming stronger. Hydrogen is considered as fuel or energy carrier in the future besides bio-diesel or solar energy. Hydrogen run fuel cells are used as propulsion for vehicles. Currently, two types of fuel cells – proton exchange membrane fuel cell (PEMFC) and solid oxide fuel cell (SOFC) – are considered as the most technologically applicable (as described in Chapter 1). In both fuel cells pure hydrogen or a reformat gas containing hydrogen can be fed to the anode, while oxygen is fed to the cathode. The main difference is the type of the electrolyte and therefore the operating temperature. A drawback of the PEMFC is the sensitivity of its anode towards poisoning with CO. This requires additional steps for CO removal if reformat gas is used as feed. With the use of a SOFC this problem can be circumvented. When analyzing the commercial viability of the fuel cell technology, the more relevant issue for commercial application of fuel cells in vehicles is the on-board production of hydrogen. Its storage, transportation and delivery are still critical steps toward a future hydrogen economy. Methane, methanol or other fuels could be converted into hydrogen within a reformer that straightway supplies it to the fuel cell. As an intermediate step for introduction of fuel cells on the market, the automobile industry is working on the on-board production of hydrogen from gasoline or diesel.

The research described in this thesis focuses on the autothermal reforming (ATR) of n-hexane as model substance for alkanes in the presence of heterogeneous catalysts.

Chapter 2 dealt with the reactions involved in n-hexane conversion to synthesis gas: steam reforming, partial oxidation, dry reforming. Thermodynamic equilibrium calculations for these reactions were performed from room temperature to 1000 °C. H₂ and/or CO are formed at temperatures higher than 300 °C, while at lower temperatures methane was thermodynamically favoured. Other possible reactions of hexane like cracking and dehydration were also considered. In the autothermal reforming of hexane the endothermicity of steam reforming is combined with the exothermicity of partial oxidation. The influence of the ratios water/hexane and oxygen/hexane on the reaction enthalpy and the thermodynamic equilibrium at different temperatures were discussed. Methane formation was favoured at low temperature and low ratios water/hexane and oxygen/hexane. The formation of CO

was favoured at high temperatures, while hydrogen passed through a maximum around 650° - 700°C. The present knowledge about catalysts investigated for steam reforming and partial oxidation and the surface reaction steps occurring were reviewed.

In Chapter 3 the activity of rhodium, platinum or nickel supported on various oxides in the autothermal reforming of n-hexane was compared. As supports ceria, zirconia, yttrium-stabilized zirconia and alumina were used. The catalysts were synthesized through wet impregnation of the powdered supports resulting in 1wt% of metal, and investigated in a temperature range from 500 - 850 °C in a fixed bed reactor. The influence of the support and the metal on the product distribution was discussed. Without metals the supports showed very low activity. Independently of the support, the activity of the catalysts increased following the sequence Ni < Pt < Rh. A correlation between the activity of hexane conversion with the total number of accessible metal atoms was not found. It was concluded that the different nature of the metals make different reaction routes accessible. For Rh the sequence of activity was Rh/Al₂O₃ > Rh/ZrO₂, Rh/YSZ > Rh/CeO₂ with approaching thermodynamic equilibrium around 800°C. Generally, the support can affect the activity of the metal catalyst through two mechanisms: (i) modification of the metal dispersion and (ii) enhanced steam adsorption followed by “inverse spillover”. As the activity over the rhodium supported catalysts was found to be independent of the metal particle size, this strongly points to the second mechanism.

The synthesis, characterisation and catalytic activity of structured catalysts impregnated with nickel, platinum or rhodium were discussed in Chapter 4. An alumina monolith was used as support. For a given feed composition the catalysts' stability was first investigated at a temperature close to the operating temperature of a solid oxide fuel cell (800 °C). Rhodium and platinum showed stable activity corresponding to thermodynamic equilibrium. An induction period for these catalysts was not observed. The induction period observed for nickel was shortened by prolonging the *in-situ* reduction step prior to reaction. Changing the feed composition from lean to rich condition in water or oxygen showed that rhodium exhibits the most stable performance close to thermodynamic equilibrium under all conditions. The platinum catalyst, on the other hand, showed decreasing activity at a low

oxygen/hexane ratio of 1.5. Nickel was deactivated by oxidation to Ni^{2+} at oxygen rich condition ($\text{O}_2/\text{C}_6\text{H}_{14} = 4.5$) and through carbon deposition at water lean condition ($\text{H}_2\text{O}/\text{C}_6\text{H}_{14} = 4$). The activity of the platinum and rhodium catalysts was compared to that of an industrial monolithic catalyst in a temperature range of 500 - 800 °C at $\text{C}_6\text{H}_{14}/\text{O}_2/\text{H}_2\text{O} = 1/3/7$. At temperatures below 750 °C the performance of the platinum catalyst deviated from the rhodium and the industrial catalyst. For platinum mainly combustion at temperatures below 570 °C occurred. Between 570 °C and 750 °C hydrogen selectivity (~10% to 120%) and carbon monoxide selectivity (10~% to 50%) increased with hexane conversion. Simultaneously, significant amounts of cracking products with a selectivity (up to 20%) were observed. The rhodium catalyst and the industrial catalyst showed high activity already at 500 °C reaching full conversion of hexane and a water conversion of around 40% at ~ 550 °C. The product distribution was close to thermodynamic equilibrium with yields from 80% to 140% in hydrogen, 10% to 50% in carbon monoxide and up to 20% in methane depending on the reaction temperature.

Chapter 5 focused on the investigation of rhodium containing catalysts (supported on alumina powder or alumina monolith, and an industrial catalyst), as the previous results showed that this noble metal has the best performance in autothermal reforming. The influence of the hexane flow rate in a temperature range of 500-800 °C and the effect of steam/hexane and oxygen/hexane ratios at selected temperatures (500 °C, 600 °C and 650 °C) were studied. Full conversion of hexane can be achieved already at temperatures as low as 550 °C. Variations in the steam to hexane and the oxygen to hexane ratios showed that the catalysts are stable for at least 2h, even under conditions only allowing partial oxidation or steam reforming. The selectivities to synthesis gas, methane and carbon monoxide were close to the thermodynamic equilibrium for the monolithic catalysts. While for the powdered catalyst intermediate cracking products (C_{2+}) could be observed at shorter residence time. For the industrial catalyst an experiment with sulfur containing hexane was included. It showed that the catalysts active sites were blocked by sulfur. While hexane and oxygen conversion remained unaffected at 800 °C the selectivity in hydrogen decreased and the yield in methane increased with time-on-stream reaching a new equilibrium after 80 min. At lower temperatures the activity in hexane and water conversion were reduced. Consequently the selectivity in

hydrogen decreased and the selectivity in CO strongly increased at low temperatures. An attempt has been made to classify the products in primary, secondary and tertiary products. From the variation in the residence time, it can be concluded that CO and H₂ were primary products through direct partial oxidation and steam reforming reaction. At low temperature, CH₄ was a secondary product obtained through methanation. At very short contact times methane could be formed as primary product through α -scissions of C-C bonds. Non-catalytic experiments showed the difficulty in operating at differential conditions as hexane conversion exceeded 20% at around 650°C. The overall reaction was found to be first order in hexane along with an indication for diffusion and heat transfer limitations.

Additionally, hydrogenolysis of n-hexane was investigated as an option to increase the methane content in the off-gas of the reformer for SOFC application. It was found that the hydrogenolysis can be catalyzed by the same Rh/Al₂O₃ catalyst used in the reformer.

Curriculum Vitae

Maria Brandmair was born on the 7th of November in 1973 in Freising, Germany. After graduating from high school in 1993, she started her study in chemistry at the Technical University of Munich, Germany. She worked on her diploma thesis, entitled *Physico-chemical and catalytic properties of Ni based molecular sieve catalysts for NO_x reduction* at the Institute for Technical Chemistry II at the Technical University of Munich, Germany under supervision of Prof. J.A. Lercher. After receiving her master degree (Diplom-Chemikerin) in September 2000 she started to work as a PhD student in the group of Prof. J.A. Lercher. The main results of this work on the autothermal reforming of n-hexane over Supported Metal Catalysts are described in this thesis.